2015-06-01

# A Simplified Performance-Based Procedure for the Prediction of Lateral Spread Displacements

Levi Thomas Ekstrom
*Brigham Young University - Provo*

# A Simplified Performance-Based Procedure for the Prediction of Lateral Spread Displacements

Levi Thomas Ekstrom

A thesis submitted to the faculty of
Brigham Young University
in partial fulfillment of the requirements for the degree of

Master of Science

Kevin W. Franke, Chair
Kyle M. Rollins
W. Spencer Guthrie

Department of Civil and Environmental Engineering

Brigham Young University

June 2015

ABSTRACT

A Simplified Performance-Based Procedure for the Prediction of
Lateral Spread Displacements

Levi Thomas Ekstrom
Department of Civil and Environmental Engineering, BYU
Master of Science

Characterization of the seismic hazard and ground-failure hazard of a site using traditional empirical lateral spread displacement models requires consideration of uncertainties in seismic loading, site conditions, and model prediction. Researchers have developed performance-based design methods to simultaneously account for these sources of uncertainty through the incorporation of a probabilistic analytical framework. While these methods can effectively handle the various sources of uncertainty associated with empirical lateral spread displacement prediction, they can be difficult for engineers to perform in a practical manner without the use of specialized numerical tools. To make the benefits of a performance-based approach accessible to a broader audience of geotechnical engineers, a simplified performance-based procedure is introduced in this paper. This map-based procedure utilizes a reference soil profile to provide hazard-targeted reference displacements across a geographic area. Equations are provided for engineers to correct those reference displacements for site-specific soil conditions and surface geometry to produce site-specific, hazard-targeted estimates of lateral spread displacement. The simplified performance-based procedure is validated through a comparative study assessing probabilistic lateral spread displacements across several cities in the United States. Results show that the simplified procedure closely approximates the results from the full performance-based model for all sites. Comparison with deterministic analyses are presented, and the place for both in engineering practice are discussed.

Keywords: Kevin W. Franke, probabilistic, simplified, lateral spread, liquefaction, earthquake, empirical, hazard, reference maps, seismic, performance-based, probability

ACKNOWLEDGEMENTS

I especially thank my advisor, Dr. Kevin W. Franke. Without his counsel, guidance, and advice I would never have been where I am today. Thank you for giving the grumpy kid who sat in the back a chance at changing his life.

I thank my graduate committee, Dr. W. Spencer Guthrie and Dr. Kyle M. Rollins, for their time and effort in reviewing this thesis and for the great advice and suggestions. A big thank you to those graduate students who were there to support and inspire me throughout my research: Kristin Ulmer and Brian Peterson. Without their daily patience and consideration for me, this process would have been much less pleasant then it turned out to be. Thanks as well to Dr. Les Youd for his wisdom and experience, and for giving me a chance to see my research in the real world.

Funding for this study was provided in part by a Federal Highway Administration Pooled Fund Study (Award No. TPF-5(296), with participation from the Utah, Alaska, Connecticut, Idaho, Montana, and South Carolina state departments of transportation) and a grant from the U.S. Geological Survey External Research Program (Award No. G14AP00031). I gratefully acknowledge this support. However, the conclusions and opinions expressed in this paper do not necessarily reflect those of our sponsors.

Last of all, thanks to my wife Mallory. Thank you for always believing in me and for encouraging me when I needed it the most. Without your love and patience, I would be lost.

TABLE OF CONTENTS

LIST OF TABLES

LIST OF FIGURES

# 1 INTRODUCTION

Liquefaction-induced lateral spread displacements have caused significant damage to structures, transportation infrastructure, and lifelines during many past earthquakes. Lateral spread, cumulatively, has caused more damage than any other liquefaction-induced ground failure (National Research Council, 1985). Prediction of the ground deformations associated with lateral spread events is essential to assessing risk to infrastructure and for designing engineering solutions to mitigate its effects. To predict the lateral spread displacements from large earthquakes, engineers have commonly relied upon empirical ground displacement predictive models developed from historic liquefaction and lateral spread case histories.

Despite the wide use and adoption of empirical lateral spread displacement models in engineering practice throughout much of the world, there typically exists considerable scatter in the predicted results, in large part due to uncertainty associated with seismic loading (e.g., source-to-site distance, earthquake moment magnitude) and with soil/site properties. To account for these uncertainties, probabilistic design approaches are being applied to the prediction of lateral spread displacement and other liquefaction effects. Performance-based earthquake engineering (PBEE) methods provide the capability to simultaneously account for uncertainty in seismic loading and soil/site parameters for a given site. Recent advances in PBEE have introduced probabilistic uniform hazard-based procedures for evaluating seismic ground deformations. Despite the advantages these probabilistic approaches provide, they have not yet been widely implemented in the engineering community due to the complexity of the methods,

the lack of convenient numerical tools, and/or engineers' lack of familiarity with probabilistic methods.

To address these challenges, a new simplified performance-based lateral spread displacement procedure based on the Youd et al. (2002) empirical lateral spread predictive model is developed. The simplified lateral spread procedure is derived and then validated against a full performance-based lateral spread procedure using multiple soil profiles, multiple selected sites in the U.S., and multiple return periods. The results of the simplified procedure are compared against a deterministic and conventional pseudo-probabilistic analysis, and recommendations are presented for how the simplified procedure should be implemented in the current state of practice.

The main result of this study is to present a simplified procedure that resembles other procedures currently used by engineering practitioners to develop probabilistic ground motions for engineering design and should therefore be understandable to most engineers and practical for implementation on even small engineering projects.

# 2 REVIEW OF LIQUEFACTION

## 2.1 Introduction

Lateral spread displacements can cause significant damage to structures and lifelines when an earthquake occurs. The horizontal movement of the ground can be particularly destructive when on sloping ground or near a free-face like near a river or port. Predicting if lateral spread will occur and the magnitude of the horizontal displacement is crucial in designing seismically resilient facilities but lateral spread displacements only occur when the soil experiences seismically-induced liquefaction. Because lateral spread is incumbent on liquefaction, a brief review of liquefaction is presented in this chapter. Lateral spread is discussed more in depth in Chapter 3.

## 2.2 Liquefaction

Liquefaction can be one of the most destructive effects of an earthquake. Though liquefaction has been observed historically in many earthquakes, it was not until the 1964 earthquakes in Prince William Sound, Alaska and Niigata, Japan that liquefaction was brought to the attention of the geotechnical engineering community. Those events initiated intense research across the world, which still continues today. The phenomenon is extremely complex, and there are still aspects that are not well understood: however, there have been many advances in characterizing how it is initiated, what soils conditions are susceptible to it, and how to predict if

it will occur. In his textbook "Geotechnical Earthquake Engineering" Kramer (1996) presents an excellent summary of the current understanding of liquefaction and is heavily referenced here.

Though liquefaction was not heavily researched until after the two 1964 earthquakes, the term was first coined by Mogami and Kubo (1953). The term has historically been used to describe a number of different of different phenomena that occur during earthquakes. In essence it describes events that involve soil deformations caused by monotonic, transient, or repeated disturbances of saturated cohesionless soils under undrained conditions (Kramer, 1996). The process is driven by the generation of excess pore pressures during the cyclic loading of the soil from an earthquake, and results in a rapid drop in shear strength and stiffness. The phenomenon is manifested, in general, in two ways: flow liquefaction and cyclic mobility.

Flow liquefaction can occur when the shear stress required for static equilibrium of a soil mass is greater than the shear strength of the soil in its liquefied state (Kramer, 1996). The cyclic shear stresses from the earthquake can cause the static strength of the soil to decrease just enough that the soil becomes unstable. This can result in the most extreme example of a liquefaction-related effect, referred to as a flow failure. These failures can result in soil masses that experience extremely large displacements that move very rapidly. Though this effect is relatively rare, the process can occur very quickly and is potentially the most dangerous of all possible failures.

Cyclic mobility is a much more common result of soil liquefaction and, though it is not as dangerous as flow liquefaction, can result in very large horizontal displacements. This expression of liquefaction occurs when the static shear stresses in the soil are less than the shear strength of the liquefied soil. This results in cyclic mobility failures that are driven by both cyclic and static shear stresses that develop incrementally in the soil during the earthquake (Kramer, 1996).

Lateral spread displacements and seismic compaction are some of the results of cyclic mobility and though usually not very dangerous, can be devastating to infrastructure.

Researchers have increased the understanding of the mechanics of liquefaction significantly over the last 50 years, and though there are many aspects of liquefaction research that could be reviewed, only a brief review of the most important aspects is reviewed here: liquefaction susceptibility, liquefaction initiation, and liquefaction effects.

## 2.3 Liquefaction Susceptibility

Not all soils are susceptible to liquefaction; therefore, the first step in a liquefaction hazard evaluation is to determine if the soil is susceptible to liquefaction. There are several ways to evaluate whether a soil is susceptible to liquefaction, and Kramer (1996) suggested the following criteria: historical criteria, geologic criteria, compositional criteria, and state criteria.

### 2.3.1 Historical Criteria

When seismic events occur, many important observations about liquefaction have been made during post-earthquake reconnaissance. The investigations have shown that liquefaction has a strong probability to occur in locations where liquefaction has already occurred, if the soil and groundwater conditions have not changed (Youd, 1984). Additionally, researchers have discovered prehistoric evidence of liquefaction, referred to as paleoliquefaction, and these observations have been used to predict future liquefaction events (Obermeier and Pond, 1999).

These researchers, from the post-earthquake reconnaissance, have also observed that liquefaction tends to occur within a particular distance of the epicenter of the earthquake. Ambraseys (1988) compiled instances where liquefaction occurred in 137 earthquake events and plotted the moment magnitude of each earthquake against the epicentral distance to the furthest

distance liquefaction occurred. He noted that the distance at which liquefaction occurs appeared to be related to the magnitude of the earthquake. This comparison can be seen in Figure 2-1.

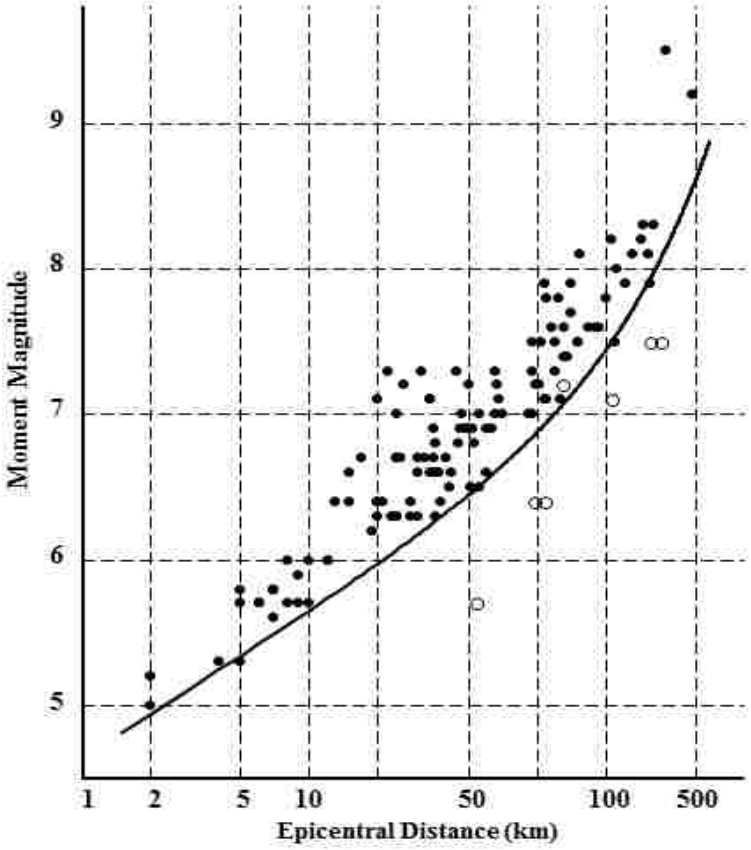


**Figure 2-1: Relationship Between Limiting Epicentral Distance of Liquefaction Sites and Moment Magnitude (after Ambraseys, 1988)**

It should be noted that this relationship does not rule out liquefaction occurring at a greater distance. The vast majority of the events used in this figure were shallow events (<50 km depth) while deeper earthquakes have been observed to cause liquefaction at greater distances.

### 2.3.2 Geologic Criteria

Depositional environment also plays an important role in determining whether a soil will be susceptible to liquefaction. The range of these environments is relatively small because susceptibility is dependent on a combination of the depositional environment, hydrological environment, and age of soil deposit (Youd and Hoose, 1977). Soils that have been deposited in loose configurations (alluvial, fluvial, Aeolian, and man-made deposits) are particularly susceptible when saturated. For liquefaction to occur, ground water is typically near the surface, as the soil must be saturated to liquefy. The age of the soil deposit also plays a role in susceptibility. The older a deposit is, the less susceptible to liquefaction (i.e. Holocene soils are more susceptible than Pleistocene, etc.) Pre-Pleistocene deposits have rarely been observed to experience liquefaction (Youd and Hoose, 1977).

### 2.3.3 Compositional Criteria

The particle size, shape, and gradation of a soil are all important factors in determining susceptibility. Soils with high volume change potential may be particularly susceptible when excess pore pressures are generated, whereas soils that resist volume change may not be. Susceptibility tends to go up the more uniform the grain size distribution is and goes down with increasing fines content and plasticity index.

Although it was originally thought that only sand was able to experience liquefaction, research has shown that gravels and silts can liquefy as well. Liquefaction was observed in the field for gravels (Coulter and Miglaccio, 1966; Wong et al., 1975; Chen et al., 2009) and coarse non-plastic silts (Ishihara, 1984; Ishihara, 1985). Fine-grained soils are still considered non-susceptible for the most part due to the difficulty in developing the high pore pressures needed for liquefaction. The "Chinese Criteria" established by Wang (1979), which provides criteria for

assessing susceptibility of clays (based on Atterberg limits, water content, and fines content), was recommended by Youd et al. (2001) and was adopted by most geotechnical engineers. However, Idriss and Boulanger (2008) have noted that low-plasticity clays can undergo a strain softening process similar to liquefaction, called "cyclic softening," though this process generally does not result in the destructive effects of liquefaction (Youd et al., 2009). This has resulted in many engineers choosing to disregard the "Chinese Criteria" (Bray and Sancio, 2006).

### 2.3.4 State Criteria

The initial stress state of a soil is highly influential in how the soil will behave in an earthquake. Since the liquefaction process is driven by the generation of excess pore pressures, the density and initial stress conditions often determine whether these pore pressures will occur. These stress and density conditions, or state, of a soil determine whether a soil will dilate or contract under cyclic earthquake loading, which will ultimately determine their susceptibility. It is also important to note that the criteria for liquefaction susceptibility are different for flow liquefaction and cyclic mobility. To understand why the state of a soil can determine its susceptibility, the concepts of critical void ratio and steady state of deformation is briefly reviewed.

#### *2.3.4.1 Critical Void Ratio*

During experiments with drained triaxial tests on sands, Casagrande (1936) observed that the same sand with the same confining pressure would either contract or dilate based on whether the sand was loosely or densely compacted and ultimately achieved the same void ratio. He referred to this void ratio as the critical void ratio (CVR). If the CVR were to be plotted for all confining stresses, then the CVR line would be created for a particular soil. It was also observed

that points plotted above the CVR represented "loose" soils that tend to contract, and points plotted below represented "dense" soils that tend to dilate. Figure 2-2 a) shows a CVR line plotted in CVR space representing this behavior.

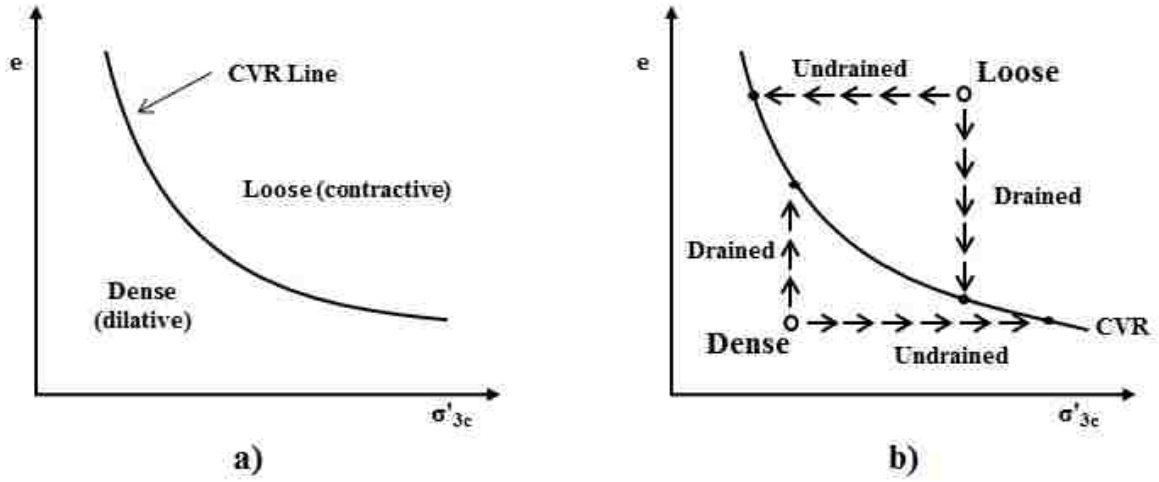


**Figure 2-2: Behavior of Loose and Dense Soil – a) With CVR Line, b) for Drained and Undrained Conditions (after Kramer, 1996)**

Casagrande predicted that if the soil were sheared in undrained conditions, where no change in volume or void ratio would occur, the loose soil would develop positive excess pore pressures and the dense soil would develop negative pore pressures, until the CVR line was reached. This can be seen in Figure 2-2 b). He concluded that the CVR line marked the boundary between contractive and dilative behavior, and because dilative soils would resist expansive volume change and not experience liquefaction. Therefore, soils that plotted above the CVR would be susceptible to liquefaction, while those below would not. Unfortunately, this theory was shown to be incorrect when the Fort Peck Dam failed in 1938 and the soil from the dam was back-calculated to plot below the CVR line (Middlebrooks, 1942).

*2.3.4.2 Steady State of Deformation*

Castro (1969) conducted static and cyclic triaxial tests on isotropically and anisotropically consolidated sand. In these tests, Castro observed three different types of stress-strain behavior. Very loose soils would tend to contract at small shear strains and then suddenly collapse, resulting in large strains at low effective confining pressure and very low residual strength. This behavior was referred to as "liquefaction". Dense specimens were observed to contract slightly but then to dilate until a high constant effective confining pressure and large-stain strength. This strength increase was due to the generation of negative pore pressures and was referred to as "dilation". For medium-dense specimens the behavior was similar to the loose specimen initially, but as the soils was strained further it would begin to dilate and regain strength similar to the dense specimen. This behavior was referred to as "limited liquefaction".

This research revealed a unique relationship between void ratio and effective confining pressure at large strains. This relationship plots below the CVR line, roughly parallel, and is called the steady state line (SSL). The difference between the lines was attributed to the development of a flow structure under stress controlled conditions. The state at which soil flowed continuously under constant shear stress, effective confining pressure, pressure, and velocity was later defined as the steady state of deformation (Castro and Poulos, 1977; Poulos, 1981). The strength of the soil in this state is referred to as the steady state strength, $S_{su}$. A soil is considered susceptible to flow liquefaction if it plots above the SSL line and its $S_{su}$ is less than the initial static stress condition, and this criteria is represented in Figure 2-3.

This criterion only applies to flow liquefaction. Cyclic mobility can occur in soil that plot above and below the SSL; therefore, cyclic mobility can occur in loose or dense soils (Kramer, 1996).

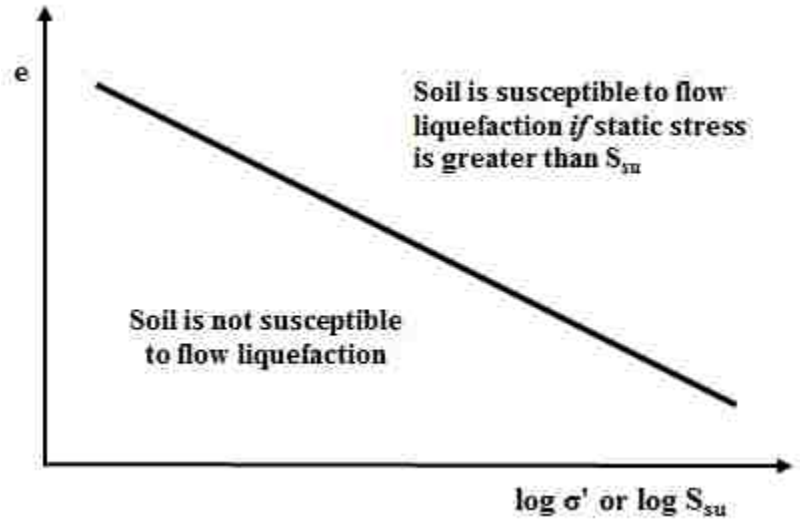


**Figure 2-3: State Criteria for Flow Liquefaction Susceptibility (after Kramer, 1996)**

## 2.4 Liquefaction Initiation

Though a soil may be susceptible to liquefaction by one or more of these criteria, liquefaction does not necessarily occur. For liquefaction to initiate, the earthquake needs to produce sufficiently large ground motions that the state of the soil is altered enough to exhibit either flow liquefaction or cyclic mobility. Understanding the initiation of liquefaction requires identification of the state of the soil when liquefaction is triggered (Kramer, 1996). Because flow liquefaction and cyclic mobility are inherently different processes, their differing initiation mechanics is briefly introduced here.

### 2.4.1 Flow Liquefaction Surface

The initiation of flow liquefaction is most easily understood when the sample is subjected to increasing monotonic stresses. Hanzawa et al. (1979) performed triaxial tests on five different

soils, initially consolidated to the same void ratio but under different effective pressures. They observed that stress paths could be used to determine if flow liquefaction would occur for a soil given a starting stress state. Figure 2-4 shows the stress paths that these samples followed after monotonic loading.

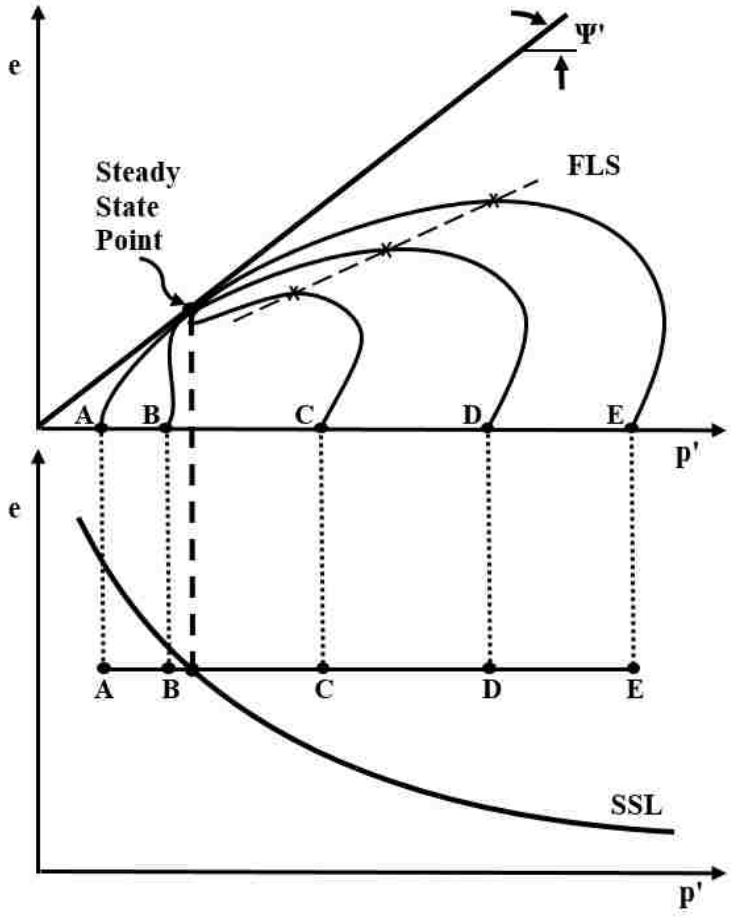


**Figure 2-4: Flow Liquefaction Surface (after Kramer, 1996)**

In Figure 2-4 it can be seen that all of the stress paths converge to a single point on the Mohr-Coloumb failure envelope. This point is referred to as the steady state strength of the soil. In the tests performed by Hanzawa et al. (1979), points A and B plotted under the SSL so they

exhibited dilative behavior and did not undergo flow liquefaction, while for points C, D, and E flow liquefaction was initiated at the peak of each stress path. The line created by connecting all of the failure points C, D and E can be used to define the flow liquefaction surface (FLS) in p-q space. The FLS marks the boundary between stable and unstable states in undrained shear. Therefore, the FLS describes the conditions at which flow liquefaction is initiated (Kramer, 1996).

For flow liquefaction to initiate, two conditions must be met. First, the effective stress path of the soil experiencing the earthquake loading needs to reach the FLS. The second is that the soil must be experiencing driving stresses that push the soil to its steady state strength, which for flow liquefaction are usually the static stresses that are already affecting the soil due to gravity. The FLS, and the necessary stress state of the soil to initiate flow liquefaction can be seen in Figure 2-5.

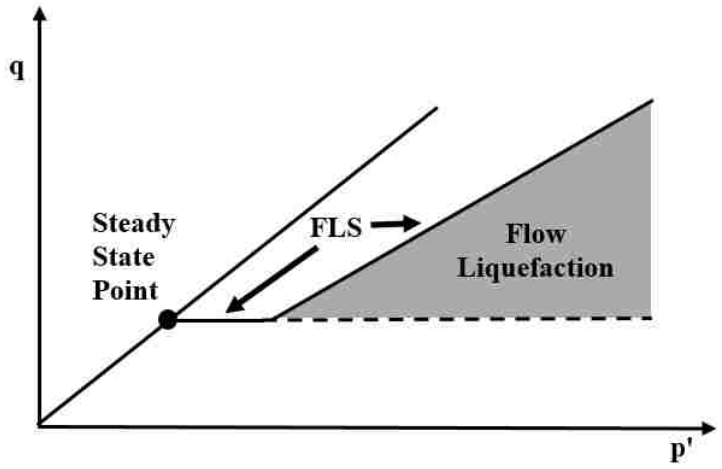


**Figure 2-5: Zone Susceptible to Flow Liquefaction (after Kramer, 1996)**

### 2.4.2 Cyclic Mobility

Unlike flow liquefaction, which cannot occur if the static stress is smaller than the steady-state strength, cyclic mobility can develop. As stated previously, cyclic mobility can initiate in loose or dense soils at low or high effective confining pressure, and so the initial state of the soil can be plotted in Figure 2-6 to evaluate its cyclic mobility potential.

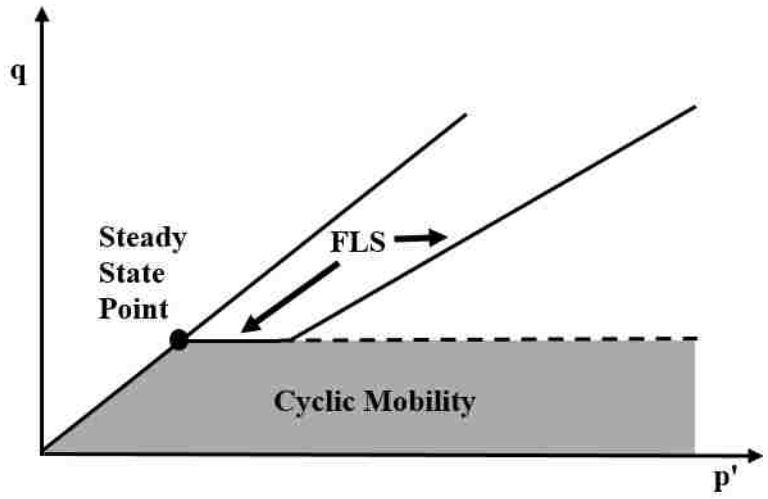


**Figure 2-6: Zone of Susceptibility to Cyclic Mobility (after Kramer, 1996)**

Cyclic mobility is the gradual loss of strength due to the buildup of pore pressure through undrained cyclic loading. This incremental loss of strength can best be explained through three cyclic loading conditions presented by Kramer (1996). The first condition, seen in Figure 2-7 a), can occur when $\tau_{static} - \tau_{cyclic} > 0$ and $\tau_{static} + \tau_{cyclic} < S_{su}$. In this condition the effective stress path moves to the left until it reaches the drained failure envelope. This is accompanied by a gradual loss of strength and increase in permanent shear strains. This behavior may result in liquefaction, but if the load were continually applied, then the steady state would be reached and the soil would cease to dilate.

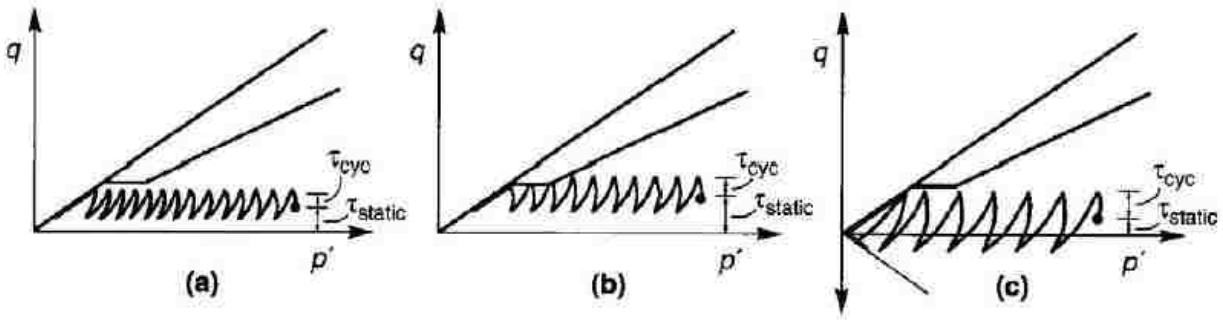


**Figure 2-7: Three Cases of Cyclic Mobility (after Kramer, 1996)**

The second condition seen in Figure 2-7 b), occurs when $\tau_{static} - \tau_{cyclic} > 0$ and $\tau_{static} + \tau_{cyclic} > S_{su}$. Similar to the first condition, the stress path moves to the left, but the collective stresses are large enough that the FLS is reached repeatedly. This results in short periods where flow liquefaction occurs, and the cumulative strains can become very large. This process is the manner in which cyclic mobility is generally initiated.

The final condition, seen in Figure 2-7 c), occurs when $\tau_{static} - \tau_{cyclic} < 0$ and $\tau_{static} + \tau_{cyclic} < S_{su}$. This results in a stress path reversal that is characterized by compressional and extensional loading. Dobry et al. (1982) and Mohamad and Dobry (1986) showed that the rate of pore pressure generation increases with increasing stress reversal. Significant cumulative strains can develop for this case, but flow liquefaction will not occur.

### 2.4.3 Evaluation of Initiation of Liquefaction

Once the basis of the behavior of liquefied soils is understood, the procedures that are used in practice today can be examined. While there are several approaches to assessing the liquefaction hazard at a site, they are generally divided into two areas: cyclic strain and cyclic stress approaches.

#### 2.4.3.1 *Cyclic Strain Approach*

The cyclic strain approach is rarely incorporated into a liquefaction initiation evaluation, but the development of strains due to pore pressure generation are closely related, and so the approach merits brief consideration. Liquefaction evaluation procedures were developed by Dobry and Ladd (1980), Dobry et al. (1982, 1984), and Vasquez-Herrera and Dobry (1988), but these procedures are not usually utilized due to the difficulty in predicting strains accumulated from seismic loading with any accuracy in a soil profile (Seed, 1980).

#### 2.4.3.2 *Cyclic Stress Approach*

The cyclic stress approach is conceptually quite simple: the earthquake-induced loading, expressed in terms of cyclic shear stresses, is compared with the liquefaction resistance of the soil, also expressed in terms of cyclic shear stresses. At locations where the loading exceeds the resistance, liquefaction is expected occur (Kramer, 1996). This process is performed by determining the earthquake-induced loading (cyclic stress ratio (CSR)) and the resistance of the soil to liquefaction (the cyclic resistance ratio (CRR)), and then comparing the two ratios to determine the factor of safety against liquefaction ($FS_L$). The determination of $FS_L$ can be seen in Equation 2-1:

$$FS_L = \frac{\tau_{cyc,L}}{\tau_{cyc}} = \frac{CRR}{CSR} \tag{2-1}$$

where the $\tau_{cyc,L}$ is the cyclic shear stress required to initiate liquefaction and $\tau_{cyc}$ is the equivalent cyclic shear stress induced by earthquake loading.

CSR is the representation of the earthquake-induced shear stresses that a given soil will experience. The actual seismic loading from an earthquake is impossible to consistently predict accurately, so correlations between ground motion parameters, pore pressure generation, and initial stress conditions are used to estimate an equivalent shear stress loading scenario. The CRR is usually determined through some correlation with the results of an in-situ test procedure. The results of the field testing are correlated to the resistance of the tested soil against earthquake ground motions.

Models have been developed to compute $FS_L$ by computing CSR and CRR for different in-situ tests including the cone penetration test (CPT) (Douglas et al., 1981; Robertson and Campanella, 1985; Seed and De Alba, 1986; Mitchell and Tseng, 1990; Martin, 1992; Kayen et al., 1992; Carraro et al., 2003; Bazier et al., 2004; Ku et al., 2004; Andrus et al., 2004, Moss et al., 2006); the shear wave velocity test (Tokimatsu et al., 1991; Finn, 1991; Kayen et al., 1992, Stokoe et al., 1998; Suzuki et al., 2004; Andrus et al., 2004); the dilatometer index (Marchetti, 1982; Robertson and Campanella, 1986; Reyna and Chameau, 1991); and the standard penetration test (SPT) (Seed et al., 1983, 1985; Youd et al., 2001; Cetin et al., 2004; Idriss and Boulanger, 2008). SPT-based methods are the most widely used procedures, though CPT methods are gaining popularity. Only the SPT procedure is reviewed in this thesis.

The SPT-based CRR procedures have been popular in practice due to how widespread the SPT is used for site characterization. Additionally, the factors that tend to increase liquefaction resistance (density, overconsolidation ratio, lateral earth pressures, seismic history, and time under sustained pressure) also tend to increase SPT resistance (Kramer, 1996). Today, there are three deterministic models that are typically used to assess liquefaction initiation: Youd et al.,

2001; Cetin et al., 2004; and Idriss and Boulanger, 2008. The following section will outline the Idriss and Boulanger (2008) procedure.

### 2.4.4 SPT-Based Evaluation of Liquefaction Initiation (Idriss and Boulanger, 2008)

The Idriss and Boulanger (2008) procedure follows the general form of Equation 2-1. The CSR and CRR need to be computed, and then the $FS_L$ can be determined. The soil profile is broken into discrete layers, based on soil type, and the $FS_L$ is determined for each layer. Generally the $FS_L$ is then plotted against depth to graphically represent liquefaction initiation potential.

Originally, research from Seed and Idriss (1967) suggested that the CSR is equal to 65% of the maximum shear stress ratio, denoted here as $CSR_{M,\sigma_v'}$ to indicate a specific moment magnitude and in-situ vertical effective stress, and is represented in Equation 2-2:

$$CSR_{M,\sigma_v'} = 0.65\frac{\tau_{\max}}{\sigma_v'} \tag{2-2}$$

where $\sigma_v$' is the total vertical stressand $\tau_{max}$ is the maximum induced shear stress

Due to the difficulties in determining $\tau_{max}$, the maximum shear stress can be estimated as a function of the total vertical stress $\sigma_v$, the maximum horizontal acceleration $a_{max}$, and the shear stress reduction parameter $r_d$. Incorporating this into Equation 2-2, the equation becomes:

$$CSR_{M,\sigma_v'} = 0.65\frac{\sigma_v}{\sigma_v'}\frac{a_{\max}}{g}r_d \tag{2-3}$$

The $a_{max}$ can be found through a seismic hazard analysis (SHA) using aground motion predictive equation in a deterministic approach, or through the USGS Interactive Deaggregation Tool (USGS, 2008). The shear stress reduction parameter, $r_d$, can be found through a variety of procedures, but Idriss and Boulanger (2008) recommend the procedure proposed by Idriss (1999) using Equation 2-4.

$$r_d = \exp[\alpha(z) + \beta(z) \cdot \mathrm{M}] \tag{2-4}$$

Where

$$\alpha(z) = -1.012 - 1.126 \sin\left(\frac{z}{11.73} + 5.133\right) \tag{2-5}$$

$$\beta(z) = 0.106 + 0.118 \sin\left(\frac{z}{11.28} + 5.142\right) \tag{2-6}$$

To compute the CRR, first the clean sand equivalent SPT resistance, first $(N_1)_{60cs}$ is determined. This correction to the field SPT resistance (N) accounts for hammer energy, confining pressure, and fines content, and is computed as:

$$(N_1)_{60cs} = (N_1)_{60} + \Delta(N_1)_{60} \tag{2-7}$$

Where

$$\Delta(N_1)_{60} = \exp\left(1.63 + \frac{9.7}{FC + 0.01} - \left(\frac{15.7}{FC + 0.01}\right)^2\right) \tag{2-8}$$

$$(N_1)_{60} = C_N C_E C_R C_B C_S N_m \tag{2-9}$$

Where $C_N$ is the overburden correction factor, $C_E$ =$ER_m$/60% ($ER_m$ is the measured value the free fall energy), $C_R$ is the rod correction factor, $C_B$ is the correction for nonstandard bore diameters, $C_S$ is the correction for using split spoons without liners, and $N_m$ is the measured field blow count. $C_R$ is determined based on Table 2-1, and $C_B$ and $C_S$ are typically 1.0. $C_N$ can be more difficult to determine. The *m* required to determine $C_N$, seen in Equation 2-10, requires $(N_1)_{60cs}$. But $C_N$ needs to be computed to find $(N_1)_{60}$. Therefore, $(N_1)_{60cs}$ needs to be solved for iteratively, which can be easily done in a spreadsheet.

**Table 2-1: Short Rod Correction Factor (after Idriss and Boulanger, 2008)**

| Rod Length | $C_R$ |
|---|---|
| < 3m | 0.75 |
| 3-4 m | 0.80 |
| 4-6 m | 0.85 |
| 6-10 m | 0.95 |
| 10-30 m | 1.00 |

$$C_N = \left(\frac{P_a}{\sigma_v'}\right)^m \leq 1.7 \tag{2-10}$$

In this procedure, the correlation for the CRR was initially determined for a magnitude 7.5 earthquake and $\sigma'_v$ of one atmosphere, which is symbolized as $CRR_{M=7.5,\sigma'_v=1}$. This can be determined with Equation 2-12 using the $(N_1)_{60cs}$ determined previously.

$$m = 0.784 - 0.0768\sqrt{(N_1)_{60cs}} \tag{2-11}$$

$$CRR_{M=7.5,\sigma'_v=1} = \exp\left(\frac{(N_1)_{60cs}}{14.1} + \left(\frac{(N_1)_{60cs}}{126}\right)^2 - \left(\frac{(N_1)_{60cs}}{23.6}\right)^3 + \left(\frac{(N_1)_{60cs}}{25.4}\right)^4 - 2.8\right) \tag{2-12}$$

Once the $CRR_{M=7.5,\sigma'_v=1}$ is determined, it can be adjusted to a specific earthquake and effective vertical stress using Equation 2-13.

$$CRR_{M,\sigma'_v} = CRR_{M=7.5,\sigma'_v} \cdot MSF \cdot K_\sigma \tag{2-13}$$

Where the MSF is the magnitude scaling factor recommended by Idriss (1999) used to adjust the CRR to the anticipated earthquake, and $K_\sigma$ is the overburden correction factor developed by Boulanger (2003) to relate the sands state parameter to that of an equivalent clean sand. The equation to determine MSF can be seen in Equation 2-14, and that for the $K_\sigma$ in Equation (2-15).

$$MSF = 6.9 \cdot \exp\left(\frac{-M}{4}\right) - 0.058 \quad \leq 1.8 \tag{2-14}$$

$$K_\sigma = 1 - C_\sigma \ln\left(\frac{\sigma_v^{'}}{P_a}\right) \leq 1.1 \tag{2-15}$$

Where

$$C_\sigma = \frac{1}{18.9 - 2.55\sqrt{(N_1)_{60cs}}} \leq 0.3 \tag{2-16}$$

Once the $CSR_{M,\sigma_v^{'}}$ and $CRR_{M,\sigma_v^{'}}$ have been computed the $FS_L$ can be found utilizing Equation 2-17.

$$FS_L = \frac{CRR_{M,\sigma_v^{'}}}{CSR_{M,\sigma_v^{'}}} \tag{2-17}$$

By plotting the $CSR_{M,\sigma_v^{'}}$ and $CRR_{M,\sigma_v^{'}}$ with depth, the layers that are susceptible to liquefaction can be easily identified. An example of this can be seen in Figure 2-8. In general if the $FS_L$ is 1.0 or more then the soil is predicted to not experience liquefaction.

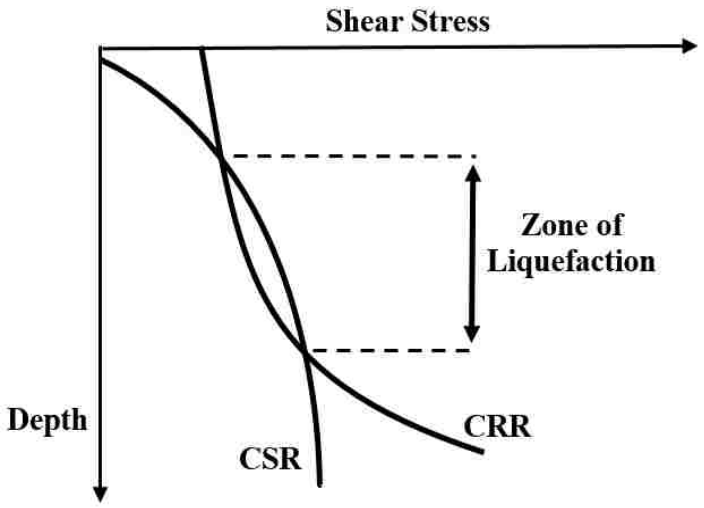


**Figure 2-8: Example of Plotting CSR vs CRR with Depth (after Kramer, 1996)**

## 2.5 Liquefaction Effects

Liquefaction has many physical manifestations, which can be very destructive to both natural and man-made structures. Once a site has been identified to have a potential liquefaction hazard, the type and extent of the effects of liquefaction should be considered. Baska (2002) identified the most significant liquefaction effects as the alteration of ground motions, ground surface settlements, loss of bearing capacity, increased lateral pressure on walls, flow failures, ground oscillation, and lateral spread. Though each of these can have serious consequences, the effects that have to do with cyclic mobility are the most pertinent and is briefly considered here.

One of the common effects of liquefaction is the settlement of the liquefied soil after the earthquake. With the generation of excess pore pressures, water will be forced from the pore space to the surface. This results in a denser configuration of the affected soil, and the cumulative change in volumetric strain will be manifest as settlement at the ground surface. This can induce damaging vertical deformations in the vicinity of infrastructure and buried lifelines.

Another effect is the loss of bearing capacity, seen most famously in the 1964 Niigata, Japan, earthquake. The severely reduced shear strength of the soil during liquefaction can reduce the resistance of the soil to the vertical pressure of the building, resulting in a global bearing capacity failure. Additionally, light-weight buried utility structures such as gas tanks or septic tanks can rise to the surface, being less dense than the liquefied soil.

The most important effect of liquefaction to this study is lateral spread displacements. This phenomenon is one of the most pervasive of all earthquake effects and has contributed to significant economic damage in many earthquakes. Lateral spread is the movement of blocks of mostly intact, surficial soil displaced down slope or towards a free face along a shear zone that has formed within the liquefied sediment (Bartlett and Youd, 1995). The horizontal deformations can be as large as 10 m and are devastating to infrastructure and lifelines.

## 2.6 Chapter Summary

Liquefaction is one of the most important, interesting, complex, and controversial topics in geotechnical earthquake engineering (Kramer, 1996). It occurs when excess pore pressures are generated due to the seismic ground shaking of an undrained soil due to an earthquake.

To assess the potential for liquefaction to occur, the susceptibility of a soil needs to be determined. This is accomplished by examining the historic, geologic, compositional, and state criteria of the soil. A soil is generally susceptible to liquefaction if is cohesionless and saturated and has low fines content and a uniform grain size distribution. The initial stress state of a soil will determine its behavior, with loose soils being contractive and dense soils being dilative.

There are two types of liquefaction: flow liquefaction and cyclic mobility. The mechanics of initiation of both of these methods are different. Flow liquefaction will occur if a soil plots above the SSL line (contractive behavior), and will not if plotted below (dilative behavior).

Dense or loose soils can experience cyclic mobility, and will liquefy if cyclic stresses drive the stress path of a soil to the FLS. To evaluate if a soil will undergo liquefaction, the CRR and CSR can be determined with models correlated with in-situ field tests. The CRR is divided by the CSR to find $FS_L$. If the $FS_L$ is greater than one, then the soil is predicted to not liquefy. SPT-based models have been te most widely accepted in engineering practice, and the Idriss and Boulanger (2008) SPT-based liquefaction initiation model was reviewed.

Liquefaction can result in many destructive effects. These effects can be destructive to infrastructure and lifelines and should be considered when performing any liquefaction hazard analysis.

# 3 REVIEW OF LATERAL SPREAD

## 3.1 Introduction

The term lateral spread describes the permanent horizontal deformations of a site located on sloping ground or near a free-face due to seismically induced soil liquefaction. These deformations can range from just a few millimeters to, in some cases, more than 10 meters (Coulter and Migliaccio, 1966) of horizontal movement. Structures located near rivers and open bodies of water are particularly at risk because the greatest displacements occur near free faces.

This chapter outlines the development of contemporary lateral spread theory and the mechanics that describe the process. Analytical and empirical methods used to predict lateral spread displacements is briefly introduced, and the procedures most commonly used today are described in depth. It should be noted that lateral spread displacements only occur where and when liquefaction occurs so, if liquefaction does not result from earthquake shaking, then lateral spread will not occur.

## 3.2 Understanding Lateral Spread Displacements

### 3.2.1 Historic Lateral Spread Examples

The phenomenon of lateral spread is one of the most damaging of all earthquake effects, and has resulted in significant economic losses throughout the world. In the great 1906

earthquake in San Francisco, California, lateral spreading destroyed buildings, bridges, and roads. However, the greatest damage came from the shearing of pipelines preventing firefighters from extinguishing fires caused by the earthquake (Youd and Hoose, 1978). In the 1964 earthquake in Prince William Sound, several coastal communities were severely damaged by lateral spread, with the city of Valdez experiencing such large displacements that the entire city was relocated (Coulter and Migliaccio, 1966). A large earthquake struck the same year in Niigata, Japan with lateral spread displacements causing the banks of the Shinano River to move as much as 10 meters into the river channel, severely damaging facilities along the waterfront (Hamada et al., 1986). More recently in the 1989 Loma Prieta earthquake, the Moss Landing Marine Laboratory was damaged beyond repair due to lateral displacements at the site over one meter (Boulanger et al., 1997). These example,s as well as similar effects in other earthquakes, have resulted in a significant amount of research into understanding and quantifying the likelihood and extent of lateral spreading.

### 3.2.2 Experimental Studies of Lateral Spread

Lateral spread is an extremely complicated process, and predicting the extent of permanent lateral deformations is an extremely difficult non-linear problem. Because the mechanics behind the process are not well understood or easily quantifiable, researchers have conducted several different types of laboratory experiments to attempt to understand the process. Through each study, greater insight into the fundamental process has been discovered, and the governing mechanics of the phenomena are slowly being revealed.

#### *3.2.2.1 Shake Table Testing*

Shake tables are used to simulate ground shaking and have often been utilized to perform experiments to liquefy sands. Test specimens are placed on the table, and then the specimen is vibrated by a harmonic wave to achieve a target acceleration value. These shake tables can be as large as several meters across and can accommodate quite large sample preparations.

Though shake table testing has been performed for over 60 years and continues today, two experiments in particular were important in characterizing lateral spread. The first of these was performed at the Kanazawa University in Japan by Miyajima et al. (1991). This experiment used boxes of sand stratum with slopes of 2, 4, and 6 percent and thicknesses of 15, 17, and 19 cm. Sixteen pins were placed on the surface of the sand, and their relative displacement was measured after the sample was vibrated for 30 seconds. Relationships between average displacement, duration of soil liquefaction, velocity of ground deformation, thickness of sand layer, and slope of sand layer were developed. Based on these relationships, the researchers concluded that the extent of lateral spread was most closely correlated to the thickness of the liquefiable layer and the slope of the surface.

The second experiment was conducted by Sasaki et al. (1991). In their experiment, samples with three layers were fashioned, with the top layer being dense gravel, the middle layer being loose sand, and the bottom layer being dense sand. After performing eight tests, the researchers concluded that the greatest displacements occurred near the bottom of the liquefied layer, and that lateral displacements were only observed when the shaking occurred.

#### *3.2.2.2 Centrifuge Testing*

Centrifuge testing has been used to model seismically-induced liquefaction since the 1970s in Cambridge University in England. The procedure is used to simulate gravity-induced stresses in soil deposits at a reduced geometrical scale through centrifugal loading. Conceptually, the technique consists of increasing the confining environment in the model soil, so that the confining stress is identical in both model and prototype at similar points. Though this procedure can be advantageous in that small models can be used, unlike the large models utilized for shake table testing, scaling effects can be a major concern.

In the 1990s a group of universities came together to verify and evaluate numerical techniques with laboratory testing performed in centrifuges. This project was called the Verification of Liquefaction Analysis by Centrifuge Studies (VELACS), and the testing was performed by nine different universities across the world (Propescu and Prevost, 1995). Nine different sample configurations were proposed, with each university performing the primary experiment on one configuration and then two others attempting to duplicate the results. Of the nine configurations, the second had a sloping profile and was useful in furthering lateral spread theory. For the second model, the primary experiment was performed by the Rensselaer Polytechnic Institute, with the California Institute of Technology and the University of California, Davis. The results of the three tests were found to be relatively similar, and all came to a similar conclusion. The researchers concluded that the lateral spread displacements were correlated less with the loading conditions, and more with the geometry of the soil layering and composition of the soil.

In 1997, the University of California, Davis conducted some centrifuge testing to quantify the effectiveness of liquefaction remediation techniques and to optimize the volume of

soil to be treated (Balakrishnan et al., 1997). Five series of tests were performed, with the fifth (referred to as BAM05) being of the most significance to lateral spread. This test consisted of three layers of soil; the bottom layer consisting of sand at 80% relative density, the middle layer of sand at 50% relative density, and the surface layer of a thin layer of overconsolidated clay (OCR=3). The test specimen was subjected to six different ground motions recorded at Port Island during the 1995 Kobe earthquake in Japan. The results of the experiment show that downslope spikes in pore pressure corresponded with upslope spikes in acceleration.

In each of the previous centrifuge experiments, lateral spread characterization was not the primary research objective. However, in 1998, Toboada-Urtuzuastegui and Dobry (1998) conducted 11 experiments to model earthquake-induced lateral spread in sand at the Rensselaer Polytechnic Institute. These researchers recognized that the maximum lateral ground displacements were a function of soil density, penetration resistance, ground surface geometry, thickness of the liquefied layer, and the duration and intensity of ground shaking. The research focused on loose sand, which was the source of most of the problems in the field. The experiment was performed in a state-of-the-art flexible wall laminar container that could approximate a continuous shear strain field and accommodate possible shear strain concentrations. The research yielded several important conclusions. As the slope increased, the pore pressures decreased or remained constant. Additionally, as the slope increased, the shear strain and permanent lateral deformation increased as well. The researchers also noted that, as the maximum acceleration was increased, the permanent shear strain and lateral displacement increased. It was also observed that, as the input frequency increased, the pore pressures and the permanent lateral displacements decreased. Lastly, as with the BAM05 tests, they noticed that downslope spikes in pores pressure corresponded with spikes in acceleration and strain

deformations. The sand would dilate under the accumulating shear strains, which would be followed by an immediate decrease in the pore pressures. The accelerations would then spike as the ground densified and the accelerations were no longer filtered out by the liquefied sand.

#### *3.2.2.3 Small Scale Laboratory Tests*

Other studies were conducted with smaller scale laboratory testing equipment. Experiments performed using undrained torsional tests (Yasuada et al., 1994; Shamoto et al., 1997), undrained triaxial tests (Nakase et al., 1997), and undrained cyclic direct simple shear tests (Wu, 2002) were conducted and confirmed many of the conclusions that were presented through the previous experiments. Of note is the conclusion of the testing performed by Wu (2002). He saw that the direction of the loading in some samples resulted in different behavior of the soil. When loaded in one direction the sample would experience cyclic mobility, and in the other it would experience flow liquefaction. He concluded that the directivity of the ground motions could affect the behavior of the liquefied soil.

### 3.2.3 Summary of Lateral Spread Theory

Based on the observations from the experiments performed to understand the mechanics of lateral spread displacements, several conclusions can be reached. First, lateral spread can occur where the soil is located at a site with sloping ground or near to a free face. The lateral displacements generally only occur where there is a layer of liquefiable soil at or near the surface. Second, the extent of the permanent lateral displacements seems to be strongly correlated with the thickness of the liquefiable layer, the density or resistance of the layer, the intensity and duration of the accelerations at the ground surface, and the geometry of the soil layering and ground surface. The greater the slope, the accelerations, or the thickness of the

layer, the greater the potential lateral displacement. Conversely, the greater the soil density or resistance, the smaller the predicted displacements. Third, the lower the frequency of the shaking, the higher the observed displacements, and the higher the accelerations, the greater the observed displacements. Therefore ground motions with low frequency and high accelerations could cause greater permanent lateral deformations. Lastly, as shear strains accumulate in sand, the soil tends to dilate, resulting in a drop in pore pressure and a spike in acceleration. This results in a complicated cycle of phase transformation and downslope movement, which makes modeling and simulating lateral spread behavior an extremely difficult challenge.

## 3.3 Analytical and Empirical Methods for Predicting Lateral Displacements

To quantify and predict the magnitude of lateral spread displacements, several different procedures have been developed by researchers. These procedures are generally divided into two different categories: Analytical Methods and Empirical Methods. Analytical methods are developed using the current understanding of the underlying mechanics behind soil behavior and general scientific knowledge. Empirical methods use large databases of earthquake case histories to regress predictive equations. Both approaches are briefly discussed, with common procedures reviewed more in depth in later sections. Some procedures incorporate both analytical and empirical procedures, often referred to as semi-empirical methods, but this method will not be directly addressed in this thesis.

### 3.3.1 Analytical Methods

Analytical methods are developed from the current understanding of soil mechanics and fundamental science. These methods typically involve closed-form mathematical solutions. Though there are several types of analytical methods that have been used to predict lateral

displacements, three in particular are reviewed for this study: Numerical Models, Elastic Beam Model, and Newmark Sliding Block Analysis.

#### *3.3.1.1 Numerical Models*

Numerical models are created by representing a system with a two- or three-dimensional mesh of nodes and elements. The displacement or force at each node is then solved for. There are generally two types of numerical models, finite element and finite difference. Finite element modeling is a numerical technique for finding approximate solutions to boundary value problems for partial differential equations. It discretizes the system into elements and develops a system of equations relating to forces and displacements at each node, which are then solved directly. The finite difference method approximates the solution to differential equations using simplified equations to approximate derivatives. Both procedures can be used on fairly complex systems and can account for many important soil parameters. These methods require a constitutive model based on soil mechanics and stress-strain behavior in soils. This does present a challenge to numerical modelers due to the complexity of soil mechanics and the uncertainty in the residual strengths and stress/strain behavior of liquefied soil.

Numerical methods also require computers for all but the most simplified models. This limited the application and usefulness of numerical methods for larger more complex systems until access to computers became more available. Starting in the latter part of the 1970s, researchers developed some early finite element models (Zienkiewicz et al., 1978; Zienkiewicz and Shiomi, 1984; Finn et al., 1986; Shiomi et al., 1987) that gradually became more sophisticated and accurate as advances in understanding fundamental soil mechanics were made. More modern models (Gu et al., 1994; Yang, 2000; Yang et al., 2003; Arduino et al., 2006;

Valsamis et al., 2010; Zhang and Wang, 2012) have become increasingly advanced and accurate and are becoming prevalent in all aspects of research that is conducted today. The potential for numerical modeling is enormous, as the sophistication of constitutive models can increase with increasing computational power of computers. The capability of numerical models to represent increasingly complicated systems and mechanical relationships will result in these methods becoming ubiquitous in research.

#### *3.3.1.2 Elastic Beam Model*

An additional analytical method is the elastic beam model. It was originally proposed by Hamada et al. (1987) as a method of predicting permanent displacements. These researchers attempted to predict the permanent displacements that were measured around the Maeyama Hills south of Nishiro City, Japan, during the magnitude 7.7 earthquake that struck there in 1983. They proposed a method that was simple because the area affected was too large for complicated and sophisticated analyses. Their procedure revolved around treating the soil layering like a board floating on water. The unsaturated surface soil layer would be the board, with its movement controlled by gravity and the boundary conditions affecting it. This layer would be floating on top of a liquefied soil layer, and there would be no friction between layers. This method would come to be known as the elastic beam model. Further research was conducted by co-authors of the original paper (Towhata et al., 1991; 1992; Yasuda et al., 1991), but little additional research beyond this has been performed.

#### *3.3.1.3 Newmark Sliding Block Analysis*

This procedure was proposed by Newmark (1965) during the 5th Rankine Lecture in London. This method consists of a block representing a soil mass on an inclined plane, with the only resistance to the block sliding down the plane coming from the friction between the block and plane. When sufficient external force is introduced, the driving force on the block will overcome the frictional force and the block will slide down the slope. This procedure was originally designated for seismic slope stability, but several researchers incorporated the process into predictive models to estimate lateral spread displacements (Dobry and Baziar, 1991; Byrne, 1991; Byrne et al., 1992; Baziar et al., 1992; Toboada et al., 1996). More recently Olson and Johnson (2008) used 39 lateral spread case histories and back calculated mobilized strength ratios using the Newmark sliding block method to develop a predictive lateral spread model. Others (Saygili and Rathje, 2008; Bray and Travarasou, 2007) have developed simplified semi-empirical models to predict seismic slope displacements and have used them to predict lateral spread displacements. Some caution should be observed when using these procedures to predict lateral displacements. These models were developed within specified bounds and extrapolation outside these bounds should be avoided.

### 3.3.2 Empirical Methods

Empirical methods are developed through a statistical process referred to as multi-linear regression (MLR) where data from earthquake case histories is used to develop a predictive relationship between lateral deformations and some quantifiable soil parameters. These models are developed independently of soil mechanics, and only the factors that reduce error in the regression are incorporated into the predictive equation. Though these empirical methods are not

based on any fundamental soil theory, because they are developed with large databases of actual earthquake data, they have found wide audience with engineering practitioners.

One issue with the empirical relationships is that the data used in the regression needs to accurate and of the highest quality possible, which may be difficult to accurately measure and quantify after an earthquake. If the data is not accurate then the regression will not provide a reliable relationship. Additionally, many of the empirical models are developed from earthquake data from Japan and the Western United States and so may not capture all the possible permutations of earthquake deformation failures everywhere. The last issue is that each model has a range of values that are acceptable for the input variables, as well as range of acceptable predictions of lateral spread displacements. Using soil parameters outside the recommend range can result in extrapolated results that do not correctly represent the relationship developed by each procedure.

Despite their limitations, empirical methods are used in practice almost universally. The predictive equations are simple to use and can be easily programmed into a spreadsheet. The implementation of the models does not require an in depth knowledge of the underlying soil mechanics theory or how the relationship was developed. While this does present some concerns about using the equations improperly, proper training and experience can reduce this possibility.

### 3.4 Deterministic Procedures for Estimation of Displacements Using Empirical Models

To gain a greater understanding of the history and development of the MLR empirical models, a few of the early, important historical models are examined. Following this several of the more modern procedures are described. Then three of the most commonly used empirical models are described in detail.

### 3.4.1 Early Empirical MLR Models

One of the earliest MLR models was developed by Hamada et al. (1987). This model considered data of permanent ground deformations from the 1983 Nihonkai-Chubu and 1964 Niigata earthquakes, as well as from the 1971 San Fernando earthquake. The regressions considered slope of the ground surface, orientation of soil stratigraphy, and thickness of the liquefiable layer and developed a simple relationship with lateral spread, the thickness of the liquefied layer, and the ground slope. The equation is fairly accurate, with 80% of the predicted displacements within a factor of two of the actual displacements. The model did have issues when predicting displacements in areas outside these three earthquakes. Notably, this model only requires two parameters so it is clear that other soil parameters also affect lateral spread.

Taking a slightly different approach, Youd and Perkins (1987) used lateral displacements from several case histories in the Western US and defined a term called the Liquefaction Severity Index (LSI). This value describes the maximum lateral displacement that could occur on wide active flood plains, deltas, or other areas of gently-sloping Holocene fluvial deposits. The relationship for LSI included the magnitude of the event and the distance from the earthquake to the site. Though it was used to predict lateral spread, it was also created as method to characterize the potential hazard of a location and was utilized in the production of hazard maps for southern California. The method was shown to be slightly more accurate than the Hamada et al. (1987) model, but failed to take into account any soil properties or site geometry.

Bartlett and Youd (1992, 1995) used a large database of lateral spread case histories from Japan and Western US to develop an MLR empirical relationship of lateral displacement with 476 displacement vectors and a number of source and site parameters. The database included source-site distances of up to 90 km and a range of magnitudes from 6.4 to 9.2. The regression

identified the source and site factors that most strongly influenced lateral ground deformations. Additionally, the researchers developed two equations for different site geometry: one for sites near a vertical or steep free-face, and one for gently sloping ground. Analyses of this procedure show that 90% of the predicted displacements were within a factor of 2 from the observed values. This accuracy, as well as the more comprehensive consideration of contributing factors to lateral spread, resulted in this procedure becoming the most widely used lateral spread predictive model, and is still used widely in practice today. The model was not without its flaws though. The model was very sensitive to source-site distance and for locations near to a seismic source the model often severely over predicted displacements. Additionally, due to lack of information in the case histories, approximate values of some of the parameters needed to be estimated which increased the uncertainty in the regression.

Using the same database compile by Bartlett and Youd (1995), Bardet et al. (1999) developed a four-parameter model to estimate lateral displacements over relatively large areas. The researchers separated the database into a data set that included all case histories, and then a data set that only included case histories with displacements two meters or less. Using MLR they developed predictive equations for both data sets. The Bardet et al. (1999) model does not incorporate site specific soil information, outside the thickness of the liquefied layer, and its predicted results can vary significantly from the Bartlett and Youd (1995) results for the same soil profile.

Research by Rauch and Martin (2000) developed an additional MLR model called the Empirical Prediction Of Liquefaction-induced Lateral Spreading (EPOLLS). This model incorporated a range of equations with increasing accuracy; regional-EPOLLS, site-EPOLLS, and geotechnical-EPOLLS. The equations were regressed from 71 lateral spread case studies

from 15 different earthquakes occurring from 1906 to 1994. This model deviated from the previous models in that the equations predicted average displacements across the surface of a site. Each of the models require an increasing amount of information, from the least accurate, regional-EPOLLS, needing only seismological parameters, while the most accurate, geotechnical-EPOLLS, requires seismological, topographical, geometrical, and geotechnical parameters. Due to the range of displacements used in this regression, this model has a slightly lower accuracy than previous models (70%) but the overall the predictions are within ± 0.75 m 71% of the time.

### 3.4.2 Recent Empirical MLR Procedures

Zhang et al. (2004) were the first researchers to incorporate CPT as well as SPT field results into their lateral spread model. They used cyclic simple shear test data on clean sand from Ishihara and Yoshimine (1992) and research on shear behavior of sands from Seed (1979) to develop correlations of factor of safety against liquefaction and relative density with maximum shear strain for a clean sand. Their model uses the SPT and CPT field results to predict the relative density to then find factor of safety against liquefaction for discrete layers over the soil profile. Then the maximum shear strain is correlated from the factors of safety and the integrated with depth to produce a value they defined as the lateral displacement index (LDI). They then correlated LDI with actual lateral displacements from earthquake case histories to develop predictive equations to estimate lateral spread as a function of LDI and site geometry. This model is referred to as semi-empirical because it incorporates soil mechanics behavior with statistical regressions. The researchers developed these equations using case histories that were found to represent three site conditions: gently sloping ground without a free face, gently sloping ground with a free face, and nearly level ground with a free face. The database for regressing the

SPT equations appears to be sufficiently large, containing information from earthquakes in the Western US, Alaska, and Japan, with 207 case histories. The database used for the CPT equations was not as extensive with 59 case histories, and so engineering judgment should be used when interpreting the results. An additional issue with the model is that the uncertainty was not provided and so it cannot be incorporated into a probabilistic framework.

Zhang and Zhao (2005) recognized that previous MLR models did not have the capability to incorporate different tectonic sources or fault mechanics. They recognized that MLR model researched by Youd et al. (2002) was regressed using earthquake case histories with a wide range of fault types and mechanics (subduction zone, normal, strike-slip). This lead to considerable scatter in the database, and to attempt to reduce some of the scatter they developed modification factors incorporating these parameters. Incorporating two attenuation models (Zhao and Zhang, 2002; Youngs et al., 1997) to develop the modification factors, they regressed new predictive equations using the Youd et al (2002) and the 1999 Kocaeli Turkey earthquake. Comparison of displacements predicted by their model appear to agree with observed displacements in the Kocaeli earthquake, but only four locations were tested. This model was updated in 2012 (Zhang et al., 2012) to include additional earthquakes and be applicable to a wider range of seismic regions.

Faris et al. (2006) also developed as semi-empirical model that differs from those previously in a few respects. They do not define site geometry in the same way as previous models, instead developing a universal variable "$\alpha$" which provided a ratio between the shear stress in the soil with the vertical effective stress. Their approach was similar to Zhang et al. (2004) in that they both incorporate a cumulative strain across the soil profile, but differ in how the shear strain is predicted. Using strain potential curves by Wu (2002), they used Bayesian

statistics to account for uncertainty in the strain data as well as in the case histories. They developed a new parameter they called the Displacement Potential Index (DPI) which they used develop the predictive equations. Similar to Zhang et al. (2004) the researchers did not provide any estimates of uncertainty so this particular model is not able to be incorporated into a probabilistic framework.

### 3.4.3 Youd et al. (2002) Procedure

Bartlett and Youd (1992, 1995) developed a procedure to estimate lateral spread displacements that incorporated a wider range of factors then previous models. They believed that a more comprehensive empirical model should contain: earthquake factors (PGA, duration, $M_w$, R), topographical factors (ground slope, distance/height of free face), geological factors (thickness and depth to liquefied layer), and soil factors (residual strength, mean grain size, fines content). They complied case history data from 448 horizontal displacement vectors from eight earthquakes (1906 San Francisco, 1964 Alaska, 1964 Niigata, 1971 San Fernando, 1979 Imperial Valley, 1983 Borah Peak Idaho, 1983 Nihonkai-Chubu, and 1987 Superstition Hills). They divided the case histories into two categories, those with gently sloping ground and those near a free face. Using these site geometry conditions, as well as all available soil properties (including SPT blow counts for resistance) and seismic loading conditions, they used MLR to determine the combination of variables that would minimize the regression coefficient ($R^2$). In Youd et al. (2002) this model was updated in several ways. Among them, they removed incorrect measures of ground displacement from the 1983 Nihonkai-Chubu earthquake, added new case histories from the 1983 Borah Peak Idaho, 1989 Loma Prieta, and 1995 Hyogo-Ken Nanbu (Kobe) earthquakes, and changed the form of the equation to include an $R^*$ term to prevent the

prediction of unrealistic ground displacements when R becomes small. The model was regressed again in a stepwise MLR procedure and the regression coefficients were re-determined.

To perform the Youd et al. (2002) procedure, first the geometry of the site needs to be characterized as either having a free-face, or being gently sloping. If a site is characterized by a free-face and gently sloping ground then both conditions should be assessed with the larger of the two predicted displacements governing. Figure 3-1 provides an aid in characterizing the site and determining the site geometry factors.

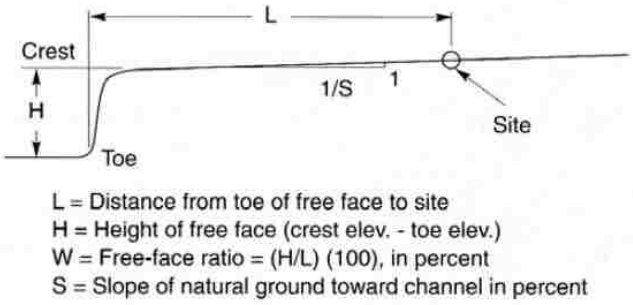


**Figure 3-1: Determination of Site Geometry for Empirical MLR Equation (after Bartlett and Youd, 1992)**

Once the site geometry is characterized then the median lateral displacement can be estimated using Equation 3-1. Terms used in the equation are defined as follows: $D_H$ = median computed lateral spread displacement in meters; M = earthquake moment magnitude; R = horizontal distance to the nearest seismic energy source or nearest fault rupture in kilometers; W = free-face ratio in percent; S = ground slope in percent; $T_{15}$ = the cumulative thickness (in the upper 20 meters) of all saturated soil layers with corrected SPT blowcounts (ie $(N_1)_{60}$) less than 15 blows/foot in meters; $F_{15}$ = the average fines content of the soil comprising $T_{15}$ in percent; and $D50_{15}$ = the average mean grain size of the soil comprising $T_{15}$ in millimeters. The $R^*$ term can

be computed using Equation 3-2. Regression coefficients for both the free-face and ground slope cases can be seen in Table 3-1.

$$\overline{\log D_H} = b_0 + b_1 M + b_2 \log R^* + b_3 R + b_4 \log W + b_5 \log S + b_6 \log T_{15} + b_7 \log\left(100 - F_{15}\right) + b_8 \log\left(D50_{15} + 0.1\right) \quad (3\text{-}1)$$

$$R^* = R + 10^{0.89M - 5.64} \quad (3\text{-}2)$$

**Table 3-1: Regression Coefficients for the Youd et al. (2002) MLR Model (after Youd et al., 2002)**

| Model | $b_0$ | $b_1$ | $b_2$ | $b_3$ | $b_4$ | $b_5$ | $b_6$ | $b_7$ | $b_8$ |
|---|---|---|---|---|---|---|---|---|---|
| Ground slope | -16.213 | 1.532 | -1.406 | -0.012 | 0 | 0.338 | 0.540 | 3.413 | -0.795 |
| Free Face | -16.713 | 1.532 | -1.406 | -0.012 | 0.592 | 0 | 0.540 | 3.413 | -0.795 |

**Table 3-2: Recommended Range of Parameters for the Youd et al (2002) Procedure (after Youd et al., 2002)**

| Variable | Range |
|---|---|
| D | 0 to 6.0 |
| M | 6.0 to 8.0 |
| R (km) | 0.2 to 100 |
| W (%) | 1 to 20 |
| S (%) | 0.1 to 6 |
| $T_{15}$ (m) | 1 to 15 |
| $Z_T$ (m) | 1 to 10 |

It should be noted that the researcher from Bartlett and Youd (1992, 1995) and Youd et al. (2002) recommended limitations on the variables entered into Equation 3-1 to ensure that the resulting displacement is not extrapolated outside the model bounds. Table 3-2 and Figure 3-2 show the recommend range for these variables, and Figure 3-3 shows a recommended flowchart

for utilizing the model. Introduced in Table 3-2 is the $Z_T$ term, which is defined as the depth to the top of the liquefiable layer in meters.

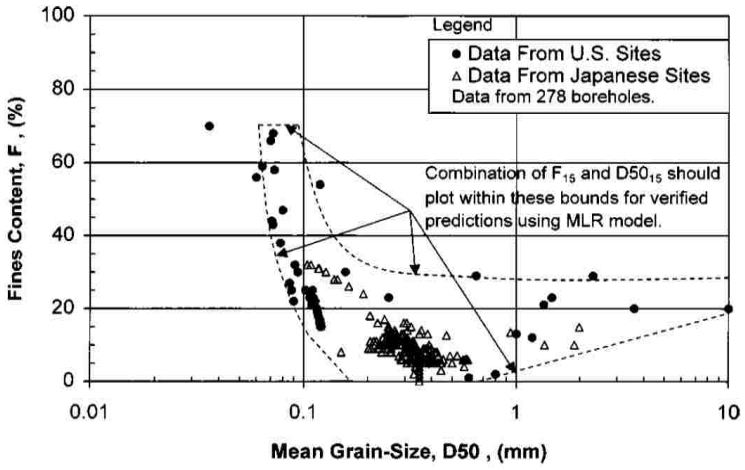


**Figure 3-2: Compiled Grain-Size Data with Ranges of $F_{15}$ and $D50_{15}$ for Use with the Youd et al (2002) Procedure (after Youd et al., 2002)**

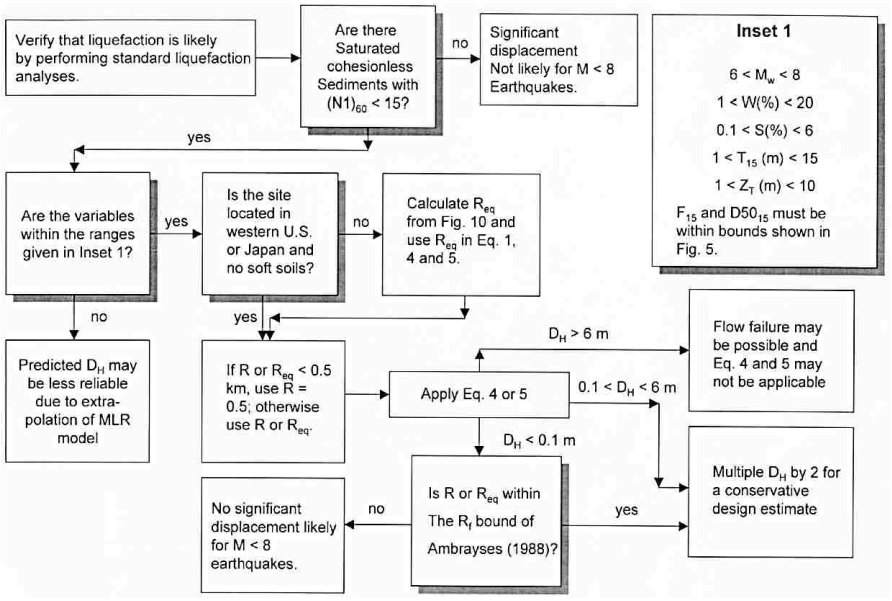


**Figure 3-3: Flow Chart for Application of the Youd et al (2002) Procedure**

### 3.4.4 Bardet et al. (2002) Procedure

Bardet et al. (1999) recognized that lateral spread displacements are not just confined to a few isolated locations, but can extend over areas as large as several square kilometers. The widespread effect can be particularly damaging to spatially distributed lifelines. In Bardet et al. (2002) the researchers developed a four-parameter MLR model that eschews most soil parameters and focuses more on the seismic loading and site geometry characteristics. They emphasize that their model is most appropriate for developing first-order approximations of the amplitude of the liquefaction-induced ground deformations over large areas.

The four-parameter MLR model was regressed essentially with the same database collected and utilized by Bartlett and Youd (1992). One of the major differences between the two models is that the Bardet et al. (2002) model divides up the earthquake case histories to develop two predictive relationships. They created one equation for all displacements (designated as Data Set A), and then developed a second only using case history data with displacements 2 meters or less (designated Data Set B). Additionally, they do not use the $F_{15}$ and $D50_{15}$ terms from the Youd et al. (2002) model. The researchers believed these variables were difficult to obtain from borehole data and determine over a large area, as well as the variables having the largest uncertainties of all the variables in the Youd et al. (2002) model. The four-parameter model is divided into two categories based on whether or not they were regressed with Data Set A or B, being referred to as FFGS-A and FFGS-B respectively. Specifying site geometry is done by selecting the appropriate regressions coefficients for the site condition (free-face or ground-slope).

Predictions of lateral spread displacements using the four-parameter MLR model can be found using Equation 3-3. Terms used in the equation are defined as follows: D = median

computed lateral spread displacement in meters; M = earthquake moment magnitude; R = horizontal distance to the nearest seismic energy source or nearest fault rupture in kilometers; W = free-face ratio in percent; S = ground slope in percent; and $T_{15}$ = the cumulative thickness (in the upper 20 meters) of all saturated soil layers with corrected SPT blowcounts (i.e. $(N_1)_{60}$) less than 15 blows/foot in meters. Regression coefficients for the FFGS-A and FFGS-B can be seen in Table 3-3 for FFGS-A and Table 3-4 for FFGS-B. .

$$\log(D+0.01) = b_0 + b_{off} + b_1 M + b_2 \log(R) + b_3 \log(W) + b_4 \log(S) + b_6 \log(T_{15}) \quad (3\text{-}3)$$

**Table 3-3: Regression Coefficients for the Bardet et al. (2002) MLR Model, FFGS-A (after Bardet et al., 2002)**

| Model | $b_0$ | $b_{off}$ | $b_1$ | $b_2$ | $b_3$ | $b_4$ | $b_5$ | $b_6$ |
|---|---|---|---|---|---|---|---|---|
| Ground slope | -6.815 | 0 | 1.017 | -0.278 | -0.026 | 0 | 0.454 | 0.558 |
| Free Face | -6.815 | -0.465 | 1.017 | -0.378 | -0.026 | 0.497 | 0 | 0.558 |

**Table 3-4: Regression Coefficients for the Bardet et al. (2002) MLR Model, FFGS-B (after Bardet et al., 2002)**

| Model | $b_0$ | $b_{off}$ | $b_1$ | $b_2$ | $b_3$ | $b_4$ | $b_5$ | $b_6$ |
|---|---|---|---|---|---|---|---|---|
| Ground slope | -6.747 | 0 | 1.001 | -0.289 | -0.021 | 0 | 0.203 | 0.289 |
| Free Face | -6.747 | -0.162 | 1.001 | -0.289 | -0.021 | 0.090 | 0 | 0.289 |

The researchers provided a range of values for the MLR variables in the data sets A and B. These ranges were the limits on the magnitudes of data from the case histories, and Bardet et al. (2002) recommend not using variables that fall outside this range. All empirical models

possess this limitation, due to the nature of the MLR process. Utilizing values outside the bounds used to regress the models can result in significant extrapolation and unrealistic magnitudes of the predicted value. The recommendation from this research can be seen in Table 3-5.

The last issue that needs to be addressed in reference to the Bardet et al. (2002) model is the sensitivity to the model to the source-site distance parameter R. Unlike the Youd et al. (2002) model, which added an $R^*$ to protect against unreasonably large predictions of displacements when R is small (<0.5 km), the Bardet et al. (2002) model can predict unrealistic displacements when source-to-site distance is small. These predictions come from extrapolation of the regressed relationship for R values at or lower then the bounds of the data used in the regression. Though no recommendations are explicitly stated in the Bardet et al. (2002) research to provide a solution to this problem, the author recommends the R parameter be limited based on magnitude as recommended in Bartlett and Youd (1995and summarized in Table 3-6. Restricting R in this manner will prevent unrealistic prediction of lateral displacement.

**Table 3-5: Recommended Range of Values for the Bardet et al. (2002) Procedure (after Bardet et al., 2002)**

| Variable | Range | |
|---|---|---|
| | FFGS-A | FFGS-B |
| D | 0 to10.15 | 0 to 1.99 |
| M | 6.4 to 9.2 | 6.4 to 9.2 |
| R (km) | 0.2 to 100 | 0.2 to 100 |
| W (%) | 1.64 to 55.68 | 1.64 to 48.98 |
| S (%) | 0.05 to 5.90 | 0.05 to 2.50 |
| T15 (m) | 0.2 to 19.7 | 0.2 to 13.6 |

**Table 3-6: Minimum Recommended R for Various Earthquake Magnitudes (after Bartlett and Youd, 1995)**

| Magnitude (Mw) | Minimum distance from seismic energy source R (km) |
|---|---|
| 6.0 | 0.5 |
| 6.5 | 1 |
| 7.0 | 5 |
| 7.5 | 10 |
| 8.0 | 20-30 |

### 3.4.5 Baska (2002) Procedure

Baska (2002) developed a semi-empirical procedure for predicting lateral spread displacements. This research incorporated actual soil liquefaction mechanics into a constitutive model, then used a nonlinear one-dimensional analysis program WAVE to develop more then 5000 "artificial" lateral spread case histories to develop a predictive model. That model was then calibrated against actual earthquake case histories and the resulting model was consistent with the current understanding of liquefied soil behavior, actual observed lateral spread case histories, and nonlinear site response (Kramer et al., 2007). The Baska (2002) model differs from the Youd et al. (2002) and Bardat et al. (2002) models in that the model does not incorporate the $T_{15}$ parameter. Instead the model uses a new parameter, $T^*$, which is the cumulative effective thickness of the laterally spread soils.

To utilize the Baska (2002) procedure, first the value of T* needs to be determined. The $T^*$ parameter is calculated for either the free-face or ground slope condition, and is found using Equation 3-4 for the ground slope and Equation 3-5 for the free-face. The variables in these equations are defined as: n = number of sublayers in the soil profile; $t_i$ = the thickness of each individual sublayer *i* in meters; $(N_{1,60,cs})_i$ = the corrected clean sand equivalent SPT blowcount

for each sublayer $i$; $z_i$ = the depth to the midpoint of each sublayer $i$ in meters; and $PI_i$ = the plasticity index for each sublayer $i$.

$$T_{gs}^{*} = 2.586\sum_{i=1}^{n} t_i \exp[-0.05(N_{1,60,cs})_i - 0.04z_i]/[1+(PI_{i/5.5})^8] \tag{3-4}$$

$$T_{ff}^{*} = 5.474\sum_{i=1}^{n} t_i \exp[-0.08(N_{1,60,cs})_i - 0.10z_i]/[1+(PI_{i/5.5})^8] \tag{3-5}$$

Once the effective cumulative thickness of the laterally spread soil is determined, the median predicted lateral spread displacement, $\hat{D}_H$, can be computed using Equation 3-6 and 3-7. The variables in these equations are defined as: M = the earthquake moment magnitude; R = the source-site distance to the seismic source in kilometers; S = the ground slope in percent; W = the free-face ratio in percent. The $R^*$ term can be determined using Equation 3-8. The regression coefficients for the free-face and ground slope conditions can be seen in Table 3-7.

$$\hat{D}_H = \begin{cases} 0 & \text{for } \overline{\sqrt{D_H}} \le 0 \\ \left(\overline{\sqrt{D_H}}\right)^2 & \text{for } \overline{\sqrt{D_H}} > 0 \end{cases} \tag{3-6}$$

$$\overline{\sqrt{D_H}} = \frac{\beta_1 + \beta_2 T_{gs}^{*} + \beta_3 T_{ff}^{*} + 1.231M - 1.151\log R^{*} - 0.01R + \beta_4\sqrt{S} + \beta_5 \log W}{1 + 0.0223(\beta_2 / T_{gs}^{*})^2 + 0.0135(\beta_3 / T_{ff}^{*})^2} \tag{3-7}$$

$$R^{*} = R + 10^{(0.89M - 5.64)} \tag{3-8}$$

**Table 3-7: Regression Coefficients for the Baska (2002) Model (after Baska, 2002)**

| Model | $\beta_1$ | $\beta_2$ | $\beta_3$ | $\beta_4$ | $\beta_5$ |
|---|---|---|---|---|---|
| Ground slope | -7.207 | 0.067 | 0 | 0.544 | 0 |
| Free Face | -7.518 | 0 | 0.086 | 0 | 1.007 |

Similar to the previously mentioned models, the Baska (2002) model has recommended bounds, which can be seen in Table 3-8.

It should be noted that the Baska (2002) model, unlike the Youd et al. (2002) and Bardat et al. (2002) models, may predict zero lateral spread for some conditions. Additionally, the Baska (2002) model may result in negative values for $\sqrt{D_H}$ which should be interpreted as zero displacement.

**Table 3-8: Recommended Bounds for the Baska (2002) Model (after Baska, 2002)**

| Variable | Range |
|---|---|
| M | 6.0 to 8.0 |
| R (km) | 0 to 100 |
| W (%) | ≤ 20 |
| S (%) | 0 to 6 |
| $T^*$ (m) | 1 to 20 |
| $(N_{1,60,cs})_i$ | unlimited |
| $z_i$ (m) | unlimited |
| $t_i$ (m) | ≤ 1.5 |

## 3.5 Incorporation of Uncertainty in the Estimation of Lateral Spread Displacements

Despite the widespread acceptance and implementation of empirical lateral spread predictive models, the estimated displacements do not directly account for the uncertainty in the predicted displacements. Because the models were regressed from data characterized by

significant scatter, many engineers and researchers have used the model standard deviations to attempt to characterize the variability in the database. Standard deviations for each model are provided in Table 3-9.

**Table 3-9: Standard Deviation Values for the Log of Displacement**

| Model | $\sigma_{\log D}$ |
|---|---|
| Youd et al (2002) | 0.202 |
| Bardat et al (2002) | 0.290 |
| Baska (2002) | 0.280 |

## 3.6 Chapter Summary

Lateral spread displacements can result in significant damage when triggered due to earthquake induced soil liquefaction. Lateral spread is the horizontal deformation of soil in ground that is gently sloped or near a free-face, and cyclic mobility due to liquefaction is predicted. Because lateral spread is an effect of liquefaction, lateral spread will not occur if the soil does not liquefy. Therefore, liquefaction susceptibility should be determined before predicting any displacements from lateral spread.

To understand the mechanics driving liquefaction-induced lateral spread, significant research has been performed. Out of this research has come a greater understanding of the process and the ability to predict lateral spread. Through laboratory and field testing, researchers have determined that the extent of lateral spread is strongly correlated to the seismic loading (magnitude, source-site distance), soil properties (density, thickness of liquefiable soil, PI), and site geometry (slope, distance to free-face). This research has led to two types of models developed to predict lateral spread, empirical and analytical. Analytical models attempt to predict

deformations based on understanding the fundamental soil mechanics of the liquefied soil behavior. Though these models incorporated the current understanding of this behavior and are considered by some to be more fundamentally correct, they have not been embraced and put into practice on the same scale as empirical models. Empirical models used databases of lateral deformations from earthquake case histories and develop statistical relationships between the displacements and related variables. These methods, though for the most part were not derived with any consideration of soil mechanics, have been adopted by most engineers due to their relatively accurate results and ease of use.

Empirical models have developed over the years, and have become more increasingly more sophisticated. Early models only considered the influence of one or two variables, but as more research was performed, empirical models became more complex. Two models in particular are used by many in the engineering community: Youd et al. (2002) and Bardat et al. (2002). These models consider the earthquake loading, soil properties, and site geometry and provide, in general, relatively accurate predictions of lateral spread. Additionally, these models can be adapted into a performance-based framework and used to perform probabilistic assessments of lateral spread. This topic is addressed in later sections.

# 4 REVIEW OF PERFORMANCE-BASED EARTHQUAKE ENGINEERING

## 4.1 Introduction

Earthquakes have had a significant impact on the manner in which engineers design buildings throughout history. With each new earthquake, building codes and ordinances have been adjusted to incorporate the expansion of the knowledge base of the engineering and geologic community. Millions of lives have been lost due to earthquakes in modern history, and seismic resistance and resiliency of structures and infrastructure has been constantly evolving to mitigate and prevent the catastrophic effects of earthquakes. One of the challenges presented to earthquake engineers is how to account for potential seismic hazard at a given site. The location, magnitude, and ground motions associated with the next major event are essentially impossible to predict. To account for this engineers have used deterministic procedures to assess seismic hazard, which consists of evaluating the major contributing seismic events and then selecting the one with the highest hazard to use for design. Following this methodology provides some confidence that the worst-case-scenario is accounted for, but this procedure does not consider the probability of the event occurring, and can lead to, in many cases, significant over design.

Many researchers and engineers feel that a more appropriate methodology is to determine the most likely event given some hazard level, and then tailoring this more probable scenario to the design. To more formally outline this approach, Performance-Based Earthquake Engineering (PBEE) has been recommended by the Pacific Earthquake Engineering Research Center (PEER).

This procedure has fundamentally altered the process whereby earthquake effects are designed for. Instead of approaching each scenario as a worst-case situation, the engineer and the owner can determine together the acceptable hazard level for the project and then develop an earthquake resistant design with an acceptable level of risk. This process allows engineers the capability to incorporate the uncertainties involved with earthquakes and then utilize the ever expanding research into design. The greater the capacity of the research community to characterize earthquake behavior, the more accurate and efficiently PBEE can account for the hazards associated with earthquakes.

This chapter will introduce the development and benefits of PBEE, provide a brief review of seismic hazard analysis for both the deterministic and probabilistic procedures, describe and outline PEER's recommended framework for PBEE, and then outline how empirical lateral spread models can be incorporated into a PBEE framework.

## 4.2 Basic Philosophy of PBEE

The development of building and seismic code provisions historically has centered on the idea of "life safety", which is in essence that buildings would be designed to a certain level of standard so that the structure would perform sufficiently in an earthquake and that the life and safety of the people inside it would be preserved. While it is important that buildings are designed to prevent loss of life, there are other factors to consider for earthquake design. Buildings designed to protect life and safety performed very well in the 1994 Northridge and 1995 Hanshin-Awaji (Kobe) earthquakes, but the level of damage to structures, economic loss due to loss of use, and cost of repair were unexpectedly high resulting in devastating economic impact on the regions (Ghobarah, 2001). With rapid growth in urban centers and many researchers concluding that seismic risk in urban environments is increasing, earthquakes pose

an ever expanding socio-economic threat. Many of the researchers agree that the solution to the increased risk is to develop more reliable seismic standards and code provisions than those currently available, and to implement these codes in the engineering of new structures and retrofitting of older structures (Bertero and Bertero, 2004). These conclusions led to the first formalized form of PBEE by the Structural Engineers Association of California (SEAOC) Visions 2000 Committee report "Performance-Based Seismic Engineering of Buildings" (Vision, SEAOC, 1995).

Krawinkler (2002) states, "PBEE implies design, evaluation, construction, monitoring the function and maintenance of engineered facilities whose performance under seismic loads responds to the diverse needs and objectives of owners, users, and societies. PBEE is based on the premise that performance can be predicted and evaluated with sufficient confidence for the engineer and client jointly to make intelligent and informed decisions based on building life-cycle considerations rather then construction cost alone." PBEE revolves around the idea that uncertainty can be quantified and used in predicting performance and then for engineers and owners to work together to identify the appropriate performance level and establish an acceptable amount of risk for a structure. This idea can be illustrated in a figure provided by Bertero and Bertero (2002) seen in Figure 4-1. This presents a criteria for a minimum performance of a structure based on a design level. A proposed new building can be evaluated under these guidelines. If the structure is not critical and does not need to remain functional after an earthquake, then the owner can comfortably assign a low performance level for potential hazards. Conversely, a critical structure that needs to remain operational after an earthquake can be given a higher minimum performance objective. This results in design procedures that more

comprehensively account for potential earthquake hazards and allow owners to make risk-based decisions.

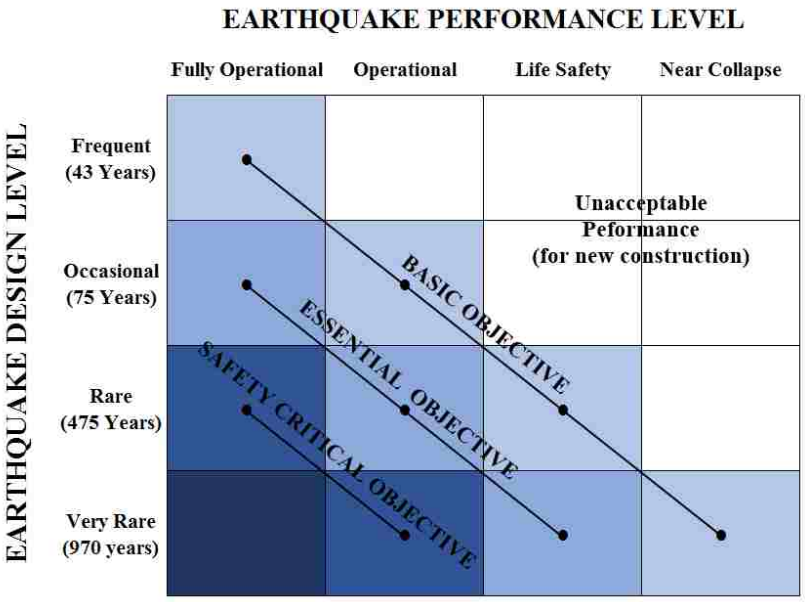


**Figure 4-1: Recommended Minimum Seismic Performance Design Objectives (after Bertero and Bertero, 2002)**

Incorporating this methodology will require that engineers move away from a deterministic approach. To predict the performance of a structure, the entire range of possible earthquake hazards needs to be evaluated and uncertainty associated with each scenario characterized, not just a single earthquake scenario. This means that design procedures that are more firmly rooted in the realistic computation of structural behavior exposed to a realistic distribution of possible earthquake loads must be developed in such a way that they are practical to apply and relatively simple to interpret, and engineers must begin to move away from purely empirical procedures (Krawinkler and Miranda, 2004). This can involve modifying existing

empirical procedures to function in a probabilistic framework or developing new models that account for all possible loading conditions.

## 4.3 Seismic Hazard Analysis

Seismic hazard analyses involve the quantitative estimation of ground-shaking hazards at a particular site (Kramer, 1996). The purpose of seismic hazard analyses is to determine the demand that a structure will experience during an earthquake. This demand is typically given as some ground motion at the site, which is referred to as the design ground motion. Determining the ground motions at a site is a difficult process, characterized with uncertainty in the location and intensity of the contributing earthquake event. To estimate the potential ground motions, empirical relationships have been developed from observed earthquake data. These empirical equations are regressed using statistical techniques and can be quite complex. They are often referred to as attenuation relationships, or also as ground motion predictive equations (GMPE), due to how the predicted ground motion attenuate with distance from the site. Ground motions can be predicted using these relationships both deterministically and probabilistically. These attenuation relationships, as well as Deterministic Seismic Hazard Analysis (DSHA) and PSHA are briefly introduced in the following sections.

### 4.3.1 Next Generation Attenuation Relationships

Ground motions at a particular site are heavily influenced by fault type, geometry, earthquake magnitude, soil and rock properties and stratigraphy, and distance from the seismic source. Attenuation relationships attempt to incorporate all of these factors in sophisticated statistical relationships to predict site-specific horizontal accelerations. Many of these models have been historically relatively straightforward empirical models (Abrahamson and Silva, 1997;

Borre et al., 1997; Campbell, 1997; Sadigh et al., 1997) In 2008, PEER released five new models that incorporated seismological and geotechnical information in addition to the empirical ground-motion data to begin transitioning from simple empirical models to full numerical simulations (Abrahamson and Silva, 2008; Boore and Atkinson, 2008; Campbell and Bozorgnia, 2008; Chiou and Youngs, 2008; Idriss, 2008). These five models are referred to as the Next Generation Attenuation (NGA) equations. All the models were developed from the same ground motion database, which is composed of recorded accelerations from earthquakes located across the world. Most of the ground motions from the database are from the western United States from crustal events, but many were also from events in Turkey, Taiwan, and Japan. Therefore the use of the equations is most appropriate in the western United States, but can also be applied in other locations for crustal events. For ease in utilizing the NGA equations, a spreadsheet was created by PEER and was released to the public for use in deterministic calculations (Al Atik, 2009). In 2013, these models were updated with the new ground motion data released by PEER, NGA-West2 (Ancheta et al., 2014), (Abrahamson et al., 2014; Boore et al., 2014; Campbell and Bozorgnia, 2014; Chiou and Youngs, 2014; Idriss, 2014). Other event types require additional attenuation relationships due to the differing fault mechanics that generate earthquake events like subduction zone and inter-plate seismic events (Youngs et al., 1997; Atkinson and Boore, 2003; and Zhao et al., 2006).

Utilizing these models to predict ground motions historically was done using a deterministic procedure. Uncertainty in the potential earthquake source, the magnitude of an event, as well as the recurrence rate demanded that seismic hazard be often times conservatively estimated through a Deterministic Seismic Hazard Analysis (DSHA). The governing, or largest, predicted ground motion at a site would be incorporated into the structural design, regardless of

the likelihood of that source actually affecting the site. This procedure would provide confidence to the owner that the structure would be protected from the largest conceivable earthquake. The DSHA is briefly introduced in the following section.

### 4.3.2 Deterministic Seismic Hazard Analysis

For the majority of the lifespan of geotechnical earthquake engineering, seismic hazard at a site was determined through a DSHA. This process involves the selection of a single event that would govern the seismic design at a given site. Based on this single event, the ground motions occurring at the site would be predicted through attenuation relationships. The process of a typical DSHA was described by Reiter (1990) and goes as follows:

1. Identification and characterization of all earthquake sources capable of producing significant ground motions at the site. This involves characterizing the fault geometry, maximum magnitude, and the likelihood of rupture for each source. These sources may be well documented active faults or little understood seismic zones.
2. Selection of a source-to-site distance parameter for each source zone. This is the shortest distance, from the fault or zone, to the site. This distance may be either the epicentral or hypocentral distance; which one will depend on the attenuation model used. The GMPE predict higher ground motions the closer the seismic source is to the site, so the shortest distance is most critical.
3. Selection of the controlling earthquake, which is generally the earthquake that produces the largest ground motion parameter. Each potential source identified in step 1 is analyzed using the GMPEs for the distance determined in step 2, and the

source with the governing ground motion parameter is described in terms of its magnitude and distance from the site.

4. The hazard at the site is formally defined, usually in terms of the ground motions produced at the site from the controlling earthquake. The characteristics of the controlling earthquake are generally described by one or more ground motion parameters obtained from the GMPEs utilized in step 3 (peak acceleration, peak velocity, spectral accelerations).

This procedure is outlined visually in Figure 4-2. The DSHA process is straightforward and relatively simple, and for many applications (nuclear power plants, large dams, and other critical facilities) the "worst-case-scenario" is a reasonable design criteria. But one of the main drawbacks of the DSHA is that no consideration is given to the likelihood of the governing earthquake actually occurring, or the uncertainty in the predicted ground motions for the event. This procedure relies on a subjective decision based on the expertise and experience of stakeholders involved in the process, which can result in differing goals and objectives and making decisions a difficult and arduous process.

The earthquake potential at a given site has been described in many terms over the years: the Maximum Credible Earthquake (MCE), Design Basis Earthquake (DBE), Safe Shutdown Earthquake (SSE), Maximum Probable Earthquake (MPE), Operating Basis Earthquake (OBE), and Seismic Safety Evaluation Earthquake (SSEE). These classifications are all defined in similar ways, and their incorporation into DSHAs has resulted in disagreements over which definition to use has resulted in delays, and even cancelations of a number of large projects. The Earthquake Engineering Research Institute (EERI) has stated that these terms are, "misleading…and their use is discouraged." (EERI, Committee on Seismic Risk, 1989). Without

the ability to objectively define the earthquake potential at a site, the classification of seismic hazard at a site using a DSHA can often result in disagreements and conflict over the preferred methodology.

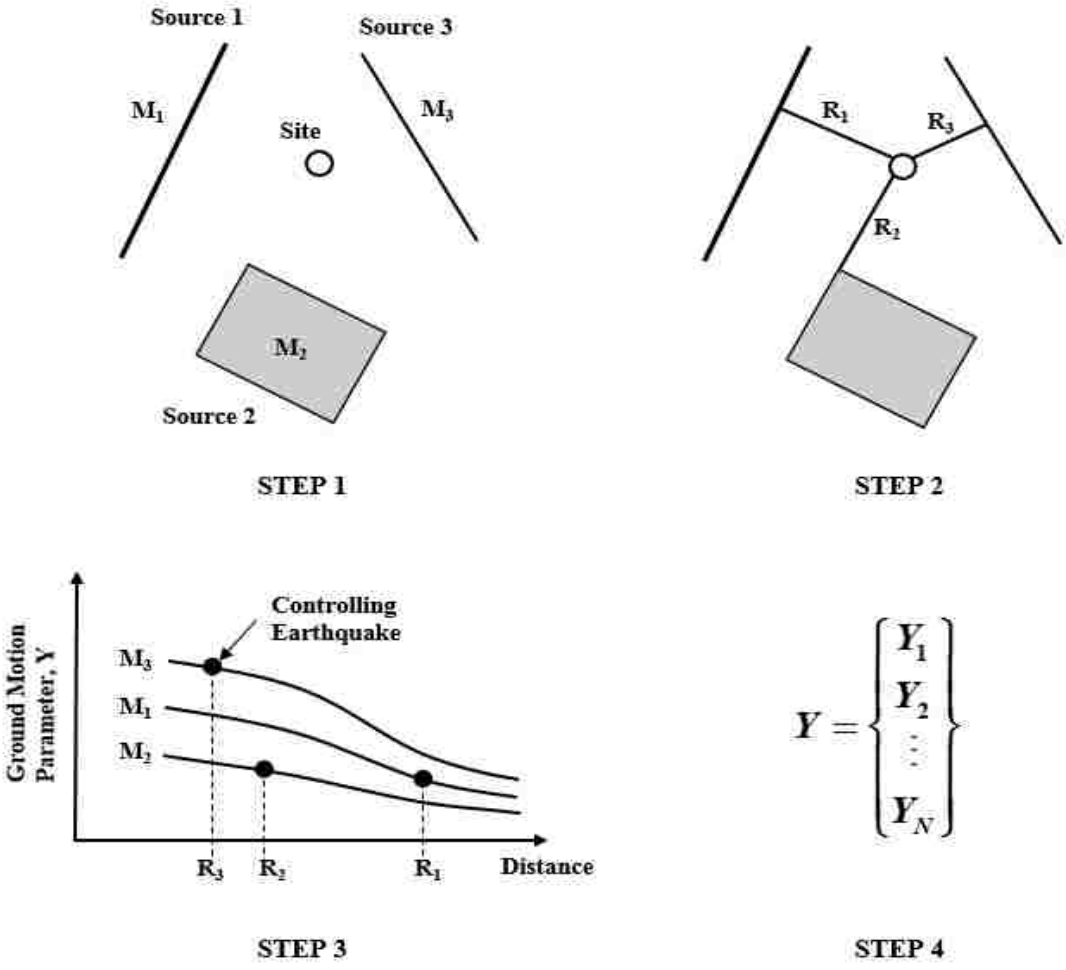


**Figure 4-2: Four Steps to Performing a DSHA (after Kramer, 1996)**

Additionally, the DSHA has no capability to account for uncertainty in the predicted ground motion parameters. The attenuation equations provide mean and median estimations of the ground motion parameters. Therefore, ground motion parameters larger than those mean values are possible at the site. If the DSHA is intended to represent a worse-case-scenario, but

the parameters predicted do not represent the worst case, what should the engineer do? Should the 84$^{th}$ percentile ground motions be utilized, or perhaps the mean plus two standard deviations. The decision becomes, once again, subjective and relies on the experience and judgment of the engineer to conservatively account for the hazard.

### 4.3.3 Probabilistic Seismic Hazard Analysis

To handle the problems and difficulties involved with performing a DSHA, researchers have developed procedures over the last 20 to 30 years (Cornell, 1968; Cornell, 1971; Merz and Cornell, 1973; Algermissen et al., 1982; McGuire, 2004) to explicitly handle the uncertainties in the potential earthquake ground motions for a given site. Such an approach is referred to as a Probabilistic Seismic Hazard Analysis (PSHA). This procedure requires familiarity with probability theory, as well as greater understanding of the geological and geotechnical mechanics of the contributing earthquake sources. The general process of a PSHA was also described by Reiter (1990) and is as follows:

1. Identify and characterize the potential contributing earthquake sources. This is essentially the same as step 1 from the DSHA, except the PSHA makes different assumptions about the source location for a given source. For the DSHA, the assumption is that the probability of the source being at the closest point on the fault or seismic zone is one, and is zero everywhere else. Of the PSHA, it is assumed that the earthquake is equally likely to occur anywhere along a fault on in a seismic zone. This spatial distribution of probability is referred to as the uniform probability distribution.
2. The seismicity or temporal distribution of earthquake recurrence must be characterized. This is done through a recurrence relationship, which is the average

rate at which an earthquake of some size will be exceeded. This recurrence rate provides a means to quantify the seismicity of each source zone. This allows a spectrum of magnitude events to be considered for each source, including the maximum magnitude, unlike the DSHA which only considers the largest event.

3. Determine the ground motion produced at the site by earthquakes of any possible size occurring at any possible point in each source zone using the predictive attenuation equations. Additionally, the uncertainty inherent in the GMPEs is considered, unlike the DSHA.
4. The uncertainties in earthquake location, earthquake size, and ground motion prediction are combined to obtain the probability that the ground motion parameter will be exceeded during a particular time period.

This process is presented visually in Figure 4-3. While the DSHA is relatively straightforward and simple to perform, the PSHA is generally complicated and requires great care that the earthquake sources are properly characterized and the uncertainties involved with each step are properly quantified. The uncertainties that are considered in the PSHA are spatial uncertainty, earthquake size uncertainty, GMPE model uncertainty, and temporal uncertainty.

#### *4.3.3.1 Spatial Uncertainty*

Attenuation relationships are very sensitive to the source-to-site distance of an earthquake event. In general, the closer to a site the earthquake occurs, the greater the intensity of the ground motions. The geometry of the seismic zone, in two- and three- dimensions, needs to be understood to accurately determine the requisite distances. Therefore, it is essential that the potential geometries in the potential location of an event be characterized.

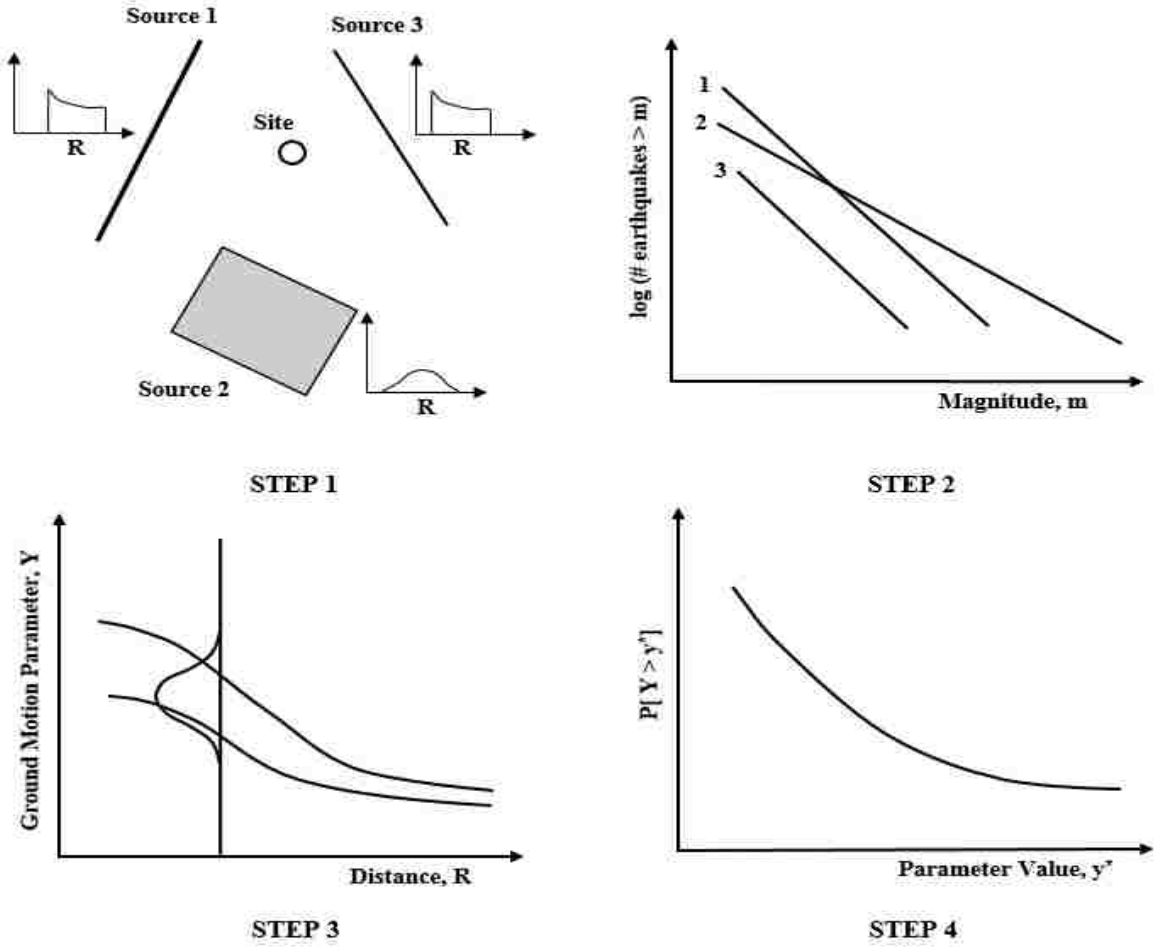


**Figure 4-3: Four Steps of a PSHA (after Kramer, 1996)**

There are three main source geometries to consider: point sources, areal sources, and volumetric sources. Point sources are from a single geographic location, like a volcano or a small fault. Areal sources are well-defined fault planes in two-dimensions on which earthquakes can occur at many different locations. Volumetric sources are three-dimensional areas where the earthquake mechanic is poorly defined, or where the faulting network is so dense and complicated that it is difficult to distinguish individual faults. Knowing how to identify each

source type and quantify the distances to each portion of the seismic zone is crucial in the PSHA process.

#### *4.3.3.2 Earthquake Size Uncertainty*

Similar to the distance from a site to an earthquake event, the magnitude of an earthquake heavily influences the intensity of the earthquake ground motions. Each seismic source zone has a maximum magnitude that can be produced, and that maximum cannot be exceeded. This maximum can be large or small depending on the source, but it must recognized that the source can produce earthquakes of any size up that maximum. The uncertainty lies in what magnitude event will be produced by a particular seismic zone.

Over the years, researchers have analyzed the observed earthquake magnitudes for particular zones over a given time period and have developed relationships that describe the source behavior. These relationships are referred to as recurrence laws. While there have been many recurrence laws developed, two in particular have been accepted by the earthquake research community. These are the Gutenberg-Richter and Characteristic Earthquake recurrence laws. The Gutenberg-Richter Recurrence Law was originally developed by Gutenberg and Richter (1944) from earthquakes in California. It was found that this law underpredicted the rate of small earthquakes and overpredicted the rate of large earthquakes (Kramer, 1996) and so McGuire and Arabasz (1990) developed a bounded Gutenberg-Richter Recurrence Law. This effectively set the lower threshold of the recurrence law to 4.0 – 5.0 magnitude events. This is due to earthquakes smaller than this rarely producing significant damage. In addition, the model creates an upper bound so that the larger magnitude events are more accurately characterized. The Characteristic Earthquake Recurrence Law was developed from paleoseismic studies that

indicated that individual points on faults and fault segments tend to move approximately the same distance in each earthquake. The researcher concluded that individual faults appear to repeatedly produce earthquakes of similar size. This recurrence law uses recorded seismicity data to predict the recurrence of small magnitude events, and the uses geologic data to predict the recurrence of higher magnitude events. Youngs and Coppersmith (1985) developed a generalized model that combined an exponential magnitude distribution at lower magnitudes with a uniform distribution in the vicinity of the characteristic earthquake.

#### *4.3.3.3 Uncertainty in the Attenuation Relationships*

Attenuation relationships are empirically derived using statistical regression. Despite the use of least-squares regression, there remain considerable scatter in the models. This scatter can be attributed to the randomness in the mechanics of rupture and from variability and heterogeneity of the source, travel path, and site conditions (Kramer, 1996). To quantity the uncertainty in the relationships due to the scatter, typically the standard deviation of the predicted parameter is used. The PSHA incorporates the uncertainty by computing the probability that a particular ground motion parameter (Y) exceeds a certain value ($y^*$), for a given magnitude (m) occurring at a given distance (r) using Equation 4-1.

$$P[Y > y^* \,|\, m, r] = 1 - F_Y(y^*) \tag{4-1}$$

Where $F_Y$ (y) is the cumulative distribution function of Y and m (magnitude) and r (source-to-site distance). This value depends on the attenuation model used and the probability distribution used to represent Y.

#### *4.3.3.4 Temporal Uncertainty*

Historically, earthquakes have been assumed to occur randomly with respect to time. Though this does seem to contradict elastic rebound theory, the ability to assume that earthquakes are random allows the use of simple probability models like the Poisson Model. This model provides a simple procedure to evaluate the probability of events, and is used frequently in PSHAs when dealing with temporal uncertainty. The Poisson model follows a Poisson process which obeys the following rules (Weisstein, 2005):

1. The number of occurrences in one time interval are independent of the number that occur in any other time interval.
2. The probability of occurrence during a very short interval is proportional to the length of the time interval.
3. The probability of more than one occurrence during a very short interval is negligible.

This Poisson process, while not appropriate for all seismic hazard applications, nonetheless is valid for most of the possible seismic scenarios (Cornell and Winterstein, 1986).

### 4.3.4 Seismic Hazard Curves

One common representation of the results of a PSHA is developing a seismic hazard curve. The seismic hazard curve indicates the annual probability of exceedance of different values of a selected ground motion parameter. Using this curve, the probability of exceeding some parameter in a given amount of time can be computed.

The basis of developing a seismic hazard curve is relatively straightforward. The probability of exceeding a specific value of a ground motion parameter is computed for a specified earthquake magnitude in a specified location and then multiplied by the probability that that magnitude earthquake will occur and by the probability that the earthquake will occur in that

location. This process is repeated for all possible combinations of magnitudes and locations. This process utilizes the total probability theorem, and is outlined with the following proof from Kramer (1996).

The probability that a ground motion parameter Y will exceed some value $y^*$ can be seen represented in Equation 4-2.

$$P\,[Y > y^*] = \iint P\,[Y > y^* \,|m,r] f_M(m) f_R(r)\; dm\; dr \tag{4-2}$$

Where $P[Y>y^*|m,r]$ is obtained from the attenuation relationship and $f_M(m)$ and $f_R(r)$ are the probability density functions for magnitude and distance, respectively. If the site of interest is in a region of $N_S$ potential earthquake sources, each of which has an average rate of threshold magnitude exceedance, $\nu_i$ (found with Equation 4-4), then the total average exceedance rate for the region cane be determined with Equation 4-3.

$$\lambda_{y^*} = \sum_{i=1}^{N_S} \nu_i \iint P\,[Y > y^* \,|m,r]\;\; f_{Mi}(m) f_{Ri}(m)\; dm\; dr \tag{4-3}$$

$$\nu_i = e^{\alpha_i - \beta_i m_o} \tag{4-4}$$

Where $\alpha = 2.303a$ and $\beta = 2.303b.$, and a and b are Gutenberg-Richter parameters.

The individual components of Equation 4-3 are sufficiently complicated that the integrals cannot be evaluated analytically. To make the development of the hazard curve possible, numerical techniques must be incorporated to approximate the result of Equation 4-3. For this

procedure the possible ranges of magnitude and distance are divided into $N_M$ and $N_R$ segments, respectively. Then Equation 4-3 can be approximated by Equation 4-5.

$$\lambda_{y^*} \approx \sum_{i=1}^{N_S}\sum_{j=1}^{N_M}\sum_{k=1}^{N_R} v_i \; P[Y > y^* \,|\, m_j, r_k] \; \mathrm{P}\,[\mathrm{M} = m_j] \; P\,[R = r_k] \tag{4-5}$$

To approximate $P[M = m_j]$ and $P[R = r_k]$, Equation 4-5 can be rewritten:

$$\lambda_{y^*} = \sum_{i=1}^{N_S}\sum_{j=1}^{N_M}\sum_{k=1}^{N_R} v_i \; P[Y > y^* \,|\, m_j, r_k] f_{Mi}(m_j) f_{Ri}(r_k) \; \Delta m \; \Delta r \tag{4-6}$$

where

$$m_j = m_o + (j - 0.5)\frac{(m_{\max} - m_o)}{N_M} \tag{4-7}$$

$$r_k = r_{\min} + (k - 0.5)\frac{(r_{\max} - r_{\min})}{N_R} \tag{4-8}$$

$$\Delta m = \frac{(m_{\max} - m_o)}{N_M} \tag{4-9}$$

$$\Delta r = \frac{(r_{\max} - r_{\min})}{N_R} \tag{4-10}$$

This procedure is relatively crude approximation of Equation 4-3, but the accuracy does increase with increasing numbers of $N_M$ and $N_R$. Additionally, this process results in just a single point on the hazard curve. The process needs to be repeated for all possible values of $y^*$. When all of the points have been computed, then the points can be plotted and the seismic hazard can be made.

## 4.4 Introduction to PEER PBEE Framework

PBEE is a methodology that incorporates probabilistic seismic hazards into a performance evaluation. PBEE is used to determine the risk at a given site from earthquake hazards, which can be expressed in terms of economic loss, fatalities, or other form of loss measurement. The PBEE framework focuses on a systems level approach, which allows an engineer to understand how the system as a whole will respond to earthquake shaking. The PBEE framework was developed by the Pacific Engineering Research Center (PEER) (Cornell and Krawinkler, 2000; Krawinkler, 2002; Deierlein et al., 2003) and is flexible enough to handle a wide range of potential hazards.

The PBEE framework is characterized by several terms, which can defined as:

1. Intensity Measure (IM) – The term represents the ground motion parameter that will be experienced at a site (peak ground acceleration, peak ground velocity, arias intensity, etc.) This mean annual rate of exceedance of this parameter is computed using a PSHA
2. Engineering Demand Parameter (EDP) – The variable characterizes the response of a system to the IM. They can be many different parameters (lateral spread displacement, probability of liquefaction, slope stability, etc.).

3. Damage Measure (DM) – This term describes the physical effect of the EDP on the system. This is the actual damage and consequence of the damage on a structure or component of a structure (interstory drift, displacement, crack width, etc.).
4. Decision Variable (DV) – This variable is the quantifiable value on which the ultimate performance of the system is based. It is, in essence, the risk associated with the DM (down time, repair cost, lives lost, etc.)

### 4.4.1 PBEE Framework

The PBEE framework is follows the same process as a PSHA, in that the mean annual rate of exceeding some variable is determined probabilistically. The variables utilized in PBEE are inter-related and are determined in a sequence, one leads in to the next and so on (IM →EDP→DM→DV). The introductory equation used in the PBEE process is given as:

$$\lambda_{edp} = \sum_{i=1}^{N_{IM}} P\left[ EDP > edp \mid IM = im_j \right] \Delta\lambda_{IM} \tag{4-11}$$

where $\lambda_{edp}$ is the mean annual rate of exceeding some EDP given some IM and likelihood of the IM being exceeded, and $P[EDP>edp|IM=im_i]$ can be found using a CDF that correlates $P[EDP>edp]$ to the IM. This type of CDF is referred to as a fragility curve.

All of the PBEE parameters can be incorporated in a single equation to find the seismic hazard curve for DV given a seismic hazard curve for IM. This equation is as follows:

$$\lambda_{dv} = \iiint P[DV \mid DM]\, dP[DM \mid EDP]\, dP[EDP \mid IM]\, d\lambda_{IM} \tag{4-12}$$

Equation 4-12 can be approximated numerically as:

$$\lambda_{dv} = \sum_{k=1}^{N_{DM}} \sum_{j=1}^{N_{EDP}} \sum_{i=1}^{N_{IM}} P\left[DV > dv \mid DM = dm_k\right] \times P\left[DM = dm_k \mid EDP = edp_j\right] P\left[EDP = edp_j \mid IM = im_i\right] \Delta\lambda_{im_i} \quad (4\text{-}13)$$

where $N_{DM}$, $N_{EDP}$, and $N_{IM}$ are the number of increments of DM, EDP, and IM, respectively. Just as with a PSHA, increasing the number in increments increase the accuracy of Equation 4-13.

The end product of Equation 4-12 or 4-13 is the mean annual rate of exceeding some DV, $\lambda_{DV}$. Additionally, the mean annual rate of exceeding any of the intermediary PBEE values is also found, due to their being incorporated into the PBEE process. All of these factors can be incorporated into a Poisson model to compute the probability that the parameter will be exceeded in a given time period. This gives stakeholders and decision makers the ability to objectively evaluate seismic hazards at any stage in the PBEE process and provides greater capability to assess risk.

## 4.5 Incorporating Empirical Lateral Spread Models into a PBEE Framework

Empirical lateral spread predictive models are characterized by uncertainty in the data used to perform the regression, and have resulted in considerable scatter of the estimated displacements. In order to account for the uncertainties involved in utilizing the empirical MLR models, researchers have incorporated these models in a performance-based framework. Franke (2005) and Kramer et al. (2007) demonstrated how the PEER PBEE framework could be adapted

to produce performance-based estimates of lateral spread displacement. This section outlines how that process was accomplished.

### 4.5.1 Loading and Site Parameters

In order to incorporate an empirical lateral spread model in to a probabilistic framework the empirical model's terms associated with seismic loading would need to be separated and distinguished from its equation associated with soil/site conditions (Franke and Kramer, 2014). Then the model could be represented as:

$$\mathcal{D} = \mathcal{L} - \mathcal{S} + \varepsilon \tag{4-14}$$

where $\mathcal{D}$ is the mean transformed (e.g. Log, Ln, square root) lateral spread displacement, $\mathcal{L}$ is the "apparent loading parameter" that characterizes seismic loading, $\mathcal{S}$ is the "site parameter" that characterizes soil/site conditions (including geometry), and $\varepsilon$ is the model uncertainty term. Using Equation 4-11, the *IM* in the PBEE framework is represented by $\mathcal{L}$, and the *EDP* is represented by $\mathcal{Z}$.

Franke and Kramer (2014) demonstrated how the Youd et al. (2002) empirical model could be adapted according to Equation 4-15 to fit within the performance-based procedure introduced by Franke (2005) and Kramer et al. (2007). This is done by modifying Equation 3-1 in accordance with Equation 4-15 as follows:

$$\overline{\log D_H} = \mathcal{L} - \mathcal{S} + \varepsilon \tag{4-15}$$

$$\mathscr{L} = b_1 M + b_2 \log R^* + b_3 R \tag{4-16}$$

$$\mathscr{S} = -\left(b_0 + b_4 \log W + b_5 \log S + b_6 \log T_{15} + b_7 \log\left(100 - F_{15}\right) + b_8 \log\left(D50_{15} + 0.1\right)\right) \tag{4-17}$$

$$\varepsilon = \sigma_{\log D_H} \Phi^{-1}\left[P\right] \tag{4-18}$$

where $P$ is the probability of exceeding the median predicted lateral spread displacement, $\hat{D}_H$, and $\Phi^{-1}$ is the inverse standard normal cumulative distribution function. Separating the $\mathscr{L}$ and $\mathscr{S}$ terms allows the different components of the model to be addressed individually.

### 4.5.2 Incorporation into PBEE Framework

Because $\overline{\log D_H}$ is conditional upon the apparent earthquake loading and site specific soil parameters (i.e., $\mathscr{L}$ and $\mathscr{S}$, respectively), then the fragility relationship to compute the probability of exceeding some given lateral spread displacement $d$ is given as:

$$P\left[\hat{D}_H > d \mid \mathscr{L}, \mathscr{S}\right] = 1 - \Phi\left[\frac{\log d - \overline{\log D_H}}{\sigma_{\log D_H}}\right] = 1 - \Phi\left[\frac{\log d - \overline{\log D_H}}{0.197}\right] \tag{4-19}$$

where $\Phi$ is the standard normal cumulative distribution function.

Equations 4-15 through 4-19 are presented graphically in Figure 4-4, where $\overline{\log D_H}$ is shown to be a linear function of $\mathscr{L}$ with a constant y-intercept equal to $\mathscr{S}$ and uncertainty

about the line characterized by $\varepsilon$. The performance-based procedure presented by Franke and Kramer (2014) assigns all of the model uncertainty to $\mathcal{M}$ and assumes that $\mathcal{S}$ remains constant for a give site. Although there can exist potential variation or uncertainty in $\mathcal{S}$, the uncertainty can be handled through a logic tree approach in which displacement hazard curves are developed for various values of $\mathcal{S}$, as shown in Figure 4-5, and then weighted accordingly.

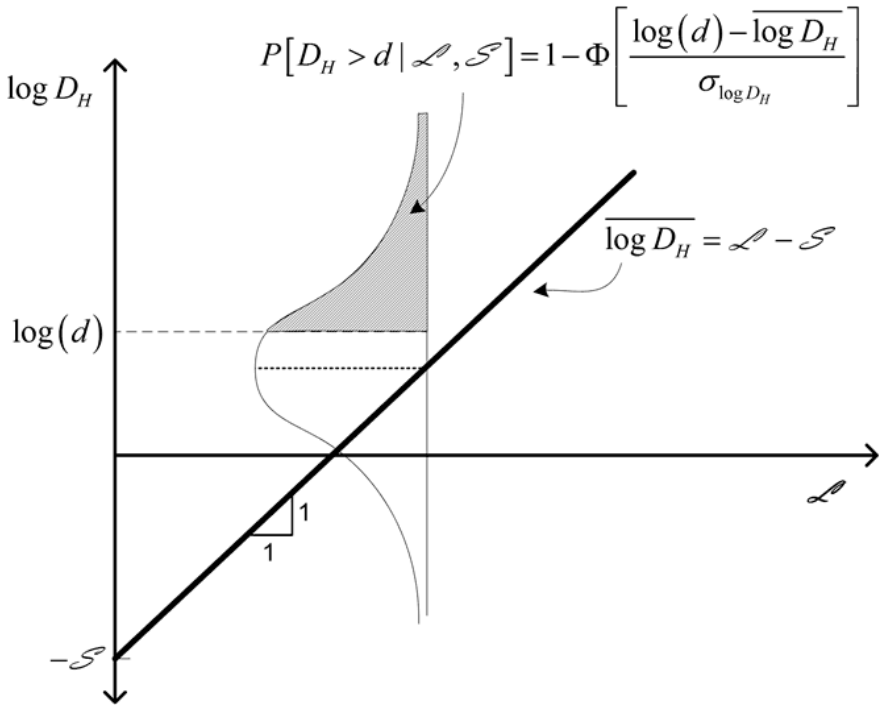


**Figure 4-4: Schematic Diagram of the Fully Probabilistic Youd et al (2002) Model (after Franke and Kramer, 2014)**

The apparent loading parameter $\mathcal{M}$ in Equation 4-16 is not a real or measurable ground motion parameter and does not represent any true statistical regression for that portion of the model alone, However $\mathcal{M}$ it is a function of magnitude and distance and has been shown to attenuate in a manner similar to measurable ground motion parameters described by traditional GMPEs (Franke and Kramer, 2014). In the context of the Youd et al. (2002) model, the apparent

loading term, therefore, can be treated as though it were an Intensity Measure (*IM)* in the PBEE framework.

By incorporating Equations 4-16 and 4-17 with the fragility relationship of Equation 4-19 in the PBEE framework of Equation 4-13, a performance-based lateral spread displacement model can be expressed as:

$$\lambda_{D_H|\mathcal{S}}(d \mid \mathcal{S}) = \sum_{i=1}^{N_{\mathcal{L}}} P\left[D_H > d \mid \mathcal{S}, \mathcal{L}_i\right] \Delta\lambda_{\mathcal{L}_i} \tag{4-20}$$

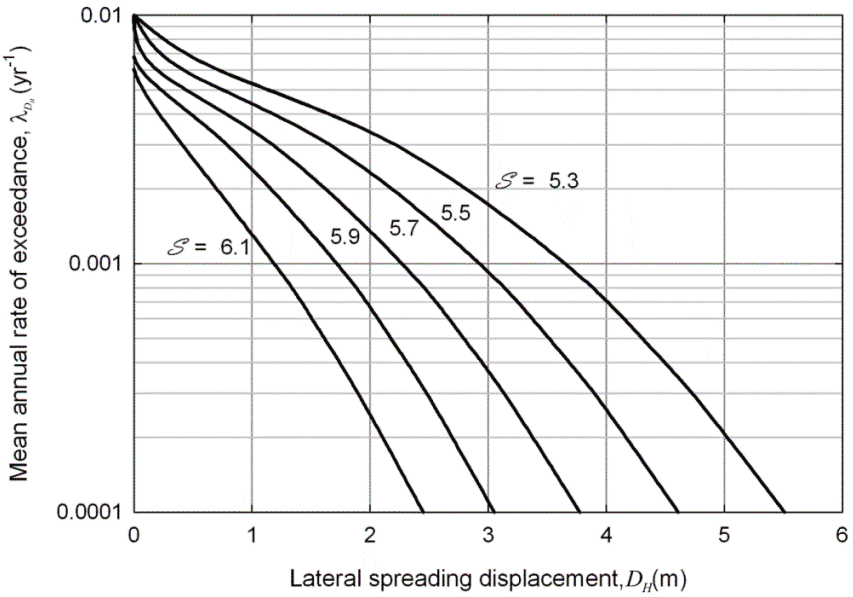


**Figure 4-5: Variations of Lateral Spread Hazard Curves as a Function of the Site Parameter, $\mathcal{S}$ (Modified from Kramer et al., 2007)**

where $\lambda_{D_H|\mathcal{S}}(d \mid \mathcal{S})$ is the mean annual rate of exceeding a displacement $d$ conditional upon site parameter $\mathcal{S}$, $N_{\mathcal{L}}$ is the number of apparent loading parameter increments required to span the

range of all possible values of $\mathscr{L}$, and $\Delta\lambda_{\mathscr{L}_i}$ is the increment of the apparent loading parameter in hazard space. For a single source, Equation 4-20 can be written as:

$$\lambda_{D_H|\mathscr{S}}\left(d \mid \mathscr{S}\right) = \nu \sum_{i=1}^{N_{\mathscr{L}}} P\left[\hat{D}_H > d \mid \mathscr{S}, \mathscr{L}_i\right] P\left[\mathscr{L}_i\right] \tag{4-21}$$

where $\nu$ is the mean annual rate of exceeding a minimum magnitude of interest for the given seismic source. However, because $\mathscr{L}$ is a function of magnitude and distance, it can be affected by multiple seismic sources. To account for these multiple possible seismic sources, Equation 4-21 can be expanded as:

$$\lambda_{D_H|\mathscr{S}}\left(d \mid \mathscr{S}\right) = \sum_{i=1}^{N_S} \nu_i \sum_{j=1}^{N_M} \sum_{k=1}^{N_R} P\left[\hat{D}_H > d \mid \mathscr{S}, M = m_j, R = r_k\right] P\left[M = m_j, R = r_k\right] \tag{4-22}$$

where $N_S$, $N_M$, and $N_R$ are the number of seismic sources, discretized magnitudes, and discretized source-site distances, respectively, and $\nu_i$ is the mean annual rate of exceeding some specified minimum magnitude for the $i^{\text{th}}$ source. Because Equation 4-22 is very similar to the typical PSHA framework commonly used to compute uniform hazard estimates of ground motions (Kramer, 1996), it can be incorporated into common PSHA software such as *EZ-FRISK 7.60* (Risk Engineering, 2013) or *OpenSHA* (Field et al., 2003) to develop lateral spread displacement hazard curves and corresponding deaggregations.

## 4.6 Chapter Summary

PBEE is an important concept in geotechnical earthquake engineering. This methodology provides the capability to quantify and incorporate uncertainty into a probabilistic framework. Methods to deal with this uncertainty give owners, engineers, and stakeholders greater capacity to quantify risk and objectively evaluate hazard at a site. The process considers all possible contributing earthquake sources and provides a much more accurate prediction of potential seismic loading. This methodology is a valuable advancement beyond the conventional DSHA.

Seismic hazard analyses are utilized by engineers to estimate ground motion parameters at a given site. There are two types of seismic hazard analyses, Deterministic and Probabilistic. Deterministic (DSHA) procedures evaluate the worst-case scenario earthquake by identifying all the contributing seismic sources for a site and then computing the ground motion associated with each source using attenuation relationships. The source that predicts the highest ground motion, becomes the governing earthquake source. Probabilistic (PSHA) procedures identify all contributing seismic sources as well, but then use attenuation relationships to determine the ground motions from all possible combinations of magnitude and distance for each source. Then using the total probability theorem, the mean annual rate of exceeding some ground motion parameter is determined. If this process is repeated over all possible ranges of the parameter, then a seismic hazard curve can be created.

The DSHA has many sources on uncertainty that are not accounted for, and relies on subjective selection of magnitude and distance to determine the governing earthquake. The likelihood of this earthquake is not considered and the selected governing seismic source may not provide a reasonable estimation of hazard. This can result in overly conservative estimations of ground motions and excessive economic costs. The PSHA incorporates the uncertainty with

the location of the earthquake, magnitude of the earthquake, scatter in the attenuation relationships, and temporal distribution of the earthquake events. The PSHA considers all possible sources of earthquake hazard, at all possible magnitudes, and all possible locations. Through the PSHA and the creation of seismic hazard maps, the hazard at a specific return period can be identified. This allows owners and engineers to evaluate and target specific levels of risk, and provides a mean to objectively and quantitatively assess the seismic hazard.

The Pacific Earthquake Engineering Research center (PEER) has developed a framework to perform PBEE assessments. The framework consists of sequentially related parameters that can be combined with their corresponding conditional probabilities to create hazard curves for each of the PBEE parameters: Intensity Measure (IM), Engineering Demand Parameter (EDP), Damage Measure (DM), and Decisions Variable (DV). These hazard curves can be used to assess the seismic risk to a structure and allows engineers and owners to make objective decisions about performance and better characterize the effects of the seismic hazards.

Empirical lateral spread displacement models are associated with uncertainties that can be quantified and accounted for by incorporating the models into a PEER PBEE framework. The Youd et al. (2002) MLR lateral spread model was incorporated into this framework and can be used to make probabilistic estimations of lateral spread displacements and develop lateral spread hazard curves. This will allow greater confidence to be placed on the predicted displacements, as well as allow hazard targeted decisions to be made where lateral displacements are a concern.

# 5 DEVELOPMENT OF SIMPLIFIED PERFORMANCE-BASED LATERAL SPREAD PREDICTION METHOD

## 5.1 Introduction

If a generic set of "reference" site conditions could be used to compute a generic and constant value of $\mathcal{S}$, then a series of performance-based lateral spread displacement analyses could be performed across a geographic grid of points to develop hazard targeted lateral spread displacement contours that correspond to the generic value of $\mathcal{S}$. These contours can be represented on a map, providing the reference lateral spread displacement for any location. An example of such a map can be seen in Figure 5-1. However, these contours would not correspond to actual, site-specific estimates of lateral spread displacement because they would be developed with generic, reference site conditions. Rather, these contours would serve as a relative indicator of regional lateral spread displacement hazard and would also represent a proxy for the seismic loading that affects lateral spread. These maps are therefore called "lateral spread reference parameter maps" to distinguish them from lateral spread hazard maps (e.g., Olsen et al., 2007), which attempt to represent actual, site-specific lateral spread hazards.

While lateral spread reference parameter maps only provide a relative indicator regarding regional lateral spread hazards at targeted return periods, it is possible to use them to compute site-specific, probabilistic estimates of lateral spread displacement for a given site at the targeted return period if soil subsurface and site geometry information are available. A similar approach is currently implemented by most seismic building codes (e.g., ASCE 2013; IBC 2014;

AASHTO 2014) to develop probabilistic ground motion estimates that account for site amplification effects (i.e., site response) from mapped, probabilistic bedrock ground motions at the desired return period. This type of mapped, simplified approach has also been used by engineering researchers to produce probabilistic estimates of liquefaction triggering (Mayfield et al., 2010; Franke et al., 2014b), as well as liquefaction-induced ground deformations for the design of a large pipeline (Honegger et al., 2014).

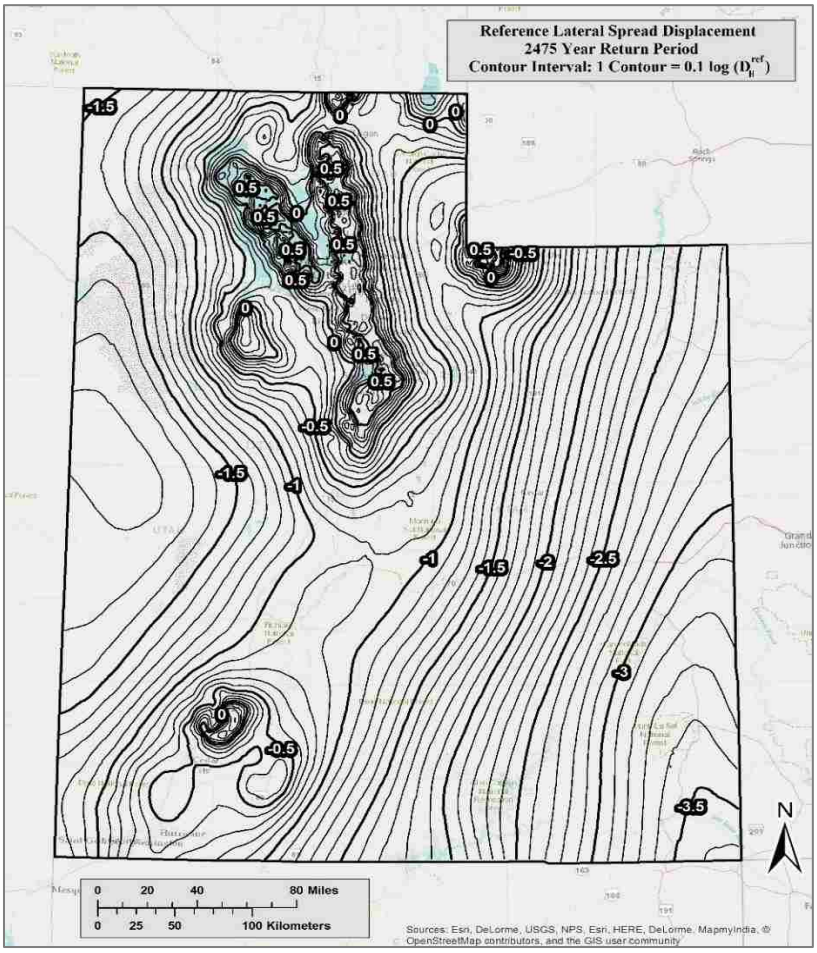


**Figure 5-1: Lateral Spread Reference Map for Utah (2475 Year Return Period)**

It should be noted that the simplified procedure is performed with the assumption that liquefaction will occur. The Youd et al. (2002) model does not possess the capability to incorporate any liquefaction parameters (factor of safety against liquefaction, probability of liquefaction) when predicting displacements, and the simplified procedure retains the same limitation. Many engineers utilize the Youd et al. (2002) model without considering liquefaction initiation, relying on engineering judgment and experience to determine whether liquefaction will occur. However, lateral spread displacements are entirely reliant on liquefaction occurring, so it is recommended that an analysis of liquefaction susceptibility and initiation should be performed before performance-based lateral spread hazard is determined.

## 5.2 Derivation of Simplified Lateral Spread Equations

To derive a simplified performance-based lateral spread procedure, a reference set of site conditions was first defined, and is presented in Figure 5-2. These site conditions were selected to be consistent with those used in the comparative lateral spread displacement study of Franke and Kramer (2014). As can be seen in Figure 5-2, the reference site conditions show a ground-slope case with $T_{15} = 3.0$ meters, $F_{15} = 20\%$, $D50_{15} = 0.2$ mm, and $S = 1\%$. Inputting the values of these site specific soil conditions in Equation 4-17, a value of 9.044 is computed for the reference value of $\mathcal{S}$.

According to the simplified procedure, a site-specific estimate of the probabilistic lateral spread displacement, $[\log D_H]^{site}$ can be computed as:

$$[\log D_H]^{site} = [\log D_H]^{ref} + \Delta D_H \tag{5-1}$$

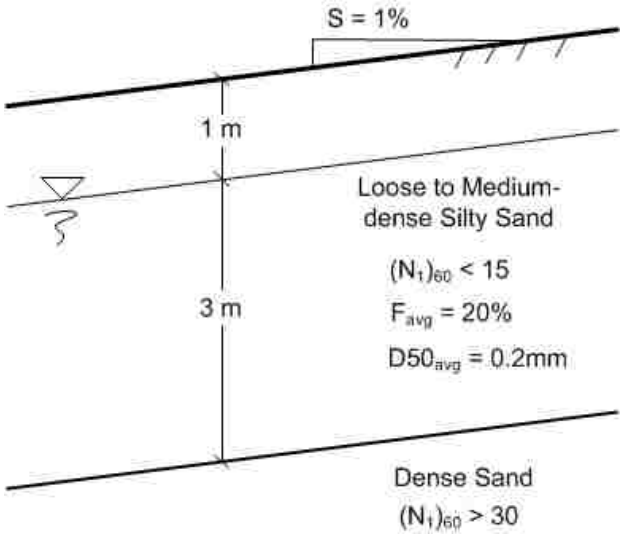


**Figure 5-2: Reference Soil Profile Used to Derive the Simplified Lateral Spread Method**

where $\left[\log D_H\right]^{ref}$ is the reference displacement obtained from a hazard-targeted lateral spread reference map, and $\Delta D_H$ is an adjustment factor that corrects the mapped reference displacement to the site-specific displacement. This adjustment factor, as proposed by Mayfield et al. (2010), is a simple linear adjustment of the log $D_H$ value, which varies linearly as can be seen in Figure 4-4. By substituting Equation 4-14 into Equation 5-1, the adjustment factor can be written as:

$$\Delta D_H = \left(\mathscr{A} - \mathscr{S}\right)^{site} - \left(\mathscr{A} - \mathscr{S}\right)^{ref} = \left(\mathscr{A}^{site} - \mathscr{A}^{ref}\right) + \left(\mathscr{S}^{ref} - \mathscr{S}^{site}\right) \tag{5-2}$$

However, because seismic loading is the same for both site-specific and reference site conditions (i.e., $\mathscr{A}^{site} = \mathscr{A}^{ref}$), Equation 5-2 can be simplified, and the calculated $\mathscr{S}$ parameter value entered in, as follows:

$$\Delta D_H = \mathscr{S}^{ref} - \mathscr{S}^{site} = 9.044 - \mathscr{S}^{site} \tag{5-3}$$

If Equation 4-17 is substituted for $S^{site}$, then Equation 5-3 can be rewritten as:

$$\Delta D_H = 9.044 + b_0^{site} + b_4^{site} \log\left(W^{site}\right) + b_5^{site} \log\left(S^{site}\right) + 0.540 \log T_{15}^{site} + 3.413 \log\left(100 - F_{15}^{site}\right) - 0.795 \log\left(D50_{15}^{site} + 0.1\right) \quad (5\text{-}4)$$

where $b_0^{site}$, $b_4^{site}$ and $b_5^{site}$ denote site-specific model coefficients conditional upon the geometry model (i.e. ground-slope or free face) and are provided in Table 5-1. Parameters with the '*site*' superscript denote site-specific soil and geometry parameters calculated from available site information. Once $\left[\log D_H\right]^{site}$ is computed using Equations 5-1 and 5-4, the probabilistic lateral spread displacement (in meters) can be computed as:

$$D_H^{site} = 10^{\left(\left[\log D_H\right]^{site}\right)} = 10^{\left(\left[\log D_H\right]^{ref} + \Delta D_H\right)} \quad (5\text{-}5)$$

**Table 5-1: Site-Specific Geometry Coefficients for Computing the Adjustment Factor $\Delta D_H$**

| Model | $b_0^{site}$ | $b_4^{site}$ | $b_5^{site}$ |
|---|---|---|---|
| Ground-Slope | -16.213 | 0 | 0.338 |
| Free Face | -16.713 | 0.592 | 0 |

Note that engineers would no longer be required to characterize seismic loading for a lateral spread displacement assessment using the simplified performance-based procedure

presented here. This is because the seismic loading for lateral spread hazard assessment would already be incorporated into the lateral spread reference map corresponding to the targeted return period or hazard level. Engineers would therefore simply need to characterize and define the site-specific soil and geometry conditions existing at the site of interest (i.e., $\zeta$ ). With such an approach, confusion regarding the selection of $(M, R)$ pairs in complex seismic environments would be eliminated, and greater consistency in the return period associated with predicted lateral spread displacements would be achieved.

## 5.3 Development of Lateral Spread Reference Parameter Maps

The lateral spread reference parameter maps are an essential part of the simplified lateral spread methodology. They are developed through a full performance-based analysis of individual grid points that span a region, resulting in a gridded set of $\log[D_H]^{ref}$ points that are interpolated to create contours representing the hazard-targeted reference lateral spread displacement over the whole area. The spacing of the grid needs to be evaluated to ensure that spacing is fine enough that the contoured results represent the actual results within a reasonable margin of error, and at the same time coarse enough that the analysis is not computationally prohibitive.

### 5.3.1 Grid Spacing Analysis

Because biases due to spacing of grid points in gridded seismic hazard analyses are known to exist, a grid spacing study is evaluated the potential for bias to occur due to grid spacing effects in a gridded probabilistic lateral spread hazard assessment. To develop robust grid spacing recommendation, this study comprises many cities in areas of varying seismicity.

The first step in the process was determining which variable to correlate with the grid spacing. A preliminary grid spacing study was performed and can be seen in the following section.

#### *5.3.1.1 Preliminary Correlation Study*

The objective of this study was to develop a simple, well-defined set of rules for determining optimum grid spacing. It was initially hypothesized that optimum grid spacing would be dependent upon peak ground acceleration (i.e. *PGA*), which is strongly correlated with magnitude and distance, similar to the Youd et al. (2002) model. Specifically, it was hypothesized that areas of high seismicity would require finer grid spacing and areas of low seismicity would not require such high resolution to achieve the desired accuracy. Four cities were selected for the preliminary study and can be seen in Table 5-2

**Table 5-2: Cities Analyzed in the Preliminary Study**

| City | Latitude | Longitude | PGA(g) ($T_R$ = 2475 years) |
|---|---|---|---|
| Berkeley, CA | 37.872 | -122.273 | 1.1340 |
| Salt Lake City, UT | 40.755 | -111.898 | 0.6478 |
| Butte, MT | 46.003 | -112.533 | 0.1785 |
| Clemson, SC | 34.683 | -82.837 | 0.1439 |

The grid spacing assessment was performed by comparing interpolated results from a simple 4-point grid with an analysis performed at the site. The gird spacing arrangement can be seen in Figure 5-3. The analysis was performed at each of the four corner points and then the value at the center was computed using simple linear interpolation. The anchor point in the center was the analyzed. The difference between the interpolated and site-specific results was

quantified, and the percent error was calculated using Equation 5-6. For the grid spacing to be acceptable, the percent error was to be, on average, five percent or less.

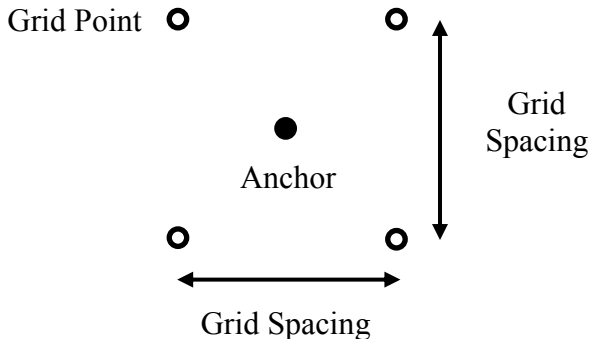


**Figure 5-3: Layout of Grid Points for Grid Spacing Analysis**

$$Percent\ Error = \frac{[Interpolated\ Value - Actual\ Value]}{Actual\ Value} \times 100\% \qquad (5\text{-}6)$$

For the preliminary study, each location was analyzed over a range of values until a grid spacing was found that resulted in five percent error or less. If the high PGA cities required finer grid spacing and the lower PGA cities coarser, then it would be concluded that the lateral spread displacement was correlated with PGA and the grid spacing study could proceed based on that correlation.

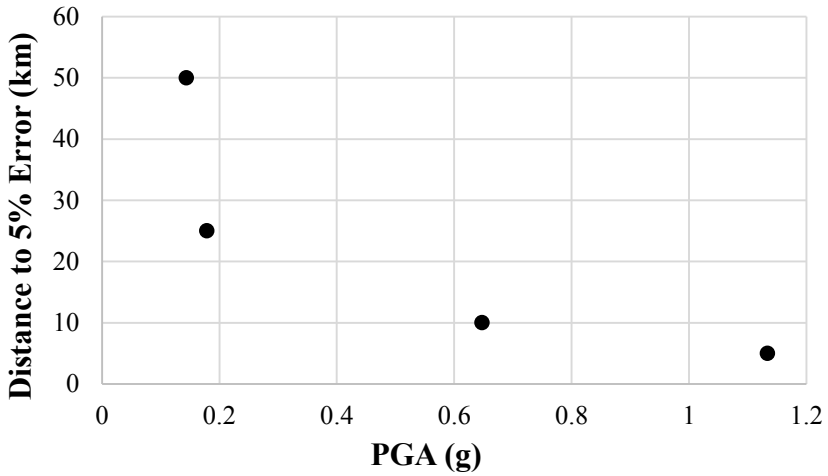


**Figure 5-4: Results of the Preliminary Grid Spacing Study**

Once the cities were analyzed, a few observations were made. For the city with the highest PGA (1.134 g), Berkeley, the optimum grid spacing was found to be 5 km. For the city with the lowest PGA (0.1439 g), Clemson, a grid spacing that resulted in 5% error was not achieved even at a 50 km spacing. Salt Lake City (PGA=0.6478g) resulted in 5% error at 10 km, and Butte (PGA=0.1785g) at 25 km. Plotting these results, the trend of the error based on PGA can be seen in Figure 5-4. From this result it appears that the grid spacing to result in 5 % error goes up as the PGA increases, therefore it was concluded that the optimum grid spacing was correlated with PGA and would be an acceptable metric for establishing optimum grid spacing.

#### *5.3.1.2 Grid Spacing Study*

A large grid spacing study was performed on 21 different cities across the United States, with varying levels of seismic hazard. The cities can be seen in Figure 5-5. Each location was analyzed based on the methodology outline in section 6.3.1.1, and the percent error was determined using Equation 5-6. The results of the grid spacing study can be seen in Figure 5-6.

The results generally show the trend of the data is consistent with the conclusion of the preliminary study. But the data starts to deviate from this trend in areas of medium and high seismicity as can be seen in Figure 6. In the PGA range from 0.4 to 0.6 g, the spread of the data increases dramatically. Some locations seem insensitive to grid spacing entirely, with Eureka, CA not reaching 5% error even with a grid spacing of 90 km. At the same time, two locations, Reno, NV and Jackson, WY, did not reach 5% error with a grid spacing of only 1 km. The explanation of this spread in the data could be attributed to three phenomena: location, model attenuation, and regional seismicity.

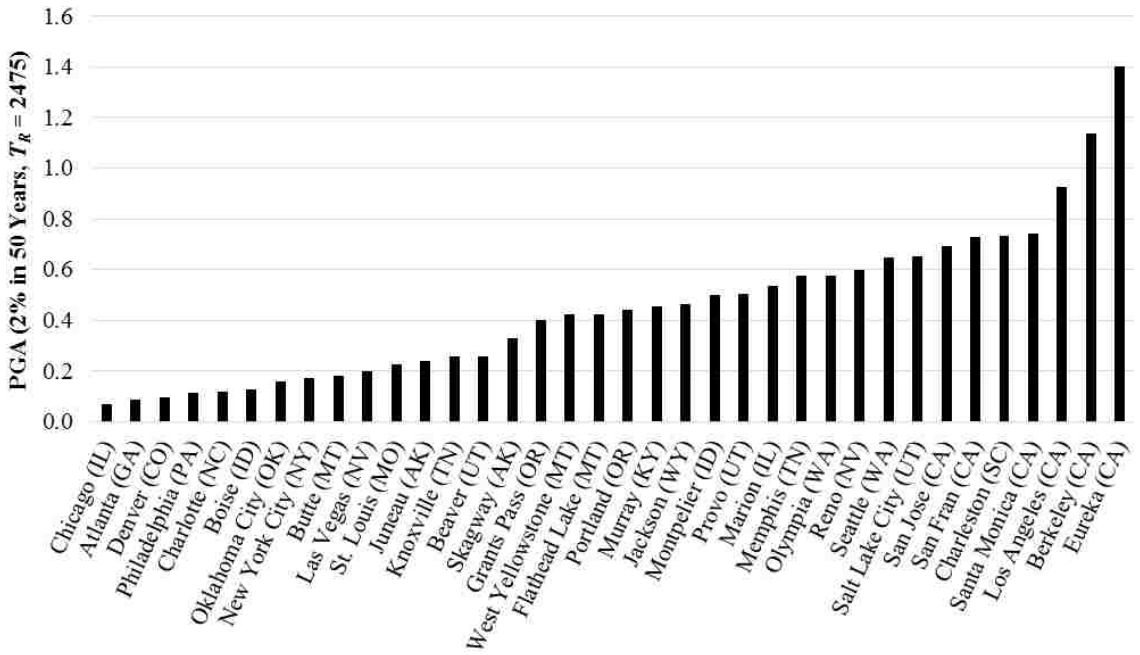


**Figure 5-5: Cities Used in the Grid Spacing Study**

First, the points that have a generally low grid spacing based on PGA were all located in or near the Basin and Range seismic region of the United States. This region is characterized by extensive normal faulting in the North-South facing valleys. The Youd et al. (2002) empirical

lateral spread model is very sensitive to source-to-site distance at low to medium magnitude events. In this region, points analyzed near (within 5 km) can predict very large displacements, even when determined with a probabilistic approach. When the grid spacing is varied locally, often one of the points used in the interpolation will end up near a fault resulting in a large error. This makes analysis of this kind very sensitive in similar regions, and would require a finer grid spacing than normal. Secondly, the Youd et al. (2002) model attenuates differently for source-to-site distance based on magnitude. High magnitude events ($M_W > 7.0$) make the model insensitive to near distances. For sites characterized by large magnitude events (especially subduction zone events), the predicted displacements are dominated by that single source. This can be seen in Figure 5-6, where Eureka, CA (which has a very high PGA of 1.41 g) maintains a low percent error even at a very large grid spacing. The last item of interest is the seismic source models used to perform the performance-based calculations. For this study, the 2008 USGS seismic source model was used. But this is not a single model, but an agglomeration of regional gridded, uniform, and local seismic zones (Peterson et al., 2008). For locations that lie on or near the boundaries of these regional seismic zones, significant spatial bias can be introduced with interpolations that draw from differing zones. Two points in particular from this study were affected by this: Reno, NV and Jackson, WY. Even with grid spacings of less than 1 km, less than 5% error was not achieved in these locations. Jackson, WY was located near five different regional seismic zones: Yellowstone Parabola, Snake River Plain, Basin and Range, and Rocky Mountain. The points examined in such a location can be analyzed with differing attenuation relationships, causing simple linear interpolations between points to introduce significant spatial bias. This is a limitation of the USGS 2008 seismic source model for points located near regional boundaries.

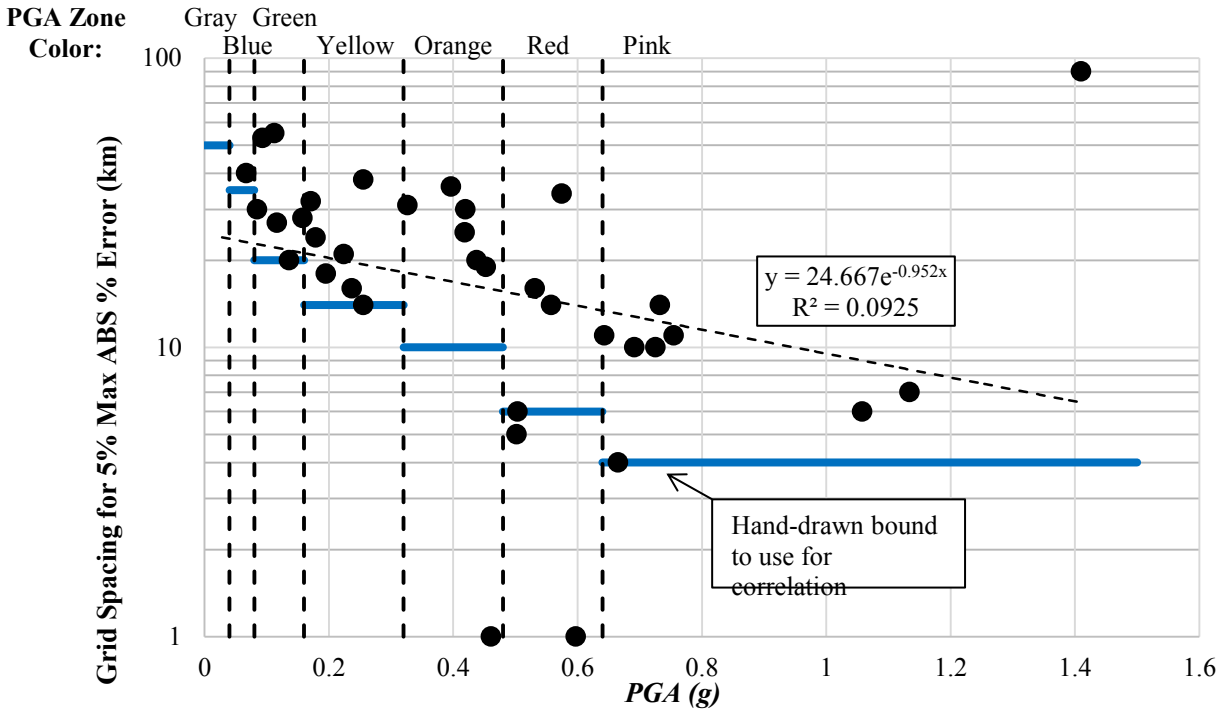


**Figure 5-6: Correlation Between PGA and Optimum Grid Spacing (Based on $D_H$)**

The recommended grid spacing for the lateral spread reference map can be seen in Table 5-3. Note that this grid spacing study does not provide estimates of accuracy between the simplified performance-based method and the full performance-based method. The measurements of error calculated in this grid spacing study reflect only the error involved in interpolation between grid points.

### 5.3.2 Development of the Lateral Spread Reference Parameter Maps

To develop a lateral spread reference map, each location needs to be divided into bins based on PGA. This can done quite conveniently using the 2008 USGS PGA Hazard Maps, seen in Figure 5-7

**Table 5-3: Proposed Grid Spacing for Development of Lateral Spread Reference Parameter Maps**

| *PGA* | Lateral Spread | |
|---|---|---|
| | Spacing (km) | Spacing (mi) |
| 0 - 0.04 | 50 | 31.1 |
| 0.04 - 0.08 | 30 | 18.6 |
| 0.08 - 0.16 | 20 | 12.4 |
| 0.16 - 0.32 | 13 | 8.1 |
| 0.32 - 0.48 | 9 | 5.6 |
| 0.48 - 0.64 | 6 | 3.7 |
| 0.64+ | 4 | 2.5 |

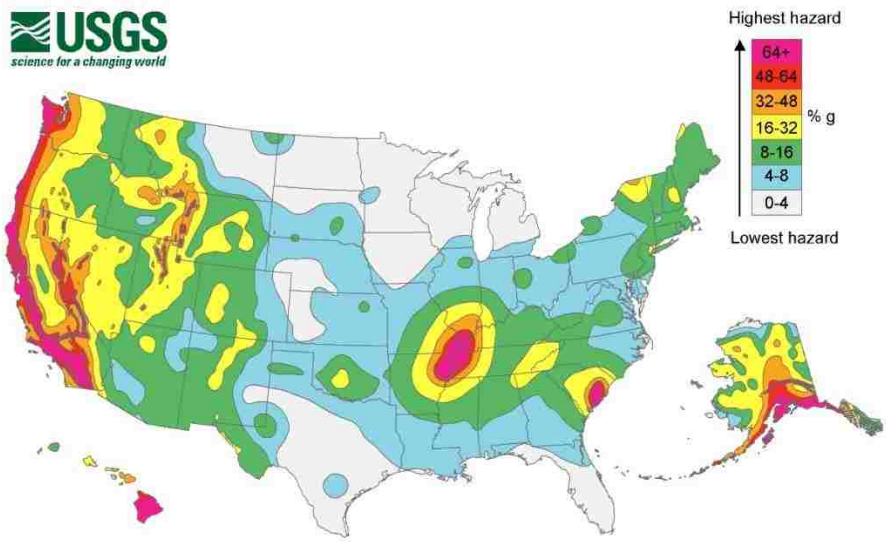


**Figure 5-7: 2008 USGS PGA Hazard Map ($T_R$=2475 years) (after USGS, 2008a)**

For this research six states were selected, and lateral spread reference maps were generated for the 475, 1033, and 2475 year return periods for the entire state. These states are: Alaska, Connecticut, Idaho, Montana, South Carolina, and Utah. The USGS has made available GIS shapefiles representing the same PGA values seen in Figure 5-7, and using ArcMap each

state was divided up into bins based on these shapefiles. The grid points were generated in ArcMap using the recommended grid spacing seen in Table 5-3 for each bin. An example of a state divided into bins based on PGA from the 2008 USGS PGA map as well as with grid points can be seen in Figure 5-8. This process was repeated for every state.

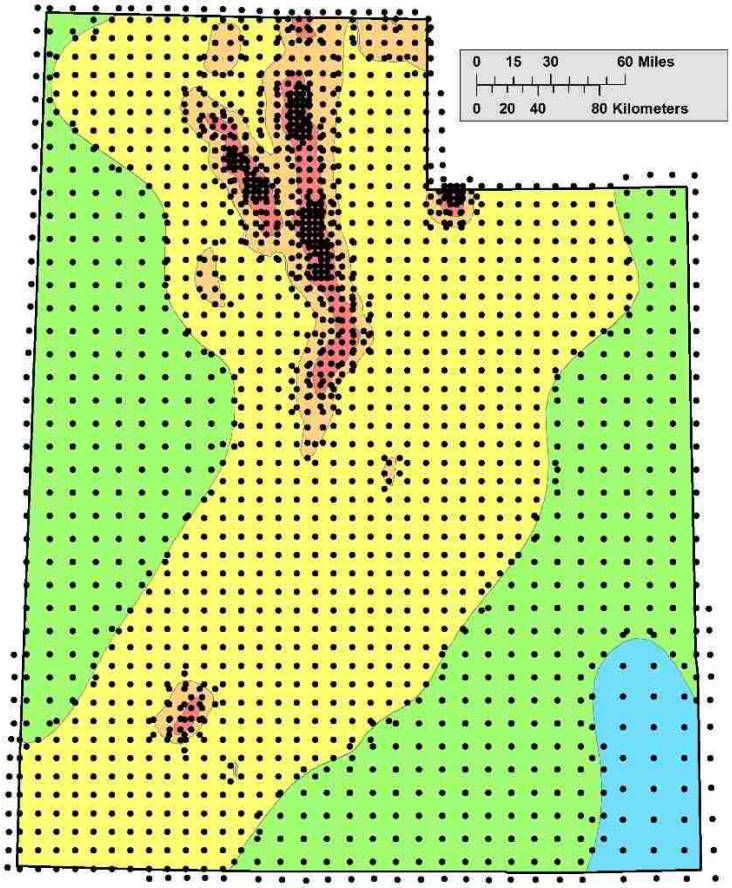


**Figure 5-8: Grid Points of Utah Combined With 2008 USGS PGA Hazard Map**

### 5.3.3 Analysis of the Grid Points

Once the grid points were developed for all the states, the location of each of the points was analyzed for the reference lateral spread displacement using the reference soil profile seen in

Figure 5-2. The performance-based analysis was performed using the commercial software EZ-FRISK (Risk Engineering, 2010). The program is usually utilized to perform probabilistic calculations of ground motions, but by creating a custom attenuation table based on magnitude and source-to-site distance, the reference lateral spread displacement was determined. The general analysis procedure in EZ-FRISK is outlined in this section.

EZ-FRISK is generally used to determine ground motion parameters using attenuation relationships. Therefore to probabilistically evaluate the Youd et al. (2002) model, the lateral spread displacement must be represented in an attenuation table. An attenuation table is created by determining the lateral spread displacement (based on the reference profile) for a range of magnitude and source-to-site distances. The attenuation table must meet the formatting guidelines presented in the EZ-FRISK help manual. An example of such a table can be seen Figure 6-9. This table needs the title of the table, the PGA (which does not matter so can be defaulted to 0.01), the number of increments of distance and magnitude, an range of distances increasing to the right, a range of magnitudes increasing downward, the displacement associated with each combination of magnitude and distance, and the uncertainty of every displacement value. Once the table is created, it is uploaded into EZ-FRISK and saved as a new attenuation equation, which can be seen in Figure 6-10. It should be noted that displacement is not a variable that is recognized by EZ-FRISK, so all the predicted displacements will be considered as accelerations, so caution should be used when performing the analysis in EZ-FRISK to keep track of variables.

| | | | | | | | |
|---|---|---|---|---|---|---|---|
| Youd et al (2002) | | | | | | | |
| 1 | | | | | | | |
| 0.01 | 20 | 20 | | | | | |
| 1 | 5 | 10 | 15 | 20 | 25 | 30 | 40 |
| 4.6 | | | | | | | |
| 0.009411 | 0.000905 | 0.000299 | 0.000147 | 8.56E-05 | 5.45E-05 | 3.68E-05 | 1.86E-05 |
| 0.454 | 0.454 | 0.454 | 0.454 | 0.454 | 0.454 | 0.454 | 0.454 |
| 4.8 | | | | | | | |
| 0.018688 | 0.001825 | 0.000603 | 0.000298 | 0.000173 | 0.00011 | 7.44E-05 | 3.77E-05 |
| 0.454 | 0.454 | 0.454 | 0.454 | 0.454 | 0.454 | 0.454 | 0.454 |
| 5 | | | | | | | |
| 0.03676 | 0.003673 | 0.001218 | 0.000602 | 0.00035 | 0.000223 | 0.00015 | 7.62E-05 |
| 0.454 | 0.454 | 0.454 | 0.454 | 0.454 | 0.454 | 0.454 | 0.454 |
| 5.2 | | | | | | | |
| 0.071334 | 0.00737 | 0.002455 | 0.001215 | 0.000708 | 0.000451 | 0.000304 | 0.000154 |
| 0.454 | 0.454 | 0.454 | 0.454 | 0.454 | 0.454 | 0.454 | 0.454 |
| 5.4 | | | | | | | |
| 0.135791 | 0.014723 | 0.004937 | 0.002448 | 0.001428 | 0.000911 | 0.000615 | 0.000312 |
| 0.454 | 0.454 | 0.454 | 0.454 | 0.454 | 0.454 | 0.454 | 0.454 |

**Figure 5-9: Example Attenuation Table for EZ-FRISK Analysis**

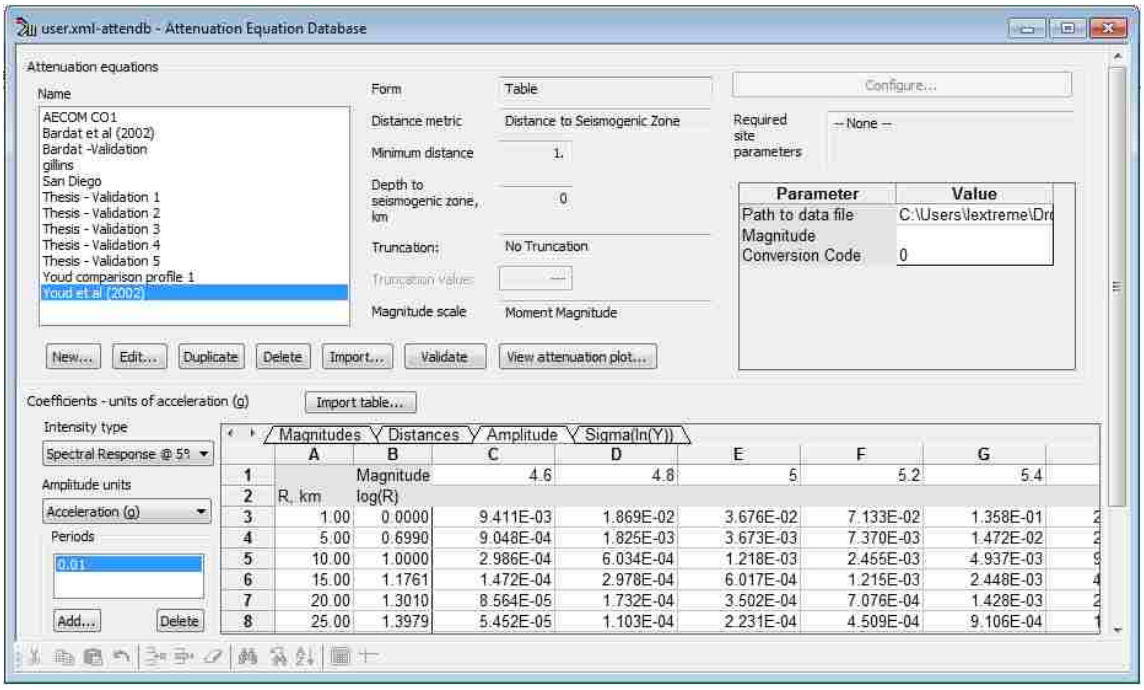


**Figure 5-10: EZ-FRISK Attenuation Equation Database (Risk Engineering, 2010)**

Before the analysis can be run, the analysis options need to be set to the appropriate settings and the correct seismic source models need to be selected. Most of the default options are acceptable, but the intensity type option needs to be set to "Geometric mean horizontal component of spectral response at 5% damping" and the amplitude units set to "Acceleration (g)". These options can be seen in Figure 6-11.

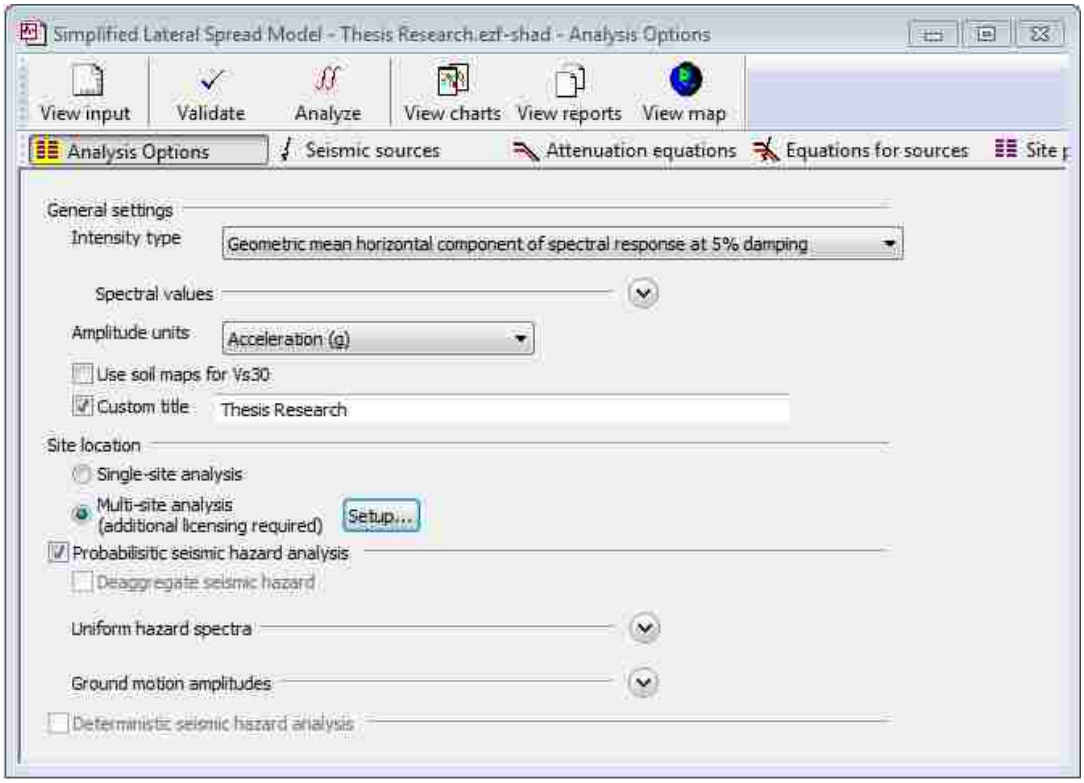


**Figure 5-11: EZ-FRISK Analysis Options (Risk Engineering, 2010)**

Utilizing EZ-FRISK requires that a seismic source model be selected. To analyze the points in Connecticut, Idaho, Montana, South Carolina, and Utah the USGS 2008 seismic source model was used (Peterson et al., 2008), and for Alaska the USGS 2002 seismic source model was used. Only area sources and faults were considered within 300 km of each site, with the

exception of subduction zone sources which were considered within 500 km. To select the appropriate seismic source, the Select Seismic Sources tool is used, which can be seen in Figure 6-12.

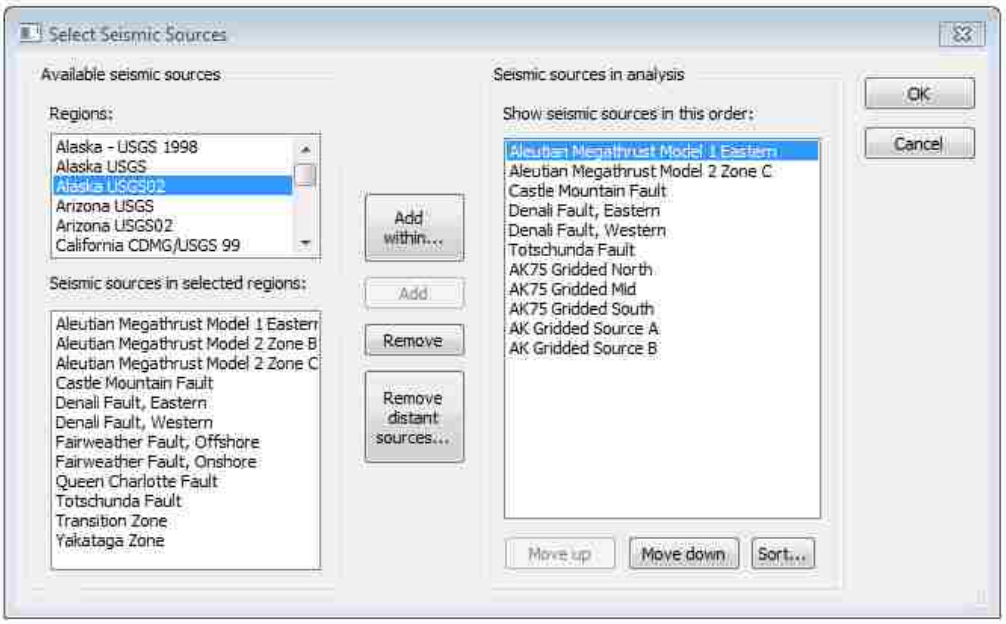


**Figure 5-12: EZ-FRISK Seismic Source Selection Tool (Risk Engineering, 2010)**

The next step is to import the grid points and then run the analysis. The results of the analysis will be saved a .txt file. Once all of the points for a particular state were successfully run, the results were compiled and then imported back into ArcMap to begin the process of making the parameter maps.

### 5.3.4 Creation of the Reference Parameter Maps

Once the analyzed grid points were imported back into ArcMap the points needed to be converted to a contour map. The conversion was done by interpolating the individual points into a surface raster using the Kriging tool. This tool interpolates between each point and makes a

surface with a value at every point. To ensure that the contours of each state run all the way to the border, the state shape is buffered slightly (10 km). The Kriging raster is created based on this buffered shape. Once the Kriging raster is made, the raster surface needs to be converted into a contour.

To make the contour with Kriging, first the spacing of the contours needed to be determined. It was important that the contour spacing be fine enough that the detail of the map could be read, but far enough apart that the contours can be read. The contour spacing will therefore generally vary from map to map based on this process. An example of a Kriging raster and contour for the state of Utah can be seen in Figure 5-13.

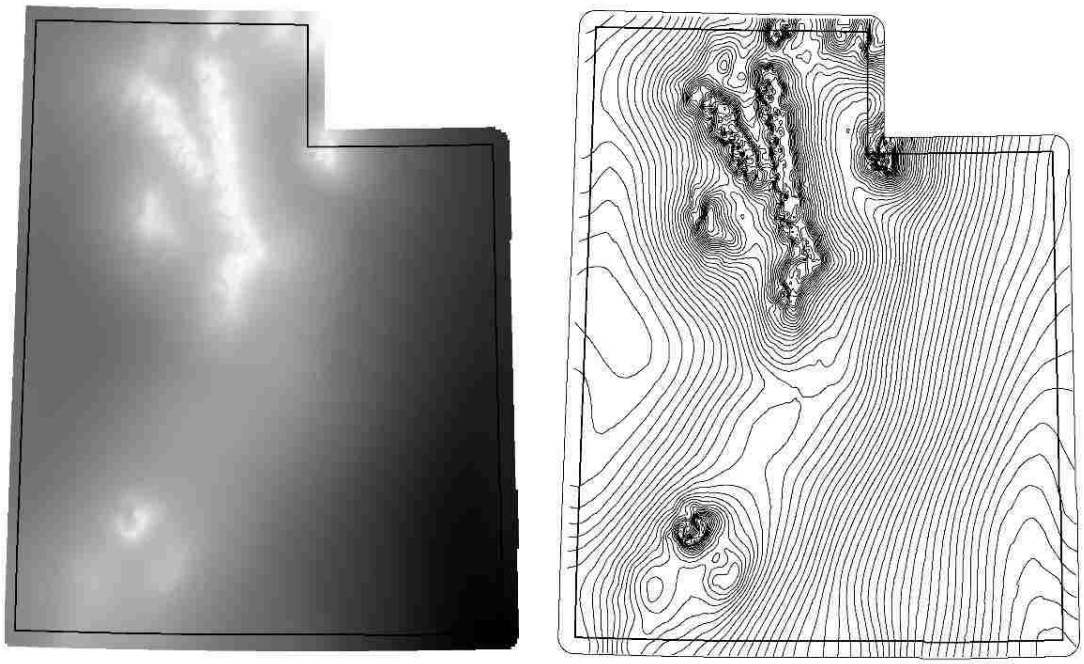

a) b)

**Figure 5-13: a) Kriging Raster and b) Contours for Utah ($T_r$ = 2475 yrs).**

Once the proper contour spacing is determined for each map, the contour is labeled and clipped to fit the state shapefile. Then a basemap and reference features are added to provide more detail about the topography to the parameter maps. Maps for each of the states for each of the three analyzed return periods can be seen in Appendix A.

The lateral spread reference map shows the reference value of displacement, $D_H^{ref}$ as calculated using the Youd et al. (2002) model, and is given in units of Log (meters). Careful attention needs to be given to the labeling of each map to ensure that map was developed with correct return period and that the reference value used in the later steps of the simplified method can be accurately read from the contours.

The maps created in this study are only of limited practical use in a simplified analysis. They were created to show the potential form of the maps, and the maps themselves are not of sufficient scale to discern the value of the reference parameter with any real accuracy. The practical result of the mapping portion of the simplified procedure is that raster shapefiles. With those, the reference value can be determine at any location, down to the width of a single pixel. Additionally, the raster can be used in a GIS program such as ArcMap to generate maps of any location, scale, and contour fineness.

### 5.3.5 Simplified Performance-Based Procedure

The overall simplified performance-based lateral spread assessment procedure can be performed with just a few simple steps:

1. Retrieve the reference lateral spread displacement from the appropriate map. These maps can be generated for any return period and essentially any location, and so once a hazard level for a site has been selected, the map that represents that hazard should be used.

2. Determine the site specific soil parameters. The simplified method allows the reference lateral spread displacement to be corrected to site specific soil information, so the appropriate soil parameters (fines content, mean grain size, thickness of liquefiable layer, etc.) need to be determined.
3. Compute the correction factor $\Delta D_H$ using Equation 5-4.
4. Compute the site specific lateral spread displacement using Equation 5-5.

As seen in these steps, the simplified procedure is simple, straightforward, and when programmed into a spreadsheet extremely quick to perform. This does not mean that the process developing the simplified method is simple. Behind every lateral spread reference map, thousands of full performance-based analyses were performed. The process allows engineers to have objectively and quantitatively assess the lateral spread hazard at a site, without having extensive experience, training, or software.

## 5.4 Chapter Summary

Developing the simplified performance-based lateral spread model involves creating lateral spread reference maps, and then correcting the reference value to a site specific lateral displacement. The Youd et al. (2002) empirical MLR lateral spread model was incorporated into a PBEE framework recommended by PEER. The simplified method equations were derived using a reference soil profile and the correction factor $\Delta D_H$ was derived.

To create the lateral spread reference maps, a grid of points was generated based on PGA and the recommended grid spacing determined in an optimum grid spacing study. The grid of points were analyzed and the results were interpolated into a kriging raster surface and then used

to make a contour map. This contour represents the reference lateral spread displacement for a given hazard level (i.e. return period).

Using the simplified procedure, the benefits of a PBEE seismic hazard analysis are available, without extensive experience, expertise, or specialized software. The process can be easily programmed into a spreadsheet and can be easily incorporated into any analysis where lateral spread is a concern.

# 6 VALIDATION OF SIMPLIFIED METHOD

## 6.1 Introduction

If the proposed simplified performance-based lateral spread displacement procedure is to be useful to engineering practitioners, then it must predict probabilistic displacements that closely approximate (i.e., $\leq 5\%$ error) the displacements that would be predicted by the full performance-based procedure (Franke and Kramer, 2014). To assess the effectiveness and accuracy of the proposed simplified procedure in approximating the results from the full performance-based procedure, a validation study was performed.

## 6.2 Methodology

To determine if the simplified method approximates the full performance-based method, 10 cities of varying seismicity were selected and then four different soil profiles were analyzed with both procedures. Then the results of the analyses were examined and the percent error and differential displacement were compared. If the average error between the two methods is five percent or less than the simplified method will be considered validated.

### 6.2.1 Soil Profiles

Four separate, hypothetical soil profiles were used in the validation study. The first two soil profiles, seen in Figure 6-1, represent ground-slope cases with $T_{15} = 1.0$ meters, $F_{15} = 25\%$,

$D50_{15} = 1.0$ mm, and $S = 1\%$ for the first profile, and $T_{15} = 4.0$ meters, $F_{15} = 15\%$, $D50_{15} = 0.5$ mm, and $S = 3\%$ for the second. Using Equation 4-17 and Figure 7-1, values of 9.846 and 8.965 for the $\mathcal{S}^{site}$ were computed for these profiles respectively. The second set of soil profiles, seen in Figure 6-2, represent two free-face cases with $T_{15} = 1.0$ meters, $F_{15} = 40\%$, $D50_{15} = 0.5$ mm, and $W = 12\%$ for the first profile, and $T_{15} = 2.0$ meters, $F_{15} = 30\%$, $D50_{15} = 0.1$ mm, and $W = 12\%$ for the second. Values of 9.829 and 9.059 for the $\mathcal{S}^{site}$ were computed for these profiles respectively. Finally, the soil profile presented in Figure 5-2 was used to develop the reference lateral spread displacements, $[\log D_H]^{ref}$ in the validation study. As previously reported, $\mathcal{S}^{ref}$ for the reference site profile was computed to be 9.043.

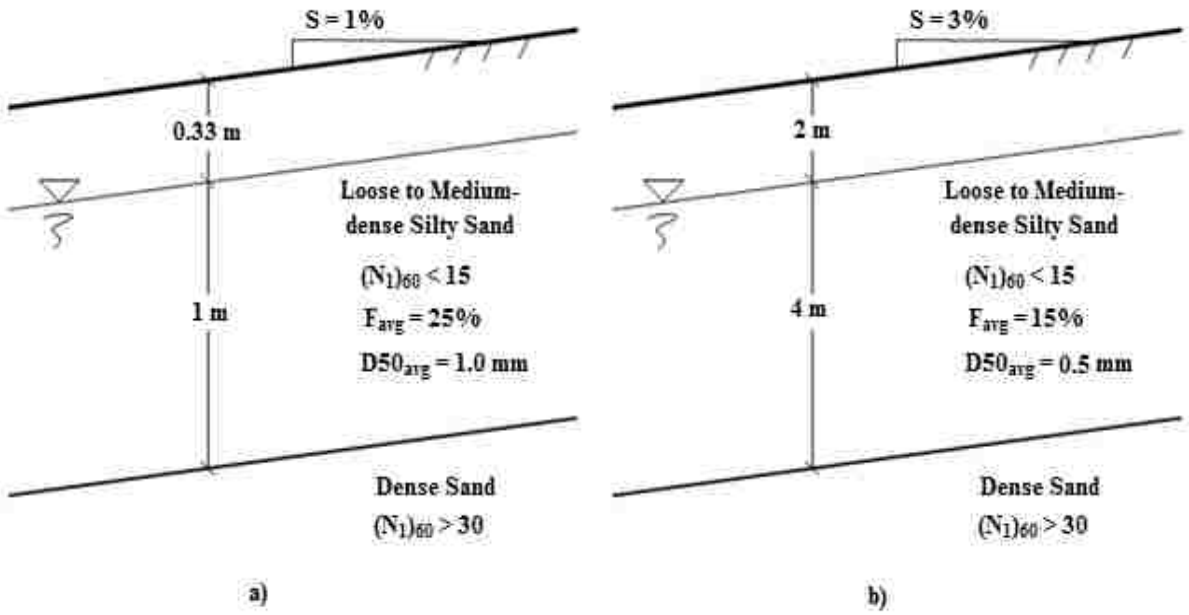


**Figure 6-1: Site-Specific Ground-Slope Profiles Used in the Validation Study**

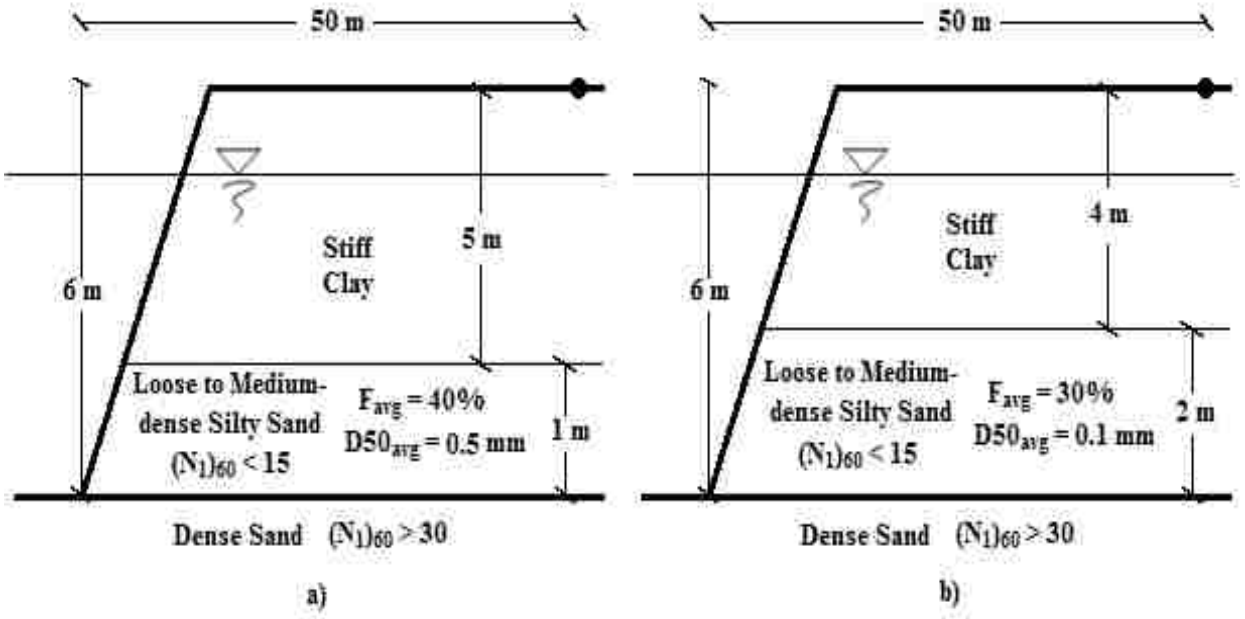


**Figure 6-2: Site-Specific Free-Face Soil Profiles Used in the Validation Study**

### 6.2.2 Site Locations

Ten cities located across the U.S. were selected as hypothetical sites for this study based on their wide ranging seismicity levels and their use in previous performance-based validation studies (Kramer and Mayfield, 2007; Franke and Kramer, 2014; Franke et al., 2014b, 2014c). The specific locations of the ten cities are provided in Table 6-1. Values of $\left[\log D_H\right]^{ref}$ for these cities were computed using *EZ-FRISK 7.60* with the Franke and Kramer (2014) performance-based procedure for the Youd et al. (2002) MLR empirical lateral spread model. The same seismic source model that was used by the U.S. Geological Survey (USGS) 2008 National Seismic Hazard Mapping Project (Petersen et al., 2008) was incorporated in this study.

**Table 6-1: Selected Cities Used in the Validation Study**

| Site | Latitude | Longitude |
|---|---|---|
| Butte | 46.003 | -112.533 |
| Charleston | 32.726 | -79.931 |
| Eureka | 40.802 | -124.162 |
| Memphis | 35.149 | -90.048 |
| Portland | 45.523 | -122.675 |
| Salt Lake City | 40.755 | -111.898 |
| San Francisco | 37.775 | -122.418 |
| San Jose | 37.339 | -121.893 |
| Santa Monica | 34.015 | -118.492 |
| Seattle | 47.53 | -122.3 |

## 6.3 Comparison Between Full and Simplified Methods

With values of $\left[\log D_H\right]^{ref}$, $\mathcal{S}^{ref}$, and $\mathcal{S}^{site}$ computed for each city and soil profile, Equations 5-4 and 5-5 were used to compute probabilistic values of $D_H^{site}$ corresponding to the three return periods of interest ($T_R$ = 475 years, $T_R$ = 1033 years, and $T_R$ = 2475 years). In addition, *EZ-FRISK 7.63* was used with the Franke and Kramer (2014) full performance-based procedure to compute "true" values of $D_H^{site}$ at each of the ten cities for each of the three return periods of interest. The resulting probabilistic values of $D_H^{site}$ were then compared to the results from the simplified procedure for the ground-slope and free face soil profiles.

The difference between the simplified and full performance-based values of $D_H^{site}$ were determined, and the resulting errors were computed. These errors, as well as the average difference between the results of both procedures, are summarized for both the ground-slope and free face soil profiles in Table 6-2. In general, the resulting error between the proposed simplified lateral spread procedure and the full performance-based lateral spread procedure is

less than 5%, and in most instances less than 3%. Only 7 out of 60 possible site/soil profile/return period combinations resulted in prediction errors greater than 5%, and of those, most were found in the Charleston and Memphis locations. Despite the error higher than 5%, the discrepancy between procedures is at the most only 4 cm for these locations, which is negligible considering the relatively large amount of variability present in the Youd et al. (2002) model.

**Table 6-2: Summary Table of the Results of the Validation Study**

| Site | Return Period | Free Face Profiles | | Ground Slope Profiles | |
|---|---|---|---|---|---|
| | | Average Difference | Average Error | Average Difference | Average Error |
| | [year] | [meter] | | [meter] | |
| Butte | 475 | < 0.01 | 1.2% | < 0.01 | 1.1% |
| | 1033 | < 0.01 | 1.0% | < 0.01 | 0.9% |
| | 2475 | < 0.01 | 0.2% | < 0.01 | 0.1% |
| Charleston | 475 | < 0.01 | 1.9% | < 0.01 | 1.8% |
| | 1033 | < 0.01 | 6.8% | < 0.01 | 6.4% |
| | 2475 | < 0.01 | 2.0% | < 0.01 | 1.9% |
| Eureka | 475 | 0.03 | 1.1% | 0.01 | 0.3% |
| | 1033 | 0.04 | 0.4% | 0.03 | 0.4% |
| | 2475 | 0.03 | 0.4% | 1.04 | 3.8% |
| Memphis | 475 | < 0.01 | 6.6% | < 0.01 | 8.7% |
| | 1033 | 0.04 | 15.1% | < 0.01 | 15.8% |
| | 2475 | < 0.01 | 1.3% | < 0.01 | 1.3% |
| Portland | 475 | < 0.01 | 2.3% | < 0.01 | 2.0% |
| | 1033 | < 0.01 | 0.2% | 0.01 | 0.6% |
| | 2475 | < 0.01 | 0.2% | 0.01 | 0.4% |
| Salt Lake City | 475 | < 0.01 | 0.8% | 0.01 | 1.1% |
| | 1033 | < 0.01 | 0.3% | 0.06 | 2.4% |
| | 2475 | < 0.01 | 0.2% | 0.11 | 2.1% |
| San Francisco | 475 | 0.01 | 0.4% | 0.01 | 0.4% |
| | 1033 | 0.02 | 0.8% | 0.02 | 0.6% |
| | 2475 | 0.01 | 0.2% | 0.02 | 0.3% |
| San Jose | 475 | < 0.01 | 0.1% | < 0.01 | 0.1% |
| | 1033 | 0.01 | 0.5% | 0.01 | 0.4% |
| | 2475 | 0.01 | 0.3% | 0.01 | 0.4% |
| Santa Monica | 475 | < 0.01 | 0.6% | < 0.01 | 0.6% |
| | 1033 | < 0.01 | 0.3% | 0.01 | 0.4% |
| | 2475 | 0.01 | 0.3% | 0.01 | 0.4% |
| Seattle | 475 | < 0.01 | 0.5% | < 0.01 | 0.6% |
| | 1033 | 0.02 | 1.6% | < 0.01 | 0.1% |
| | 2475 | 0.14 | 8.3% | 0.01 | 0.2% |

The simplified and full performance-based values of $D_H^{site}$ from Table 6-2 are compared graphically in Figure 6-3. The data presented in Figure 6-3 suggest that the simplified performance-based lateral spread procedure provides a very good approximation of the full performance-based lateral spread procedure at the analyzed return periods. The data shown in Fig. 5 form a straight line with 1H:1V slope and very little scatter. Additionally, the $R^2$ value corresponding to all three analyzed return periods for the free-face and ground-slope profiles is 0.997.

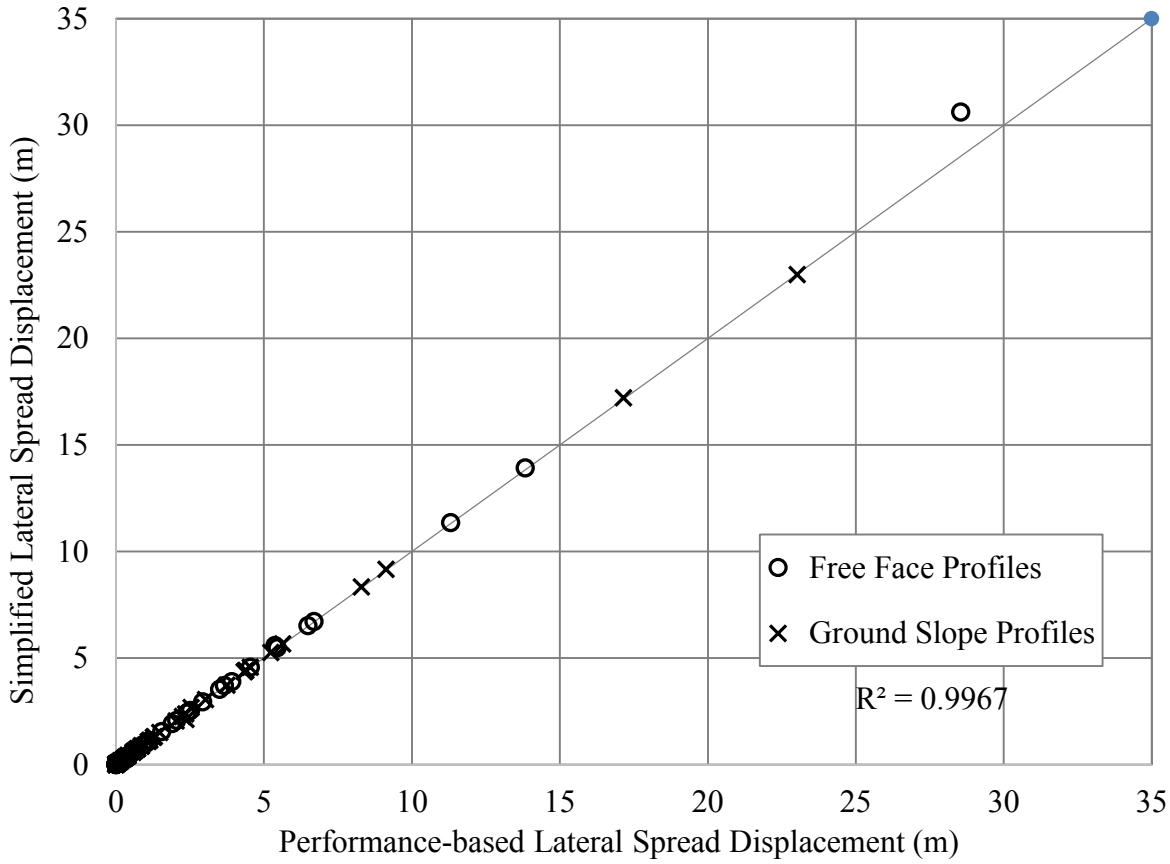


**Figure 6-3: Comparison of the Computed Lateral Dispalcements from the Validation Study**

## 6.4 Discussion of Results

The results of the validation study show a very close fit of the data. The lack of any significant scatter in the results seems too good to be true. But unlike many other simplified procedures, the simplified lateral spread model was mathematically derived. There would be more worry if the fit was not so close. This is one of the strengths of the simplified procedure; though it is simple to perform, there are full performance-based analyses backing up every reference value. The value of the simplified method is that the method overall is simple, but the procedure requires that full performance-based lateral spread assessments for the reference maps to be developed. Therefore, the end user is using the results of the full procedure without having to personally run the more sophisticated and difficult analysis.

There are some limitations with the simplified performance-based procedure. Like all empirically derived models, there are limits on the magnitudes of parameters that can be entered into the model and the range of predicted values. All of the requirements that apply to the Youd et al. (2002) empirical lateral spread model still apply to the simplified models. For example, the Youd et al. (2002) model limits predicted displacements to 6 m. In many areas of high seismicity, the model can predict displacements far greater than 6 m. Therefore, it is essential to understand the limits of the Youd et al. (2002) model to ensure that results from the simplified procedure are within reason.

An additional issue with the simplified model, and probabilistic procedures in general, is that in areas of high seismicity, the model predicts unreasonably high values of lateral spread. The probabilistic approach considers all potential seismic sources, at all possible magnitudes, but also consider multiple faults rupturing simultaneously. This is extremely unlikely, but the probabilistic process considers it. To handle the unreasonably large predicted values in high

seismic locations, a deterministic cap is recommended. In areas of high hazard, a probabilistic and deterministic analysis should be performed and the lower of the two results should govern. This should ensure that the magnitude of lateral spread displacements are not over predicted in zones of high seismic hazard

## 6.5 Chapter Summary

To validate the simplified method, 10 sites selected and four differing soul profiles were analyzed using the simplified and full performance-based lateral spread displacement methods. The results of the validation study show that the simplified method can approximate the results of a full performance-based procedure within an acceptable amount of error (<3% on average).

When using any empirical model, ensure that the parameters inputted into the model are within the bounds recommended by the researchers. This will prevent extrapolation outside the recommended range of predicted values. Additionally, probabilistic procedures can predict very high hazard in areas of high seismic, so great care should be taken when utilizing performance-based approaches in such areas.

# 7 COMPARISON WITH DETERMINISTIC ANALYSIS

## 7.1 Introduction

This section provides comparisons between the pseudo-probabilistic, deterministic, and simplified performance-based procedures for estimating liquefaction initiation hazard and lateral spread displacement. The purpose of these comparisons is to identify how the deterministic procedure should be used in the proposed simplified procedure, and when, if at all, it would be appropriate to forgo the PBEE approach for the deterministic methodology.

Three cities of varying seismicity were selected for the comparison study: San Francisco (high seismicity), Salt Lake City (medium seismicity), and Butte (low seismicity). For each city, three analyses were performed: probabilistic (simplified performance-based procedure developed as part of this research), pseudo-probabilistic (AASHTO), and deterministic. A description of the deterministic and pseudo-probabilistic methods is provided in the following section.

### 7.1.1 Deterministic Analysis

The deterministic procedure to predict lateral spread displacements is very similar to the manner in which ground motions are obtained through a DSHA. The seismic sources in the nearby region of the site of interest are identified, and their maximum magnitude and smallest distance are determined. The source which produces the largest lateral displacement in the area becomes the governing earthquake.

The software EZ-FRISK was used to identify the top five seismic sources within 200 km for San Francisco and Salt Lake City. The 2008 USGS Seismic Source Model within EZ-FRISK does not include some smaller faults in low seismic regions, such as Butte. Thus, the governing fault for Butte (Rocker Fault) was identified using the USGS quaternary fault database (Haller, 1994). In the case of Salt Lake City and San Francisco, values of $M_w$ and $R$ were determined using the seismic source models provided by EZ-FRISK. For Butte, the 50$^{th}$ and 84$^{th}$ percentile $M_w$ values were estimated using a correlation with surface rupture length developed by Wells and Coppersmith (1994), and the R was found using measured dimensions of the Rocker Fault available in the fault database. Summaries of the seismic sources considered in this DSHA and details of the Rocker Fault calculations are provided in Tables B.1 and B.2, respectively, in the Appendix. Once the model inputs have been determined through the DSHA they are entered into the Youd et al. (2002) empirical lateral spread model. A summary of the governing input variables utilized in the lateral spread displacement models are provided in Table 7-1.

**Table 7-1: Input Variables Used in the Deterministic Analysis**

| Location | Latitude | Longitude | Distance [km] | Mean $M_w$ |
|---|---|---|---|---|
| Butte | 46.003 | -112.533 | 4.92 | 6.97 |
| Salt Lake City | 40.755 | -111.898 | 1.02 | 7.00 |
| San Francisco | 37.775 | -122.418 | 12.4 | 8.05 |

Once the seismic components of the Youd et al. (2002) model have been determined, then those values and the site specific are entered into the model suing the procedure outline in Chapter 3, Section 3.4.3.

### 7.1.2 Pseudo-probabilistic Analysis

In the pseudo-probabilistic procedure, the variables used in the empirical lateral spread hazard models are obtained from a Probabilistic Seismic Hazard Analysis (PSHA). Then these variables are used in the same deterministic procedure outlined previously to determine the lateral spread displacement. To find these variables using a PSHA the USGS 2008 interactive deaggregation website (USGS, 2008) was utilized. This procedure involved entering the latitude and longitude of the target cities, then selecting the return period for the analysis. Using this tool, the mean magnitude $M_w$ and source-to-site distance $R$ were obtained for a return period of 1,039 years for each city of interest. The resulting values are summarized in Table 7-2.

**Table 7-2 Input Values Found Using USGS 2008 Deaggregations ($T_R$ = 1,039 years)**

| Location | Latitude | Longitude | Distance (km) | Mean $M_w$ |
|---|---|---|---|---|
| Butte | 46.003 | -112.533 | 24.9 | 6.03 |
| Salt Lake City | 40.755 | -111.898 | 4.20 | 6.84 |
| San Francisco | 37.775 | -122.418 | 12.0 | 7.38 |

## 7.2 Comparison of the Simplified and Deterministic Methods

Each city was evaluated using the three analysis types discussed previously (probabilistic, pseudo-probabilistic, and deterministic). The results of each analysis is plotted together for each city, which will allow easy comparison between the three methods. These comparisons can be seen in Figure 7-1, Figure 7-2, and Figure 7-3 for Butte, Salt Lake City, and San Francisco respectively.

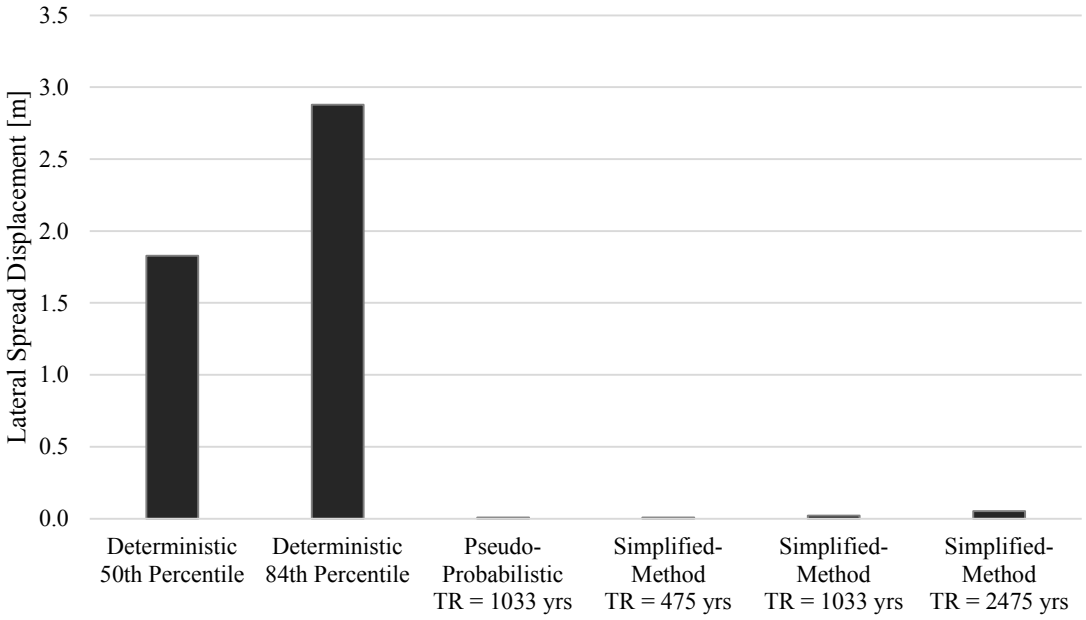


**Figure 7-1: Comparison of Deterministic, Pseudo-probabilistic, and Simplified Methods for Butte, MT**

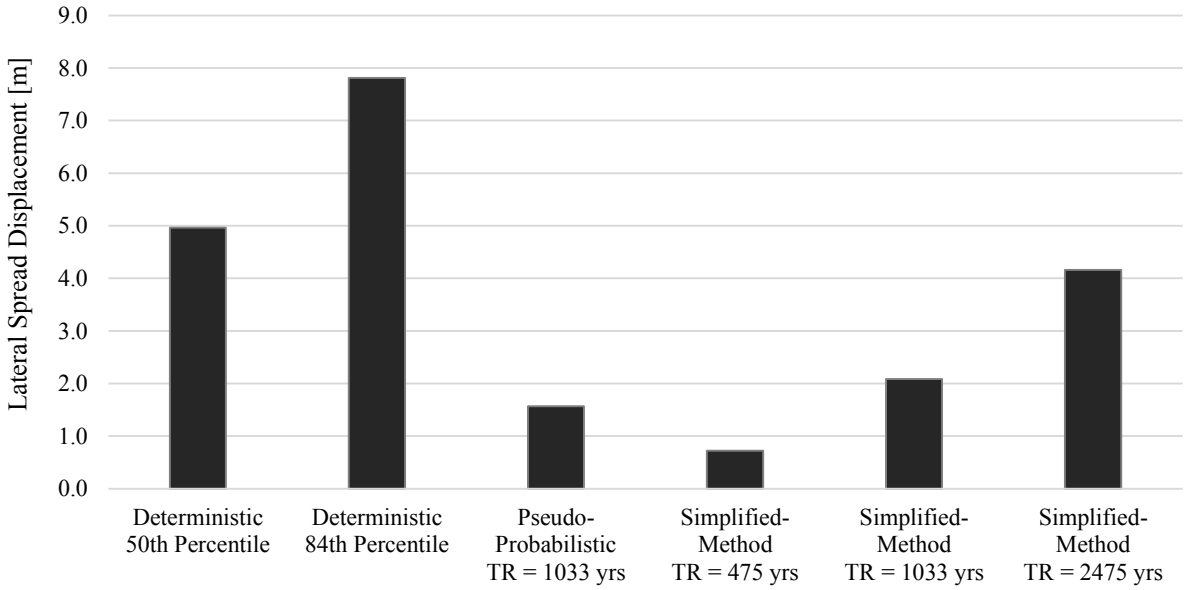


**Figure 7-2: Comparison of Deterministic, Pseudo-probabilistic, and Simplified Methods for Salt Lake City, UT**

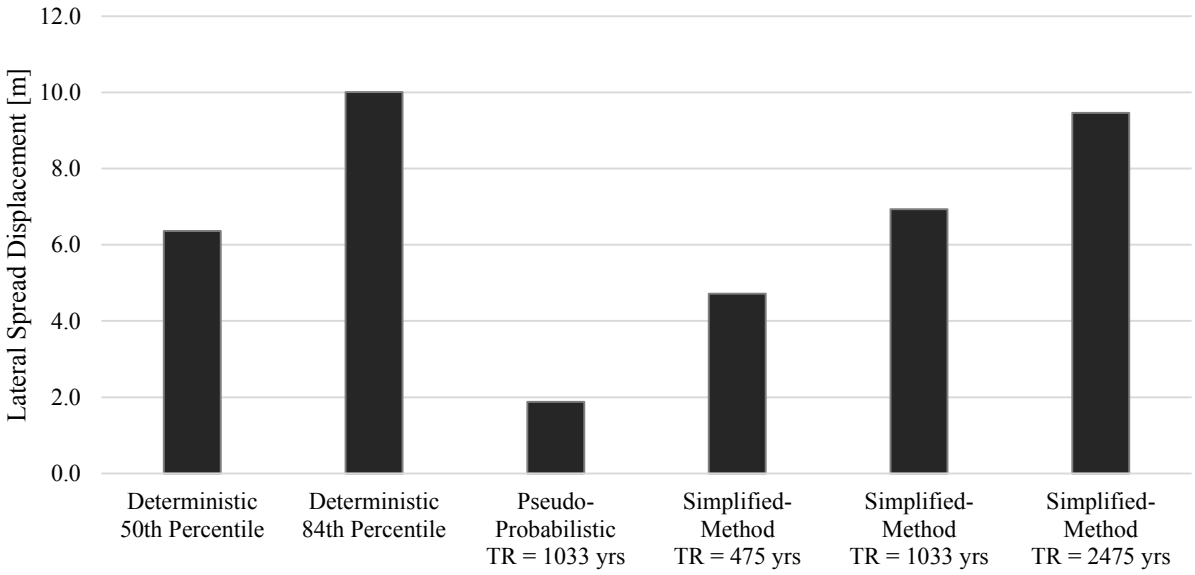


**Figure 7-3 Comparison of Deterministic, Pseudo-probabilistic, and Simplified Methods for San Francisco, CA**

The different cities are associated with regions of differing seismicity, and the deterministic comparisons with the simplified results yield some interesting conclusions. In the city with low seismicity, Butte seen in Figure 7-1, the deterministic method massively over-predicts the displacements predicted by the simplified and pseudo-probabilistic methods. This result can be attributed to the deterministic procedure not accounting for the likelihood of the Rocker fault rupturing, and predicts a displacement that may have an extremely low probability of occurring. The medium seismicity city, Salt Lake City seen in Figure 7-2, shows as well that the deterministic method predicts displacements higher than the simplified and pseudo-probabilistic procedures. In San Francisco, the high seismicity city, the results are much more similar at the 2475 return period, as can be seen in Figure 7-3. In this area the simplified method for the 2475 year return period predicts a slightly higher displacement than the deterministic

mean value. The deterministic 84$^{th}$ percentile still predicts a higher value than the simplified method at the 2475 year return period.

### 7.3 Discussion of Results

The results of this comparison show that deterministic methods severely over-predicted liquefaction hazard in Butte—an area of low seismicity. The deterministic results also slightly over-predicted liquefaction hazards at high return periods in Salt Lake City—an area of medium seismicity. In San Francisco—an area of high seismicity—the deterministic methods slightly under-predicted liquefaction hazard when considering the 50$^{th}$ percentile ground motions in the deterministic method and the 2,475-year return period in the simplified performance-based procedures. These results suggest that the deterministic results could be used as an upper-bound in areas of high seismicity, but in areas of low seismicity, the deterministic analysis could be optional. Engineers performing analyses in areas of medium to high seismicity could choose to use a deterministic analysis as a "reality check" against the simplified performance-based results. If both deterministic and performance-based methods are considered, the *lower* result is the governing value. When deciding whether the deterministic or performance-based results should be accepted, engineers should apply the following rule: the *lower hazard governs*.

This rule may seem counter-intuitive, but the idea is not completely foreign—when developing a spectral acceleration design envelope, the lower of the deterministic and probabilistic values is the governing acceleration. Likewise, in a liquefaction hazard analysis, the lower value governs. If the deterministic value is lower than the performance-based value, the combination of multiple seismic sources in the performance-based analysis may suggest greater liquefaction hazard then would be caused by a single, nearby, governing fault. Therefore, the deterministic analysis provides a type of "reality check" against the performance-based

analysis, and the deterministic results should be accepted. If the performance-based value is lower than the deterministic value, the nearby governing fault may have a significantly low likelihood of rupturing and achieving the 50$^{th}$ or 84$^{th}$ percentile ground motions. In this case, the deterministic results could be considered too extreme (especially for some projects which do not need to be designed to withstand such large events). Therefore, the performance-based results should be accepted as a representation of the more *likely* liquefaction hazard.

## 7.4 Chapter Summary

The result of a simplified performance-based lateral spread model was compared against the results of a deterministic and pseudo-probabilistic lateral spread analysis for three cities of varying seismicity. Based on the results, the deterministic method over-predicts lateral displacements in an area of low seismicity. The deterministic results also slightly over-predicted lateral displacements at high return periods in an area of medium seismicity. In an area of high seismicity the deterministic method slightly under-predicted liquefaction hazard when considering the 50$^{th}$ percentile lateral spread in the deterministic method and the 2,475-year return period in the simplified performance-based procedures. These results suggest that the deterministic results could be used as an upper-bound in areas of high seismicity, but in areas of low seismicity, the deterministic analysis could be optional. Engineers performing analyses in areas of medium to high seismicity could choose to use a deterministic analysis as a "reality check" against the simplified performance-based results.

# 8 SUMMARY AND CONCLUSIONS

Lateral spread is the horizontal movement of soil due to earthquake-induced liquefaction. It is one of the most destructive effects of earthquakes, and can be devastating to infrastructure and lifelines. Over the last 50 years, extensive research has been performed to understand this phenomenon and learn how to design for its effects. Lateral spread is a consequence of liquefaction, and so the history and process of liquefaction were briefly reviewed. The mechanics of lateral spread were examined, and some of the most widely used empirical predictive models were reviewed.

Accurately predicting the extent of lateral spread displacements is difficult, due to the uncertainty in the variables associated with earthquakes (location, size, and temporal occurrence) and uncertainty in the predictive relationship. To account for these sources of uncertainty, probabilistic seismic hazard analysis (PSHA) and performance-based earthquake engineering were introduced. These methodologies allow engineers to objectively quantify sources of uncertainty and provide results that more accurately represent a site.

PBEE and PSHAs are complicated and require specialized experience and expertise to perform, and make utilizing them difficult for practicing engineers. To provide the benefit of PBEE to the engineering community, this study introduced a simplified performance-based adaptation of the Youd et al. (2002) empirical procedure. This procedure incorporates lateral spread reference parameter maps developed with a reference soil profile. Using this simplified

model, practitioners can account for the uncertainties associated with predicting lateral spread without requiring extensive experience or specialized software. To ensure this, a validation study was performed that confirmed that the simplified procedure produces results that approximate the full-performance based procedure. Additionally, the simplified method was compared to a conventional deterministic lateral spread predictive procedure to determine the appropriate application of the simplified procedure in engineering practice.

This study resulted in several important observations about the simplified performance-based procedure, the development of the lateral spread reference maps, and the comparison with the deterministic procedure. These observations include:

1) Lateral spread is conditional upon liquefaction occurring, and needs to be assessed in tandem with liquefaction initiation. If liquefaction is not predicted to occur, then lateral spread will not occur.
2) Deterministic empirical lateral spread models can predict reasonably accurate results, if the appropriate seismic loading parameters are utilized. The determination of magnitude and source-to-site distance is the most crucial aspect of the procedure, and improper selection of these variables may result in unrepresentative predictions of lateral spread displacements.
3) Utilizing variables outside the bounds recommended by the model can result in extrapolation, and while this can be unavoidable at times, great caution and engineering judgment should be used in interpreting the results.
4) PBEE procedures allow greater ability to assess risk for a given site. The capability to analyze seismic hazards at a variety of return periods allows owners, engineers, and

stakeholders to more objectively account for the appropriate level of risk. This can lead to more resilient, cost effective structures and facilities.

5) The simplified performance-based models approximated the results of the full performance-based procedure within an acceptable amount of error, in most occasions within 3% of the full procedure.
6) When creating maps that require gridded analysis, great care should be taken for locations at or near the border between different seismic source models. Interpolating across such regions can introduce significant error into the mapped values.
7) The simplified procedure can be easily incorporated into current engineering practice due to the similarities between similar existing procedures for assessing other hazards, and how simply the simplified procedure can be incorporated into a spreadsheet. With access to lateral spread reference maps, site-specific soil information, and a pre-programmed spreadsheet, a PBEE estimation of lateral spread can be found in minutes.
8) The incorporation of performance-based procedures does not mean that deterministic procedures should be ignored. Probabilistic methods tend to overestimate hazard in area of high seismicity, so in such areas both performance-based and deterministic analyses should be performed, with the lower result governing.

## 8.1 Recommendations for Further Research

As a consequence of this research, several areas were recognized where further research is needed. The optimum grid spacing study, revealed many interesting aspects of the development of liquefaction hazard maps. Though the correlation of PGA and optimum grid

spacing utilized in this thesis was effective in determining optimum grid spacing, other correlations could be examined that could better represent the optimum grid spacing.

Additionally, the simplified procedure outlined in this thesis is only applicable to purely empirical models. Yet there are many semi-empirical and analytical models that could be incorporated into a probabilistic analysis. Adapting these models into a performance-based framework would provide additional tools to predict lateral spread hazard.

Lastly, the Youd et al. (2002) model and database have not been updated in nearly 13 years. Several significant earthquakes have occurred since the last model update (particularly the Christchurch, New Zealand sequence in 2011-2012) with many new case histories of lateral spread displacements. Incorporating these case histories into the model and re-regressing a new relationship would allow the prediction of lateral spread displacements to account for the additional data from these more recent events

## REFERENCES


Abrahamson, N.A., Silva, W.J., (1997). Empirical response spectral attenuation relations for shallow crustal earthquakes. *Seismological Research Letters*, 68, 94-127.

Abrahamson, N.A., Silva, W.J., (2008). Summary of the Abrahamson & Silva NGA ground-motion relations. *Earthquake Spectra*, 24(1), 67-98.

Abrahamson, N.A, Silva, W.J., Kamai, R. (2014). Summary of the ASK14 ground motion relation for active crustal regions. *Earthquake Spectra*, 30(3), 1025-1055.

Al Atik, L. (2009). "NGA Excel Spreadsheet, Version 1.0" *Pacific Earthquake Engineering Research Center*. <http://peer.berkeley.edu/products/rep_nga_models.html> (May, 2015).

Algermissen, S.T., Perkins, D.M., Thenhaus, P.C., Hanson, S.L., Bender, B.L. (1982). Probabilistic estimates of maximum acceleration and velocity in rock in the contiguous United States. *Open-File Report 82-1033,* U.S. Geological Survey, Washington, D.C., pp. 99.

American Association of State Highway and Transportation Officials. (2014). *AASHTO LRFD Bridge Design Specifications, 7th Ed.*, ISBN: 1-56051-592-0, AASHTO, Washington, D.C.

Ambraseys, N. (1988). Engineering Seismology. *Journal of Earthquake Engineering and Structural Dynamics*, 17, 1-105.

American Society of Civil Engineers. (2013). *Minimum Design Loads for Buildings and Other Structures (ASCE Standard ASCE/SEI 7-10, third printing)*, ISBN: 978-0-7844-1085-1, ASCE, Reston, VA.

Ancheta, T.D., Darragh, R.B., Stewart, J.P., Seyhan, E., Silva, W.J., Chiou, B., Woodell, K.E., Graves, R.W., Kottke, A.R., Boore, D.M., Kishida, T., Donahue, J.L. (2014) NGA-West2 database. *Earthquake Spectra*, 30(3), 989-1005.

Andrus, R.D., Piratheepan, P., Ellis, B.S., Zhang, J., Hsein Juang, C. (2004). Comparison of liquefaction evaluation methods using penetration-VS relationships. *Soil Dynamics and Earthquake Engineering*, 24(9-10), 713-721.

Arduino, S.A., Ilankatharan, M., Kramer, S.L., Kutter, B.L., Shin, H.S. (2006), Experimental and numerical analysis of seismic soil-pile-structure interaction of a two-span bridge.

*Proceedings, 8th U.S. National Conference on Earthquake Engineering, Paper No. 504.* Sand Francisco, CA.

Atkinson, G.M., Boore, D.M. (2003). Empirical ground-motion relations for subduction-zone earthquake and their application to Cascadia and other regions, *Bulletin of the Seismological Society of America*, 93(4), 1703-1729.

Baker, J.W. and Faber, M. (2008). Liquefaction risk assessment using geostatistics to account for soil spatial variability. *J. Geotech. Geoenviron. Eng.* 134(1), 14-23.

Balakrishnan, A., Kutter, B.L., Idriss, I.M. (1997). Liquefaction remediation at bridge sites-centrifuge data report for BAM05. *Report No. UCD/CGMDR-91/10*, Center for Geotechnical Modeling: University of California at Davis.

Bardat, J.P., Mace, N., and Tobita, T. (1999). "Liquefaction-induced ground deformation and failure." *Report to PEER/PG&E, Task 4A – Phase I*, May 4, 1999, 125 pp.

Bardat, J.P., Tobita, T., Mace, N., Hu, J. (2002). Regional modeling of liquefaction-induced ground deformation. *Earthquake Spectra*, 18(1), 19-46.

Bartlett, S.F. and Youd, T.L. (1992). "Empirical analysis of horizontal ground displacement generated by liquefaction-induced lateral spread." *Report No. NCEER-92-0021*, NCEER, State University of New York, Buffalo, 114 pp.

Bartlett, S.F., and Youd, T.L. (1995). "Empirical prediction of liquefaction-induced lateral spread." *J. Geotech. Eng.,* 121(4), 316-329.

Baska, D. (2002). "An analytical model for prediction of lateral spread displacement." *Ph.D. Dissertation,* Univ. of Washington, Seattle, WA.

Bazier, M.H., Dobry, R., Elgamal, A.W. (1992). Engineering evaluation of permanent ground deformations due to seismically-induced liquefaction. *Technical Report NCEER-92-0007*, Buffalo, New York: National Center for Earthquake Engineering Research, State University of New York.

Bertero, R.D., Bertero, V.V. (2002). Performance-based seismic engineering: the needs for a reliable conceptual comprehensive approach. *Earthquake Engineering and Structural Dynamics*, 31, 627-652.

Boore, D.M., Joyner, W.B., Funal, T.E. (1997). Equations for estimating horizontal response spectra and peak acceleration from western North American earthquakes: A summary of recent work. *Seismological Research Letters*, 68, 128-153.

Boore, D.M., Atkinson, G.M. (2008). Ground-motion prediction equations for the average horizontal component of PGA, PGV, and 5%-damped PSA at spectral periods between 0.01 s and 10.0 s. *Earthquake Spectra*, 24(1), 99-138.

Boore, D.M, Stewart, J.P., Seyhan, E., Atkinson, G.M (2014). NGA-West2 equations for predicting PGA, PGV, and 5% damped PSA for shallow crustal earthquakes. *Earthquake Spectra*, 30(3), 1057-1085.

Boulanger, R.W. (2003). High overburden stress effects in liquefaction analyses. *Journal of Geotechnical and Geoenvironmental Engineering*, ASCE 129(1), 1071-1082.

Bradley, B.A., Cubrinovski, M., and Haskell, J.J.M. (2011). Probabilistic pseudo-static analysis of pile foundations in liquefiable soils. *Soil Dynamics and Earthquake Eng.,* 31, 1414-1425.

Bray, J.D., Sancio, R.B. (2006). Assessment of the liquefaction susceptibility of fine-grained soils. *Journal of Geotechnical and Geoenvironmental Engineering*, 132(9), 1165-1177.

Bray, J.D. and Travasarou, T. (2007). Simplified procedure for estimating earthquake-induced deviatoric slope displacements. *J. Geotech. Geoenviron. Eng.* 133(4), 381-392.

Bryne, P.M. (1991). A model for predicting liquefaction-induced displacements. *Proceedings, 2nd International Conference on recent Advances in Geotechnical Earthquake and Engineering and Soil Dynamics*, 2, 1027-1035. St. Louis, Missouri.

Bryne, P.M., Jitno, H., Salgado, R. (1992). Earthquake-induced displacements of soil-structure systems. *Proceedings, 10th World Conference on Earthquake Engineering*, 3, 1407-1412. Madrid, Spain.

Campbell, K.W. (1997). Empirical near-source attenuation relationships for horizontal and vertical components of peak ground acceleration, peak ground velocity, and pseudo-absolute acceleration response spectra. *Seismological Research Letters*, 68, 154-179.

Campbell, K.W., Bozorgnia, Y. (2008). NGA ground motion model for the geometric mean horizontal component of PGA, PGV, PGD and 5% damped linear elastic response spectra for periods ranging from 0.01 to 10 s. *Earthquake Spectra*, 24(1), 139-171.

Campbell, K.W., Bozorgnia, Y. (2014) NGA-West2 Campell-Bozorgnia ground motion model for the horizontal components of PGA, PGV, and 5% damped elastic pseudo-acceleration response spectra for periods ranging from 0.01 to 10 sec. *Earthquake Spectra*, 30(3), 1089-1116.

Carraro, J.A., Bandini, P., Salgado, R. (2003). Liquefaction resistance of clean and nonplastic silty sand based on cone penetrometer resistance. *Journal of Geotechnical and Geoenvironmental Engineering*, 129(11), 965-976.

Casagrande, A. (1936). Characteristics of cohesionless soil affecting the stability of slopes and earth fills. *Journal of the Boston Society of Civil Engineers*, 257-276.

Castro, G. (1969). Liquefaction of sands. *PhD Dissertation*, Cambridge, Massachusetts: Harvard University.

Castro, G., Poulos, S.J. (1977). Factors affecting liquefaction and cyclic mobility. *Journal of the Geotechnical Engineering Division*, 106(GT6), 501-506.

Cetin, K.O., Seed, R.B., Der Kiureghian, A., Tokimatsu, K., Harder Jr., L.F., Kayen, R.E. (2004). Standard penetration-based probabilistic and deterministic assessment of seismic soil liquefaction potential. *Journal of Geotechnical and Geoenvironmental Engineering*

Chen, L., Yuan, X., Zhenzhong, C., Sun, R., Dong,L. (2009). Liquefaction macrophenomena in the great Wenchauan earthquake. *Earthquake Engineering and Engineering Vibration*, 8(2), 219-229.

Chiou, B.S.J, Youngs, R.R. (2008). An NGA model for the average horizontal component of peak ground motion and response spectra. *Earthquake Spectra*, 24(1), 173-215.

Chiou, B.S.-J., Youngs, R.R. (2014). Update of the Chious and Youngs NGA model for the average horizontal component of peak ground motion and response spectra. *Earthquake Spectra*, 30(3), 1117-1153.

Cornell, C.A. (1968). Engineering seismic risk analysis. *Bulleting of the Seismological Society of America*, 58, 5.

Cornell, C.A. (1971). Probabilistic analysis of damage to structures under seismic loading. *Dynamic Waves in Civil Engineering*. London, England: Interscience.

Cornell, C.A., Winterstein, S.R. (1986). Applicability of the Poisson earthquake-occurrence model. *Seismic Hazard Methodology for the Central and Eastern United States, Report No. NP-4726*. Palo Alto, CA: Electric Power Research Institute.

Cornell, C.A., and Krawinkler, H. (2000). Progress and challenges in seismic performance assessment. *PEER News,* April, 1-3.

Coulter, M., & Migliaccio, L. (1966). Effects of the earthquake of March 27, 1964 at Valdex, Alaska. *Professional Paper 542-C*, Washington, D.C.:U.S. Geological Survey, U.S. Department of the Interior.

Deierlein, G.G., Krawinkler, H., and Cornell, C.A. (2003). A framework for performance-based earthquake engineering. *Proc.*, *2003 Pacific Conference on Earthquake Engineering*, Wellington, New Zealand.

Dobry, R., Ladd, R.S. (1980). Discussion to "Soil liquefaction and cyclic mobility evaluation for level ground during earthquakes," by H.B. Seed and "Liquefaction potential: science versus practice," by R.B. Peck. *Journal of Geotechnical Engineering*, 106 (GT6), 720-724.

Dobry, R., Ladd, R.S., Yokel, F.Y., Chang, R.M., Powell, D. (1982). Predictions of pore water pressure buildup and liquefaction of sanfs during earthquake by the cyclic strain method. *NBS Building Science Series 138,* Gaithersburg, Maryland, National Bureau of Standards, 150 pp.

Dobry, R., Mohamad, R., Dakoulas, P., Gazetas, G. (1984). Liquefaction evaluation of earth dams – a new approach. *Proceedings, 8th World Conference on Earthquake Engineering*, 3, 333-340.

Dobry, R., Mohamad, R. (1986). Undrained monotonic and cyclic triaxial strength of san. *Journal of Geotechnical Engineering*, 112(10), 941-958.

Dobry, R., Baziar, M.H. (1991) Evaluation of ground deformation caused by lateral spreading. *Proceedings, 3rd- Japan-U.S. Workshop on Earthquake Resistant Design of Lifeline Facilities and Countermeasures for Soil Liquefaction, Technical Report NCEER-91-0001*, 209-223.

Douglas, B.J., Olsen, R.S., Martin, G.R. (1981). Evaluation of the cone penetrometer test for SPT liquefaction assessment. *Proceedings, In Situ Testing to Evaluate Liquefaction Susceptibility*, New York, New York: ASCE.

Earthquake Engineering Research Institute (EERI) Committee on Seismic Risk. (1989). The basics of seismic risk analysis, *Earthquake Spectra*, 5, 675-702.

Elgamal, A., Yang, Z., Parra, E., and Ragheb, A. (2003). "Modeling of cyclic mobility in saturated cohesionless soils." *Int. J. Plast.,* 19(6), 883-905.

Faris, A.T., Seed, R.B., Kayen, R.E., and Wu, J. (2006). "A semi-empirical model for the estimation of maximum horizontal displacement due to liquefaction-induced lateral spreading, *Proc, 8th U.S. Nat. Conf. Earthquake Eng.,* EERI, Oakland, CA.

Field, E.H., Jordan, T.H., and Cornell, C.A. (2003). OpenSHA: A developing community-modeling environment for seismic hazard analysis. *Seism. Res. Letters,* 74(4), 406-419.

Finn, W.D., (1990). Assessment of liquefaction potential and post-liquefaction behavior on earthquake structures: Development 1981-1991 (State-of-the-art paper). *Proceedings, 2nd International Conference on Recent Advances in Geotechnical Engineering and Soil Dynamics,* 3, 1833-1850. St. Louis, Missouri.

Finn, W.D., Yogendrakumar, M., Yoshida, M., Yoshida, N. (1986). TARA-3: A program to compute the response of 2-D embankments and soil-structure interaction systems to seismic loadings. Vancouver, British Columbia: Department of Civil Engineering, University of British Columbia.

Franke, K.W. (2005). "Development of a performance-based model for prediction of lateral spreading displacements." *M.S. Thesis*, Univ. of Washington, Seattle, WA.

Franke, K.W. (2011). A performance-based model for the computation of kinematic pile response due to lateral spread and its application on select bridges damaged during the M7.6 earthquake in the Limon Province, Costa Rica. *Ph.D. Dissertation*, Brigham Young University, 437 pp.

Franke, K.W. and Kramer, S.L. (2014). A procedure for the empirical evaluation of lateral spread displacement hazard curves. *J. Geotech. Geoenviron. Eng.*, 140(1), 110-120.

Franke, K.W., Lingwall, B.N., and Youd, T.L. (2014a). The sensitivity of empirical liquefaction assessment to seismic loading in areas of low seismicity and its implications for sustainability. *Geo-Congress 2014 Technical Papers, Geo-characterization and Modeling for Sustainability,* ASCE GSP 234, 1284-1293.

Franke, K.W., Mayfield, R.T., and Wright, A.D. (2014b). Simplified uniform hazard liquefaction analysis for bridges. *Trans. Research Record*, 2407, 47-55, DOI: 10.3141/2407-05.

Franke, K.W., Wright, A.D., and Ekstrom, L.T. (2014c). "Comparative study between two performance-based liquefaction triggering models for the standard penetration test." *J. Geotech. Geoenviron. Eng.*, 140(5), 04014010.

Gillin, D.T. and Bartlett, S.F. (2014). "Multilinear regression equations for predicting lateral spread displacement soil soil type and CPT data." *J. Geotech. Geoenviron. Eng.,* 140(4), 04013047.

Ghobarah, A. (2001). Performance-based design in earthquake engineering: state of development. *Engineering Structures*, 23, 878-884.

Gu, W.H., Morgenstern, N.R., Robertson, P.K. (1994). Post-earthquake deformation analysis of wildlife sites. *Journal of Geotechnical Engineering*, 120(2), 274-289.

Guternberg, B., Richter, C.F. (1944). Frequency of earthquakes in California. *Bulletin of the Seismological Society of America*, 34(4), 1985-1988.

Haller, K.M. (1994). Fault number 669, Rocker fault, in Quaternary fault and fold database of the United States: US Geological Survey. < http://earthquakes.usgs.gov/hazards/qfaults> (January, 2015).

Hamada, M., Yasuda, S., Isoyama, R., Emoto, K. (1986). Study on liquefaction induced permanent ground displacements. *Association for the Development of Earthquake Prediction in Japan*, 87.

Hamada, M., Towhata, I., Yasuda, S., and Isoyama, R. (1987). "Study of permanent ground displacement induced by seismic liquefaction." *Computers and Geotechnics,* 4, 197-220.

Hanzawa, H., Itoh, Y., Suzuki, K. (1979). Shear characteristics of a quick sand in the Arabian Gulf. *Soils and Foundations*, 14(3), 1-5.

Honegger, D.G., Wijewickreme, D., and Youd, T.L. (2014). "Regional pipeline vulnerability assessment based upon probabilistic lateral spread hazard characterization." *Proc., 10th Nat. Conf. on Earthquake Eng.,* Paper 1022, EERI, Oakland, CA.

Idriss, I.M. (1999). An update to the Seed-Idriss simplified procedure for evaluating liquefaction potential. *Procedeedings, TRB Workshops on New Approaches to Liquefaction*. Publication No. FHWA-RD-99-165, Federal Highway Administration.

Idriss, I.M. (2008). An NGA empirical model for estimating the horizontal spectral values generated by shallow crustal earthquakes. *Earthquake Spectra*, 2491), 217-242.

Idriss, I.M. (2014). An NGA-West2 empirical model for estimating the horizontal spectral values generated by shallow crustal earthquakes. *Earthquake Spectra,* 30(3), 1155-1177.

Idriss, I.M. and Boulanger, R.W. (2008). *Soil Liquefaction During Earthquakes,* EERI Monograph MNO-12. Oakland, CA.

International Building Code. (2014). *2015 International Building Code*, ISBN: 978-1-60983-468-5, International Code Council, Inc., Country Club Hills, IL.

Ishihara, K. (1984). Post-earthquake failure of a tailings dam due to liquefaction of the pond deposit. *Proceedings, International Conference on Case Histories in Geotechnical Engineering*, Vol 3, 1129-1143.

Ishihara, K. (1985). Stability of natural deposits during earthquakes. *Proceedings, 11th International Conference on Soil Mechanics and Foundation Engineering*, Vol. 1, 321-376.

Ishihara, K., Koseki, J. (1989). Discussion of the cyclic shear strength of fines-containing sands. *Proceedings, Earthquake Geotechnical Engineering,XII Int. Conf. on Soil Mechanics*, pp. 101-106.

Ishihara, K., Yoshimine, M. (1992). Evaluation of settlements in sand deposits following liquefaction during earthquakes. *Soils and Foundations*, 21(1), 173-188.

Juang, C.H., Li, D.K., Fang, S.Y., Liu, Z., and Khor, E.H. (2008). Simplified procedure for developing joint distribution of amax and Mw for probabilistic liquefaction hazard analysis. *J. Geotech. Geoenviron. Eng.* 134(8), 1050-1058.

Juang, C.H., Ching, J.Y, Wang, L., Khoshnevisan, S., and Ku, C.S. (2013). Simplified procedure for estimation of liquefaction-induced settlement and site-specific probabilistic settlement exceedance curve using cone penetration test (CPT). *Canadian Geotech. J.,* 50(10), 1055-1066.

Kayen, R.E., Mitchell, J.K., Seed, R.B., Lodge, A., Nishio, S., Cotinho, R. (1992). Evaluation of SPT-, CPT-, and shear wave-based methods for liquefaction potential assessment using Loma Prieta data. *Proceedings, 4th U.S.-Japan Workshop on Earthquake Resistant Design of Lifeline Facilities and Countermeasures for Soil Liquefaction*, 1, 177-204.

Koester, J.P. (1994). The influence of fines type and content on cyclic strength. *Ground failures under seismic conditions*, ASCE. 17-33.

Kramer, S.L. (1996). *Geotechnical Earthquake Engineering*, Prentice Hall, Inc., Upper Saddle River, NJ, 653 pp.

Kramer, S.L. (2008). "Performance-based earthquake engineering: Opportunities and implications for geotechnical engineering practice." *Proc., Geotech. Earthquake Eng. Soil Dyn. IV, ASCE Geotechnical Special Publication 181*, 1-32.

Kramer, S.L., and Mayfield, R.T. (2007). Return period of soil liquefaction. *J. Geotech. Geoenviron. Eng.* 133(7), 802-813.

Kramer, S.K., Franke, K.W., Huang, Y.-M., and Baska, D. (2007). "Performance-based evaluation of lateral spreading displacement." *Proceedings, 4th International Conference on Earthquake Geotechnical Engineering*, Paper No. 1208, Thessaloniki, Greece, June 2007.

Kramer, S.L., Huang, Y.M., and Greenfield, M.W. (2014). Performance-based assessment of liquefaction hazards. *Geotechnics for Catastrophic Flooding Events,* Iai ed., ISBN 978-1-138-02709-1, Taylor and Francis Group, London, 17-26.

Krawinkler, H. (2002). A general approach to seismic performance assessment. *Proc., Int. Conf. on Advances in New Challenges in Earthquake Engineering Research*, ICANCEER, Hong Kong.

Krawinker, H., Miranda, E. (2004). Performance-based earthquake engineering. *Chapter 9, Earthquake Engineering: From Seismology to Performance-Based Engineering*. (Y. Bozorgnia, & V.V. Bertero, Eds.). Boca Raton, FL: CRC Press, LLC.

Ku, C.S., Lee, D.H., Wu, J.H. (2004) Evaluation of soil liquefaction in the Chi-Chi, Taiwan earthquake using CPT. *Soil Dynamics and Earthquake Engineering*, 24(9-10), 659-673.

Lam, I., Arduino, P., and Mackenzie-Helnwein, P. (2009). "OpenSees soil-pile interation study under lateral spread loading." International Foundation Congress & Equipment Expo '09, ASCE, Reston, VA.

Ledezma, C., and Bray, J. D. (2010). Probabilistic performance-based procedure to evaluate pile foundations at sites with liquefaction-induced lateral displaement. *J. Geotech. Geoenviron. Eng.,* 136(3), 464-476.

Marchetti, S. (1982). Detection of liquefiable sand layers by means of quasi-static penetration tests. *Proceedings, Stability and Performance of Slopes and Embankments*, 1, 116-142. Geotechnical Special Publication No. 31, ASCE.

Marrone, J., Ostadan, F., Youngs, R., and Itemizer, J. (2003). Probabilistic liquefaction hazard evaluation: Method and application. *Proc., 17th Int. Conf. Struct. Mech. in Reactor Tech. (Smart 17)*, Prague, Czech Republic, Paper No. M02-1.

Martin, G.R. (1992). Evaluation of soil properties for seismic stability of slopes. *Proceedings, Stability and Performance of Slopes and Embankments*, 1, 116-142. Geotechnical Special Publication No. 31, ASCE.

Mayfield, R.T., Kramer, S.L., and Huang, Y.M. (2010). Simplified approximation procedure for performance-based evaluation of liquefaction potential. *J. Geotech. Geoenviron. Eng.* 136(1), 140-150.

McGann, C.R. and Arduino, P. (2014). Numerical assessment of three-dimensional foundation pinning effects during lateral spreading at the Mataquito River Bridge. *J. Geotech. Geoenviron. Eng.* 140(8), 04014037.

McGuire, R. (2004). Seismic hazard and risk analysis. *Second Monograph Series MNO-10*. Earthquake Engineering Research Institute.

McGuire, R.K., Arabasz, W.J. (1990). An introduction to probabilistic seismic hazard analysis. *Geotechnical and Environmental Geophysics*, 1, 333-353.

Merz, H.I., Cornell, C.A. (1973). Seismic risk analysis based on quadratic magnitude-frequency law. *Bulletin of the Seismological Society of America*, 63(6) 1999-2006.

Middlebrooks, T.A. (1942). Fort Peck Slide. *Transactions of the American Society of Civil Engineers*, 107, 723-764.

Mitchell, J.K., Tseng, D.J. (1990). Assessment of liquefaction potential by cone penetration resistance. *Proceedings, H. Bolton Seed Memorial Symposium*, 2, 335-350. Berkeley, California.

Miyajima, Kitaura, Ando. (1991). Experiments on liquefaction-induced large ground deformation. *Proceedings, 3rd Japan-U.S. Workshop on Earthquake Resistant Design of Lifeline Facilities and Countermeasures for Soil Liquefaction, Technical Report NCEER-91-0001,* 269-292. (O'Rourke & Hamada, Eds.).

Mogami, T., and K. Kubo. (1953). "The behavior of soil during vibration. *Proceedings of the Third International Conference of Soil Mechanics and Foundation Engineering*. Vol.1, 152-155.

Moss, R.E., Seed, R.B., Kayen, R.E., Steward, J.P., Der Kiureghian, A., Cetin, K.O. (2006). CPT-based probabilistic and deterministic assessment of in situ seismic soil liquefaction potential. *Journal of Geotechnical dna Geoenvironmental Engineerning*, 132(8), 1032-1051.

Nakase, H., Hiro-oka, A., Yanagihata, T. (1997). Deformation characteristics of liquefied loose sand by triaxial compression tests. *Proceedings, IS-Nagoya 97, Deformation and Progressive Failure in Geomechanics*, 559-564. (A. Asaoka, T. Adachi, F. Oka, Eds.) Pegamon, Elsevier Science.

National Research Council (US). (1985). *Liquefaction of soil during earthquakes*. Vol 1., National Academies.

Newmark, N. (1965). Effects of earthquakes on dams and embankments. *Geotechnics*, 152(2), 139-160.

Obermeier, S.F., & Pond, E.C. (1999) Issues in using liquefaction features for paleoseismic analysis. *Seismological Research Letters*, 70(1), 34-58.

Olsen, M.J., Bartlett, S.F., and Solomon, B.J. (2007). "Lateral spread hazard mapping of the Northern Salt Lake Valley, Utah, for M7.0 scenario earthquake." *Earthquake Spectra,* 23(1), 95-113.

Olson, S.M., and Johnson, C.I. (2008). "Analyzing liquefaction-induced lateral spreads using strength ratios." *J. Geotech. Geoenviron. Eng.* 134(8), 1035-1049.

Parra, E. (1996). Numerical modeling of liquefaction and lateral ground deformation including cyclic mobility and dilation response in soil system." *Ph.D. Dissertation*, Rensselaer Polytechnic Institute, Troy, NY.

Petersen, M. D., Frankel, A. D., Harmsen, S. C., Mueller, S. C., Haller, K. M., Wheeler, R. L., et al. (2008). Documentation for the 2008 update of the United States National Seismic Hazard Maps. *USGS Open-File Report 2008-1128*, 128 pp.

Poulos, S.J. (1981). The steady state of deformation. *Journal of Geotechnical and Geoenvironmental Engineering*, 107, ASCE 16241 Proceedings.

Popescu, R., Prevost, J.H. (1995). VELACS Numerical "Class A" Predictions and Centrifuge Experimental Soil Test Results. *Soil Dynamics and Earthquake Engineering*, 14(2), 79-92.

Rathje, E.M. and Saygili, G. (2008). Probabilistic seismic hazard analysis for the sliding displacement of slopes: scalar and vector approaches. *J. Geotech. Geoenviron. Eng.* 134(6), 804-814.

Rathje, E.M. and Saygili, G. (2009). Probabilistic assessment of earthquake-induced slifing displacements of natural slopes. *Bull. New Zealand Soc. Earthquake Eng.*, 42(1), 18-27.

Rathje, E.M., and Saygili., G. (2011). Estimating fully probabilistic seismic sliding displacements of slopes from a pseudoprobabilistic approach. *J. Geotech. Geoenviron. Eng.,* 137(3), 208-217.

Rauch, A.F., and Martin, J.R. (2000). "EPOLLS model for predicting average displacements on lateral spreads." *J. Getech. Geoenviron. Eng.* 126(4), 360-371.

Reiter, L. (1990). *Earthquake Hazard Analysis – Issues and Insights*. New York, NY: Columbia University Press.

Reyna, F., Chameau, J.L. (1991) Dilatometer-based liquefaction potential of sites in the Imperial Valley. *Proceedings, 2nd International Conference on Recent Advances in Geotechnical Earthquake Engineering and Soil* Dynamic, 1, 385-392. St. Louis, Missouri.

Risk Engineering. (2010). EZ-FRISK version 7.43. Boulder, CO.

Robertson, P.K., Campanella, R.G. (1985). Liqeufaction potential of sands using the CPT. *Journal of Geotechnical Engineering*, 111(3), 384-403.

Robertson, P.K., Campanella, R.G. (1986). Estimating liqeufaction potential of sands using the flat dilatometer. *Geotechnical Testing Journal*, 9(1), 38-40.

Sadigh, K., Chang, C.Y., Egan, J.A., Makdisi, F.I., Youngs, R.R. (1997). Attenuation relationships for shallow crustal earthquakes based on California strong motion data. *Seismological Research Letters*, 68(1), 180-189.

Sasaki, Tokaida, Matsumoto, Saya. (1991). Shake table tests on lateral ground flow induced by soil liquefaction. *Proceedings, 3rd Japan-U.S. Workshop on Earthquake Resistant Design of Lifeline Facilities and Countermeasures for Soil Liquefaction, Technical Report NCEER-91-0001*, 371-385. (O'Rourke & Hamada, Eds.).

Saygili, G. and Rathje, E.M. (2008). Empirical predictive models for earthquake-induced sliding displacements of slopes. *J. Geotech. Geoenviron. Eng.,* 134(6), 790-803.

Seed, H.B. (1979). Soil liquefaction and cyclic mobility evaluation for level ground during earthquakes. *Journal of Geotechnical and Geoenvironmental Engineering*, 105(2), 201-255.

Seed, H.B. (1980). Closure to soil liquefaction and cyclic mobility evaluation for level ground during earthquakes. *Journal of Geotechnical Engineering*, 106(GT6), 724.

Seed, H.B., Idriss, I.M. (1967). "Analysis of liquefaction: Niigata earthquake." Proc. ASCE, 93(SM3), 83-108.

Seed, H.B., Idriss, I.M. (1971). Simplified procedure for evaluating soil liquefaction potential. *Journal of Soil Mechanics and FoundationsDiv., 97(SM9), 1249-1273.*

Seed, H.B., De Alba, P. (1986). Use of SPT and CPT test for evaluating soil liquefaction potential. *Proceddings, In Situ '86*, ASCE.

Seed, H.B., Idriss, I.M., Arango, I. (1983). Evaluation of liquefaction potential using field performance data. *Journal of Geotechnical Engineering*, 109(3), 458-482.

Seed, H.B., Tokimatisu, K., Harder, L.F., Chung, R.M. (1984). The influence of SPT procedures in soil liquefaction resistance evaluations. *Report No. UCB.EERC-84/15*. Berkeley, California: University of California.

Seid-Karbasi, M., and Byrne, P.M. (2007). "Seismic liquefaction, lateral spreading and flow slides: A numerical investigation into void redistribution." *Canadian Geotech. J.*, 44(7), 873-890.

Shamoto, Y., Zhang, J.M., Goto, S. (1997). Mechanism of large post-liquefaction deformation in saturated sands. *Soils and Foundations*, 37(2), 71-80.

Shiomi, T., Tsukuni, S., Hatanaka, M., Tanaka, Y., Suzuki, Y., Hirose, T. (1987). Simulation analysis of ground liquefaction induced by earthquake. *Computers and Geotechnics*, 4(4), 221-245.

Stokoe, K.H., Roesset, J.M., Bierschwale, J.G., Aouad, M. (1988). Liquefaction potential of sands from shear wave velocity. *Proceedings, 9th World Conference of Earthquake Engineering*, 3, 213-218. Tokyo, Japan.

Suzuki, Y., Tokimatsu, K., Koyamada, K. (2004). Correlation between soil liquefaction during earthquake and shear wave velocity. *Journal of Structural and Construction Engineering*, (578), 67-74.

Toboada, V.M., Andoun, T., Dobry, R. (1996). Prediction of liquefaction-induced lateral spreading by dilateral sliding block model calibrated by centrifuge tests. *Proceedings, 11th World Conference on Earthquake Engineering*, Paper No. 1037. Acapulco, Mexico.

Toboadao-Urtuzuastegui, V.M., Dobry, R. (1998). Centrifuge modeling of earthquake-induced lateral spreading in sand. *Journal of Geotechnical and Geoenvironmental Engineering*, 124(12), 1195-1206.

Tokimatsu, K., Kuwayama, S., Tamura, S. (1991). Liqeufaction potential evaluation based on Rayleigh Wave investigation and its comparison with field behavior. *Proceedings, wnd Internationals Conference on Recent Advances in Geotechnical Earthquake Engineering and Soil Dynamics*, 1, 357-364. St Louis, Missouri.

Towhata, I., Sasaki, K., Tokida, K., Matsumoto, H., Tamari, Y., Yamuda, K. (1992). Prediction of permanent displacements of liquefied ground by means of minimum energy principle. *Soils and Foundations*, 32(2), 97-116.

Towhata, I., Tokida, K., Tamari, H., Matsumoto, H., Yamada, L. (1991). Prediction of permanent lateral displacement of liquefied ground by means of variational principle. *Proceedings, 3rd Japan-U.S. Workshop on Earthquake Resistant Design of Lifeline Facilities and Countermeasures for Soil Liquefaction*, Technical Report NCEER-91-0001, 237-251. (O'Rourke & Hamada, Eds.).

Travasarou, T., Bray, J.D., and Der Kiureghian, A. (2004). A probabilistic methodology for assessing seismic slope displacements. *13th World Conf. on Earthquake Eng.*, Paper No. 2326, IAEE, Tokyo, Japan.

United States Geologic Survey (USGS). (2008)." 2008 Interactive Deaggregations" Geologic Hazards Science Center, < http://geohazards.usgs.gov/deaggint/2008> (January, 2014).

USGS. (2008a)." Simplified 2008 Hazard Map" Geologic Hazards Science Center, < http://earthquake.usgs.gov/hazards/products/conterminous/2008/maps/ > (June, 2014).

Valsamis, A.I., Bouckovalas, G.D., Papadimitrou, A.G. (2010). Parametric investigation of lateral spreading of gently sloping liquefied ground. *Soil Dynamics and Earthquake Engineering*, 30(6), 490-508.

Vasquez-Herrera, A., Dobry, R. (1988). The behavior of undrained contractive sand and its effect of seismic liquefaction flow failures of earth structures. *Report to the U.S. Army Core of Engineers*, 510 pp., Troy, New York: Rennsalaer Polytechnic Institute.

Vision, SEAOC. (1995). Performance based seismic engineering of buildings. *Structural Engineers Association of California*, Sacramento, CA.

Wang, W. (1979). Some findings in soil liquefaction. *Water Conservancy and Hydroelectric Power Scientific Research Institute*, Earthquake Engineering Department.

Weisstein, E.W. (2005). "Poisson Process," *MathWorld*. <http://mathworld.wolfram.com/PoissonProcess.html> (February, 2015).

Wells, D.L., Coppersmith, K.J. (1994). New empirical relationships among magnitude, rupture length, rupture width, rupture area, and surface displacement. *Bulletin of the Seismological Society of America*, 84(4), 974-1002.

Wong, R.T., Seed, H.B., Chan, C.K. (1975). Liquefaction of gravelly soil under cyclic loading conditions. *Journal of the Geotechnical Engineering Division*, 101(GT6), 571-583.

Wu, J. (2002). Liquefaction triggering and post-liquefaction deformations of Monterey 0/30 sand under uni-directional cyclic simple shear loading. *PhD Dissertation*, Berkeley, California: University of California.

Yang, Z. (2000). "Numerical modeling of earthquake site response including dilation and liquefaction." *Ph.D. Dissertation*, Columbia Univ., New York.

Yang, Z., Elgamal, A., Parra, E. (2003). A computational model for liquefaction and associated shear deformation. *Journal of Geotechnical and Geoenvironmental Engineering*, 129(12), 1119-1127.

Yasuda, S., Nagase, H., Kiku, H., Uchida, Y. (1991). A simplified procedure for the analysis of the permanent ground displacement. *Proceedings, 3rd Japan-U.S. Workshop on Earthquake Resistant Design of Lifeline Facilities and Countermeasures Against Soil Liquefaction*, NCEER-91-0001, 225-236. (O'Rourke & Hamada, Eds.).

Yasuda, S., Masuda, T., Yoshida, N., Kiku, H., Itafuji, S., Mine, K. (1994). Torsional shear and triaxial compression tests on deformation characteristics of sands before and after liquefaction. *Proceedings, 5th U.S.-Japan Workshop on Earthquake Resistant Design of Lifeline Facilities and Countermeasures Against Soil Liquefaction*, NCEER-94-0026, 249-266, Salt Lake City, UT.

Youd, T.L. (1984). Recurrence of liquefaction at the same site. *Proceedings, 8th World Conference on Earthquake Engineering*, Vol. 3, 231-238.

Youd, L.T., Hoose S.N. (1978). *Historic ground failures in northern California triggered by earthquakes*. Vol. 993, U.S. Govt. Print Off., Washington D.C.

Youd, T.L., and Perkins, D.M. (1987). "Mapping of liquefaction severity index." *J. Geotech. Eng.*, 113(11), 1374-1392.

Youd, T.L., Idriss, I.M., Andrus, R.D., Arango, I., Castro, G., Christian, J.T. (2001). Liqeufaction resistance of soils; summary report from the 1996 NCEER and 1998 NCEER/NSF Workshops on evaluation of liquefaction resistance of soils. *Journal of Geotechnical and Geoenvironmental Engineering*, 127(10), 817-833.

Youd, T.L., Hansen, C.M., and Bartlett, S.F. (2002). "Revised multilinear regression equations for prediction of lateral spread displacement." *J. Geotech. Geoenviron. Eng.,* ASCE, 128(12), 1007-1017.

Youd, T.L., DeDan, D.W., Bray, J.D., Sancio, R.B., Cetin, K.O., Gerber, T.M. (2009). Zero-displacement lateral spreads, 1999 Kocaeli, Turkey, earthquake. *Journal of Geotechnical and Geoenvironmental Engineering*, 135(1), 46-61.

Youngs, R.R., Coppersmith, K.J. (1985). Implications of fault slip rates and earthquake recurrence models to probabilistic seismic hazard assessments. *Bulleting of the Seismological Society of America*, 75(4), 939-964.

Youngs, R.R., Chiou, S.J., Silva, W.J., Humphrey, J.R. (1997). Strong ground motion attenuation relationships for subduction zone earthquakes. *Seismological Research Letters,* 68(1), 58-73.

Zhang, G., Robertson, P.K., and Brachman, R.W.I. (2004). "Estimation liquefaction-induced lateral displacements using the standard penetration test or cone penetration test," *J. Geot. Geoenv. Eng.,* 130(8), 861-871.

Zhang, J., Zhao, J.X. (2005). Empirical models for estimating liquefaction-induced lateral spread displacements. *Soil Dynamics and Earthquake Engineering*, 25, 439-450.

Zhang, J.-M., Wang, G. (2012). Large post liquefaction deformation of sand, part I: physical mechanism, constitutive description, and numerical algorithm. *Acta Geotechnica*, 7, 69-113.

Zhang, J., Yang, C., Zhao, J.X., McVerry, G.H. (2012). Empirical models for predicting lateral spreading considering the effect of regional seismicity. *Earthquake Engineering and Engineering Vibration*, 11(1), 121-131.

Zhao, J.X., Zhang, J.J. (2002). Development of attenuation models from Japanese strong-motion data accounting for source-type effects. *Insitute of Geological and Nuclear Sciences Limited*, Client Report 2002/142.

Zhao, J.X., Zhang, J., Asano, A., Ohno, Y., Ouchi, T., Takahashi, T. (2006). Attenuation relations of strong ground motions in Japan using site classification based on predominant period. *Bulletin of Seismological Society of America*, 96(3), 898-913.

Zienkiewics, O.C., Shiomi, T. (1984). Dynamic behavior of saturated porous media: the generalized Biot formulation and its numerical solution. *International Journal for Numerical and Analytical Methods in Geomechancis*, 8, 71-96

Zienkiewics, O.C., Chang, C.T., Hinton, E. (1978). Non-linear seismic response and liquefaction. *International Journal for Numerical and Analytical Methods in Geomachanics*, 2, 381-404.

# APPENDIX A. SAMPLE LATERAL SPREAD PARAMETER MAPS

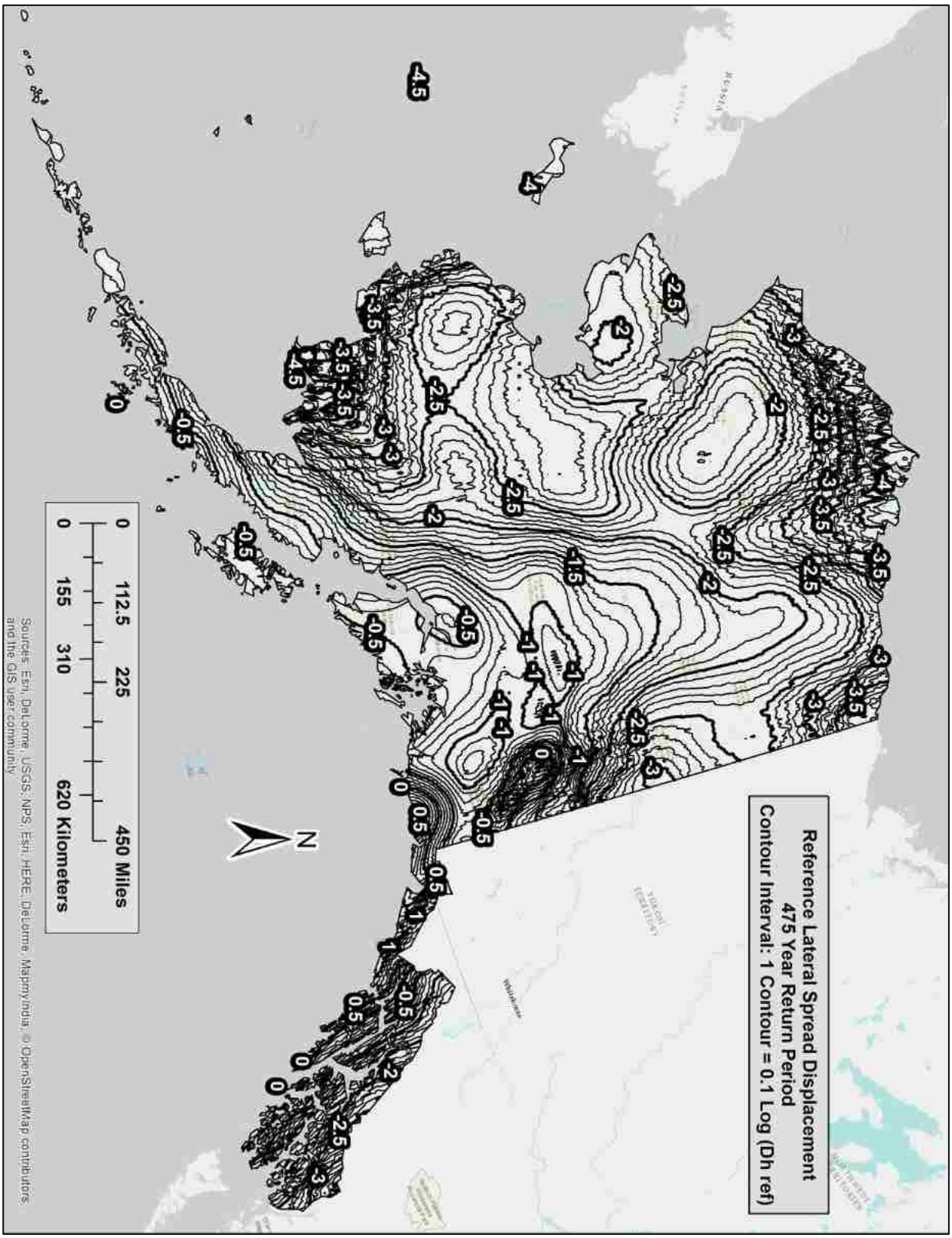


**Figure A-1: Lateral Spread Parameter ($D_H^{ref}$) Map for Alaska ($T_r$ = 475)**

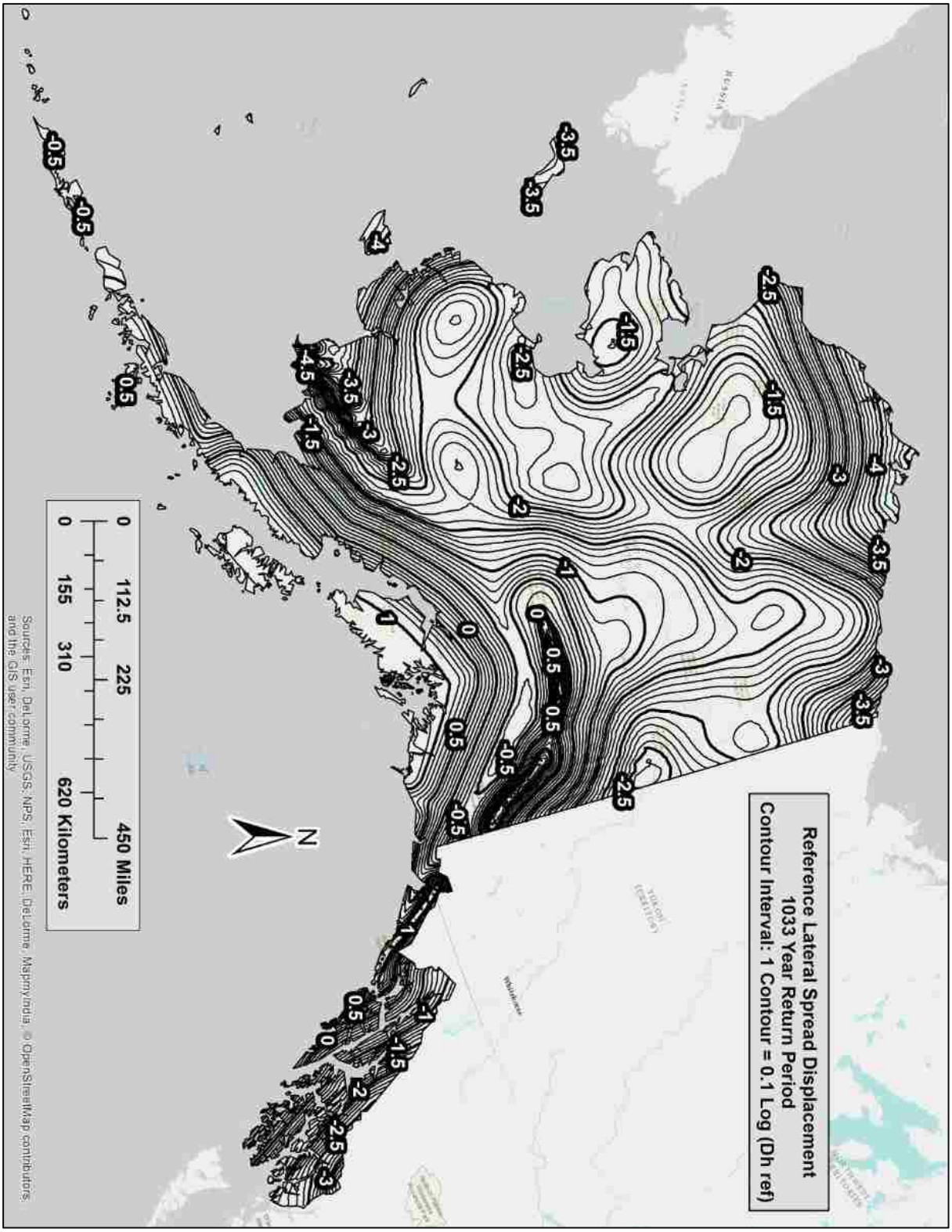


**Figure A-2: Lateral Spread Parameter ($D_H^{ref}$) Map for Alaska ($T_r$ = 1,033)**

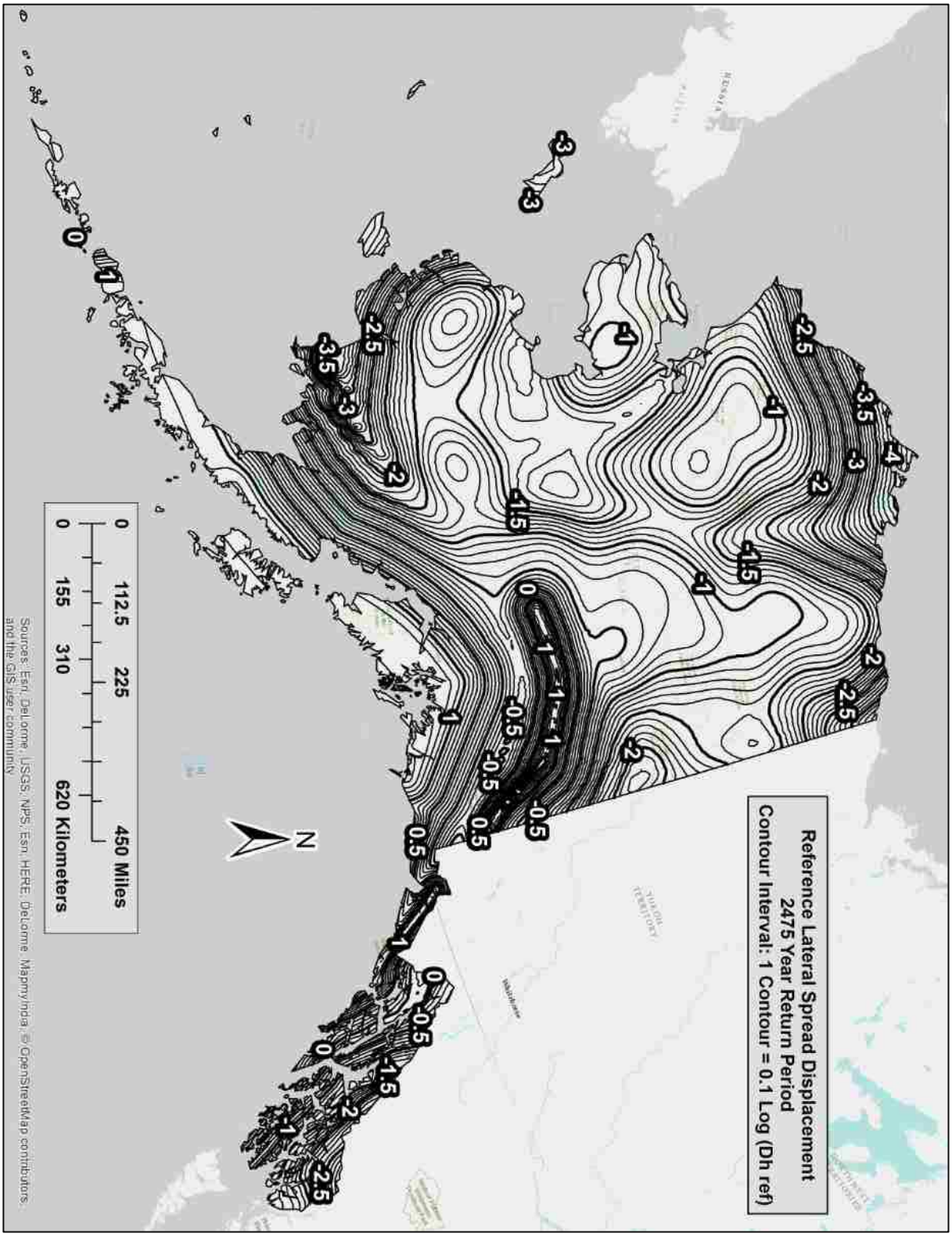


**Figure A-3: Lateral Spread Parameter ($D_H^{ref}$) Map for Alaska ($T_r$ = 2,475)**

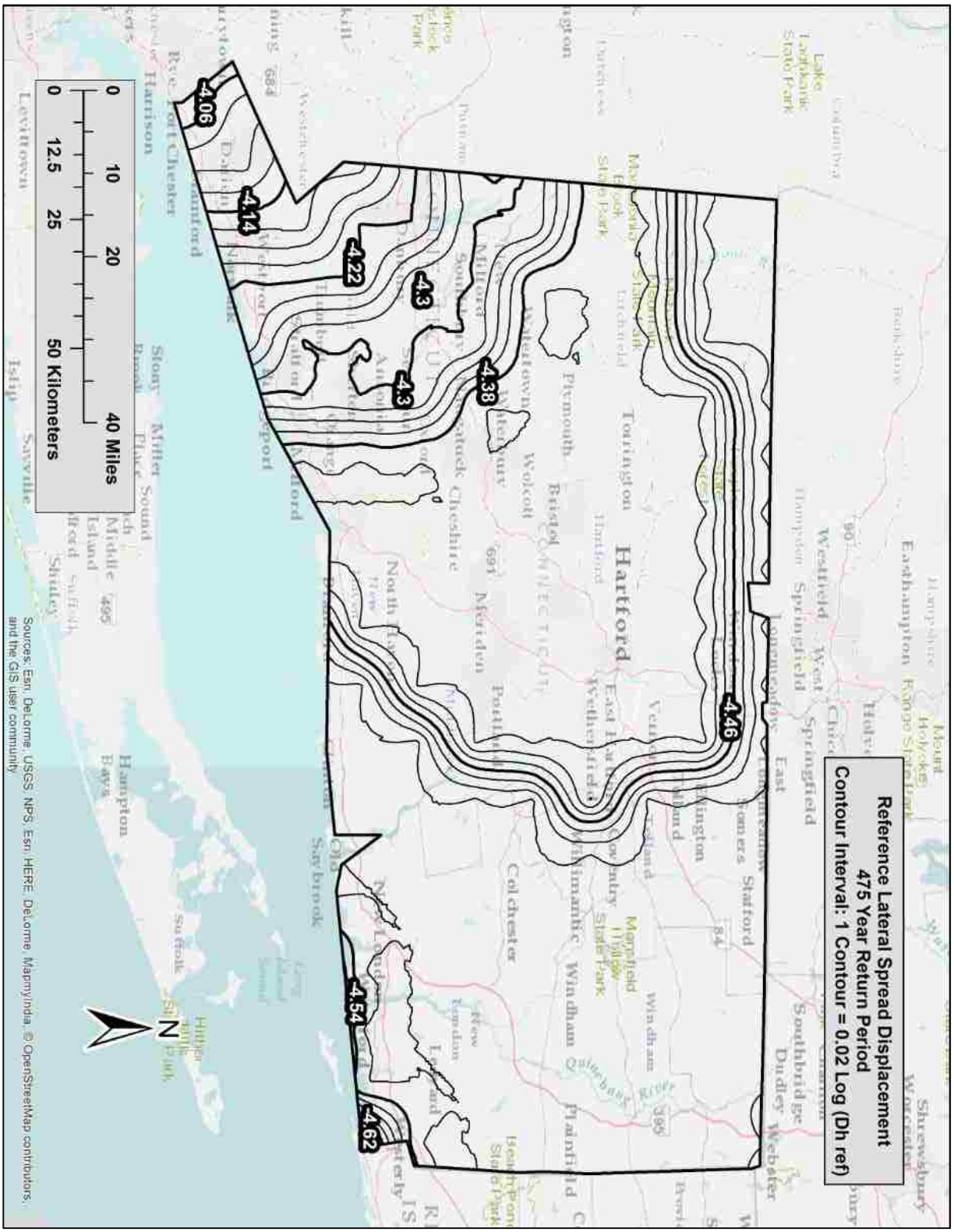


**Figure A-4: Lateral Spread Parameter ($D_H^{ref}$) Map for Connecticut ($T_r$ = 475)**

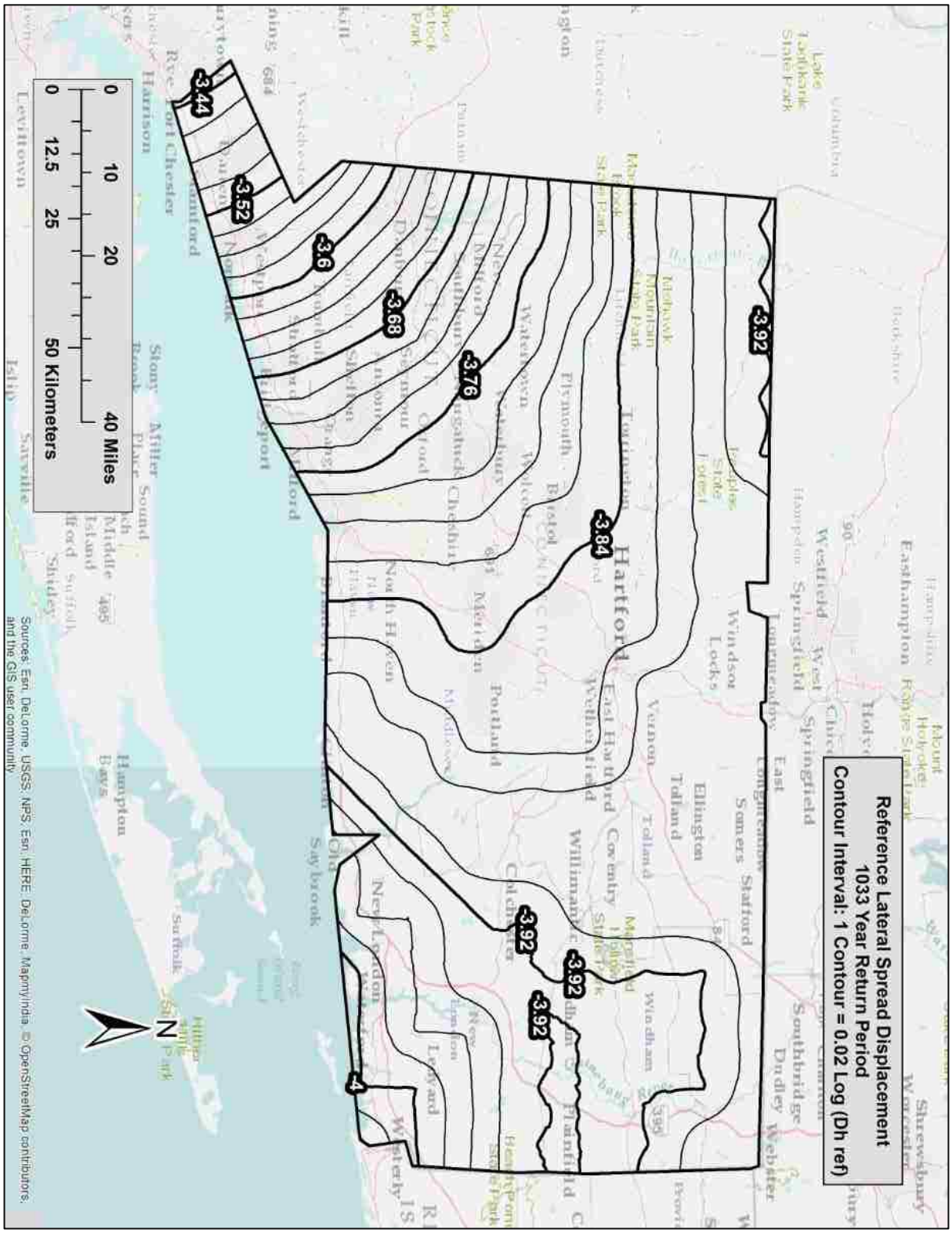


**Figure A-5: Lateral Spread Parameter ($D_H^{ref}$) Map for Connecticut ($T_r$ = 1,033)**

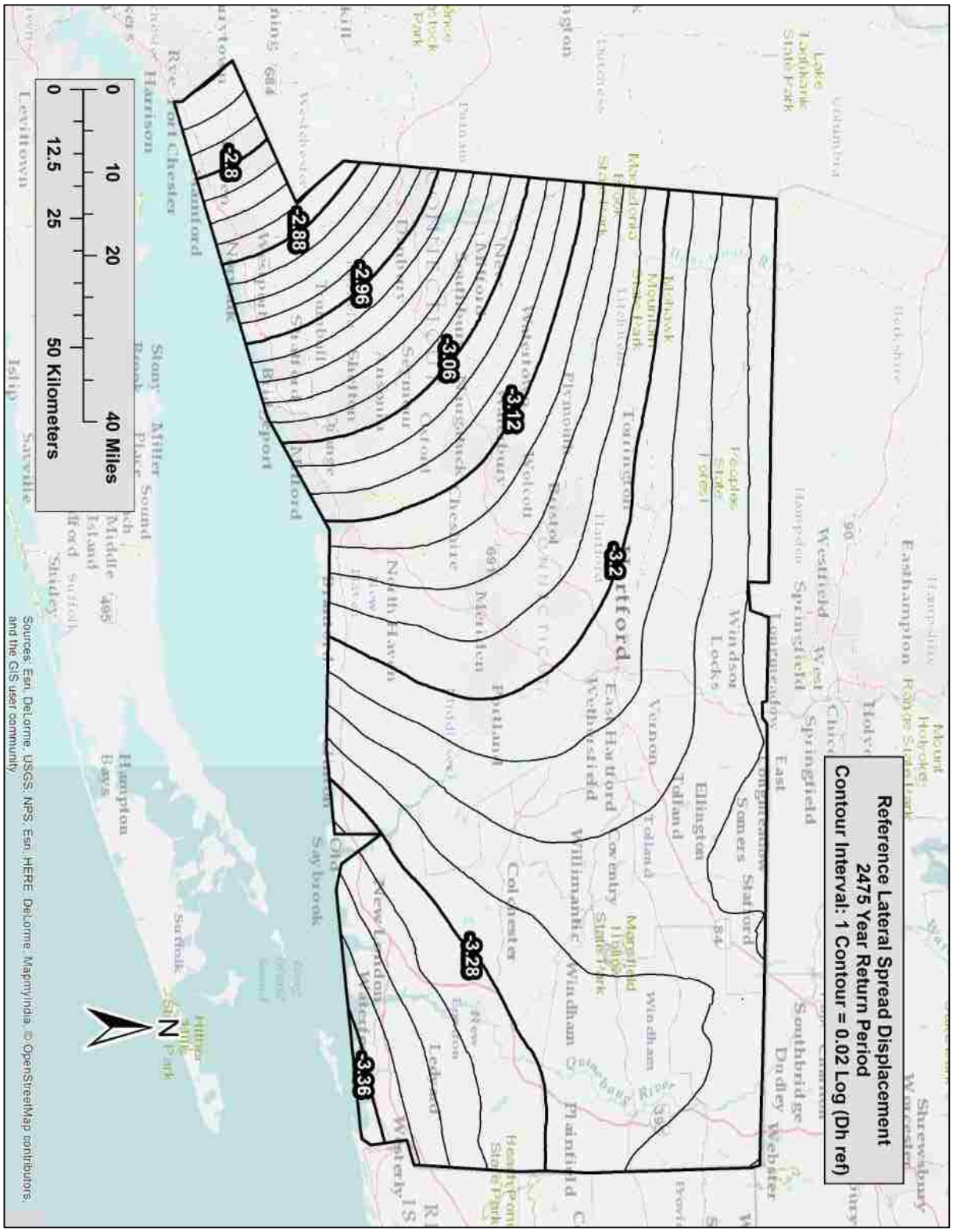


**Figure A-6: Lateral Spread Parameter ($D_H^{ref}$) Map for Connecticut ($T_r$ = 2,475)**

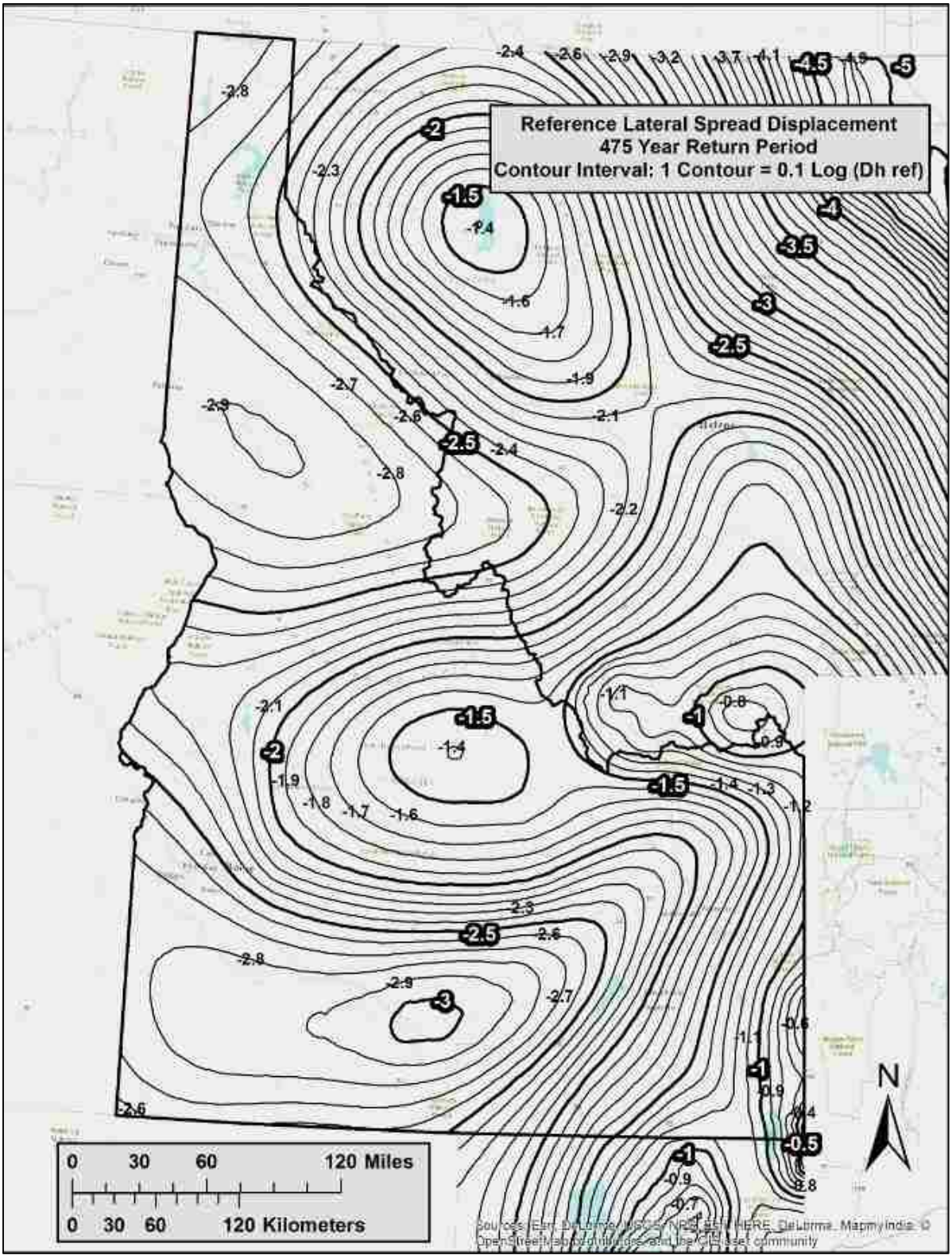


**Figure A-7: Lateral Spread Parameter ($D_H^{ref}$) Map for Idaho ($T_r$ = 475)**

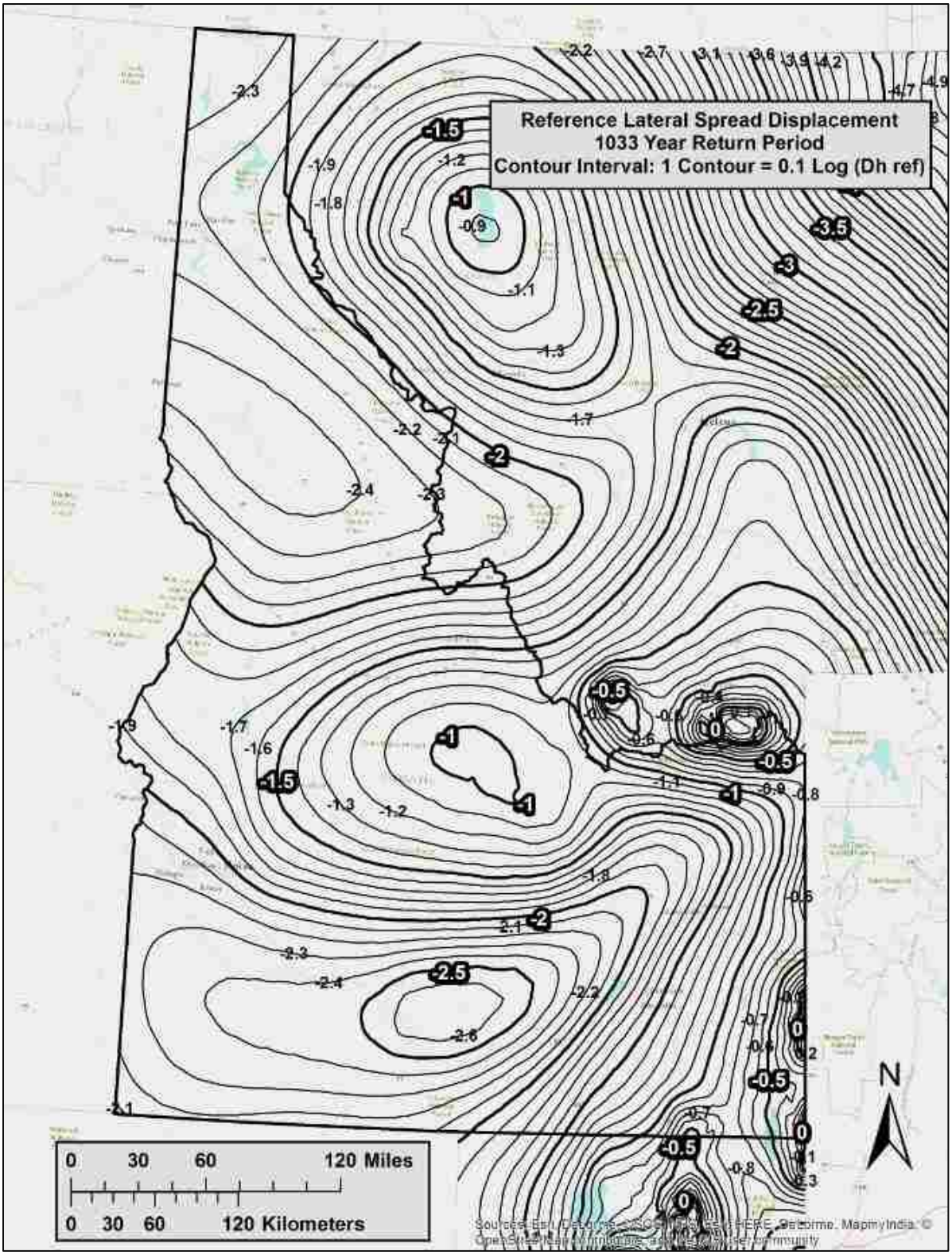


**Figure A-8: Lateral Spread Parameter ($D_H^{ref}$) Map for Idaho ($T_r$ = 1,033)**

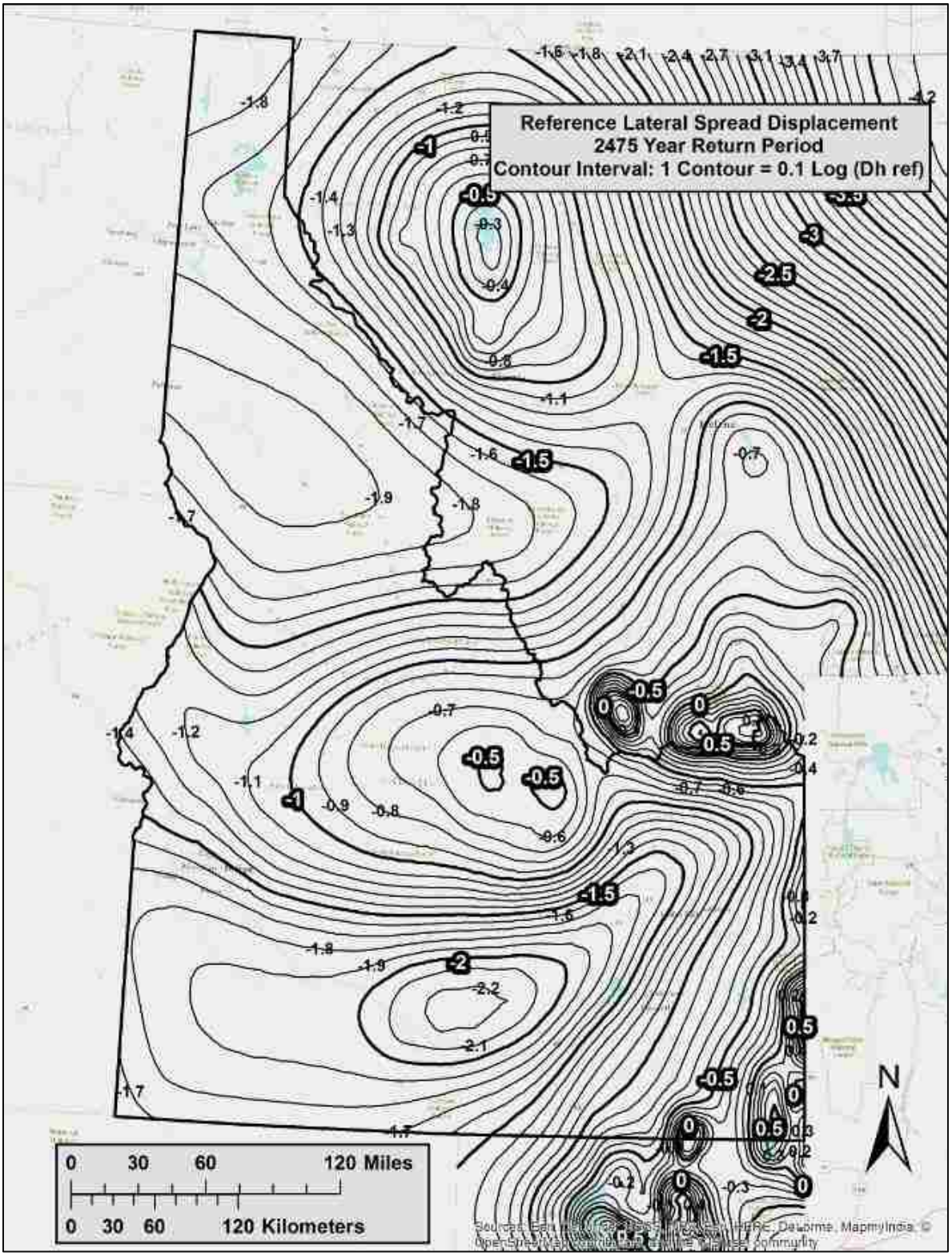


**Figure A-9: Lateral Spread Parameter ($D_H^{ref}$) Map for Idaho ($T_r$ = 2,475)**

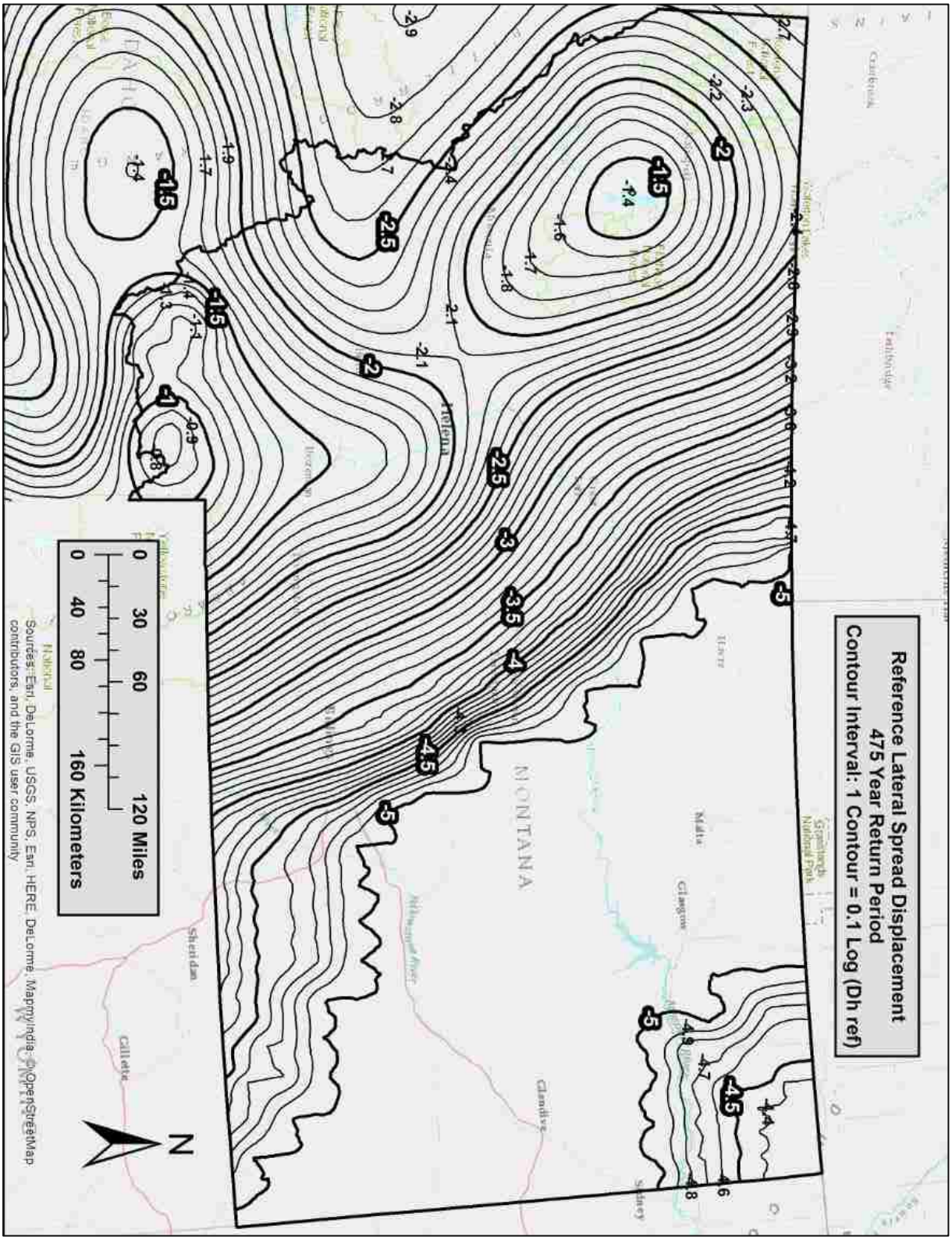


**Figure A-10: Lateral Spread Parameter ($D_H^{ref}$) Map for Montana ($T_r$ = 475)**

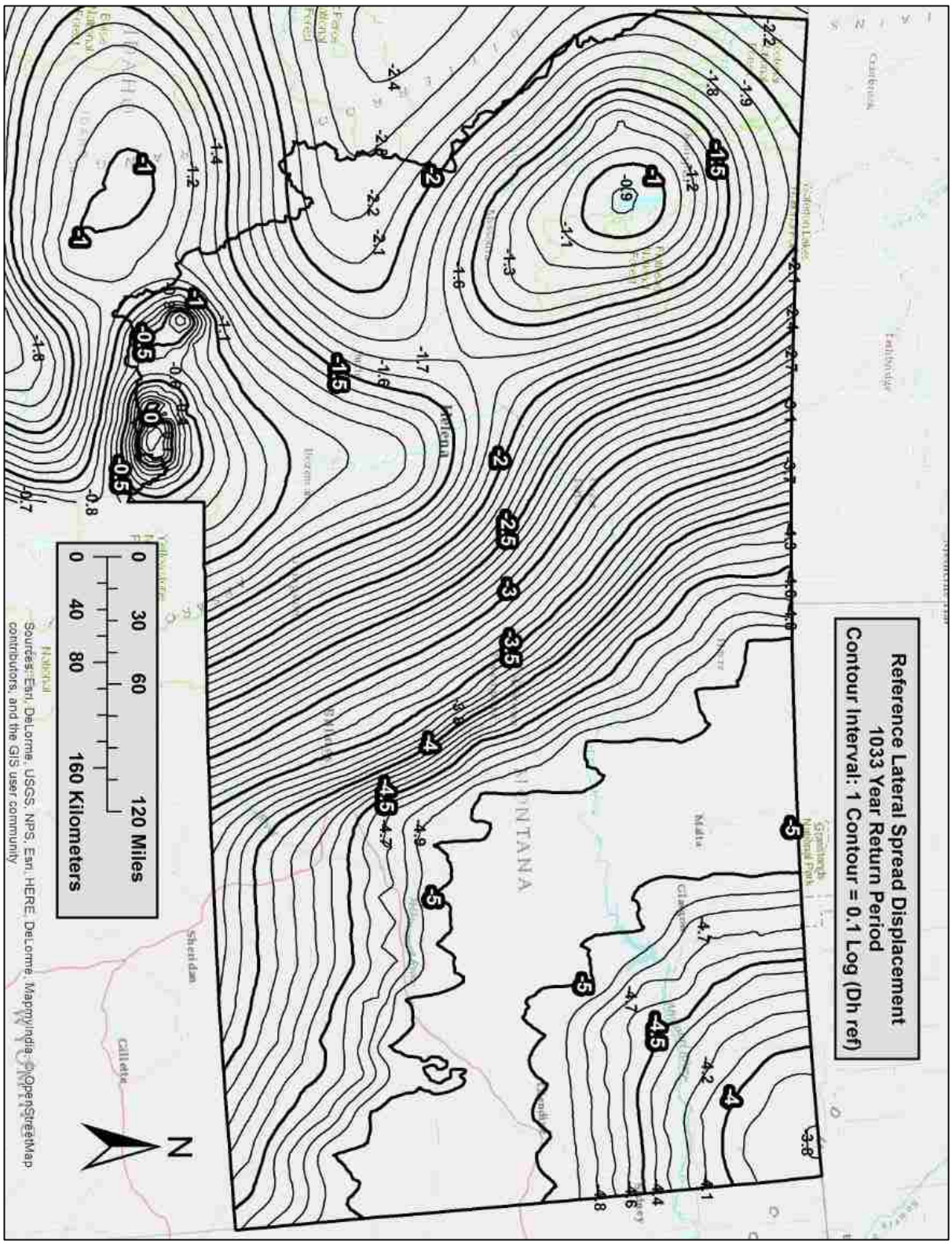


**Figure A-11: Lateral Spread Parameter ($D_H^{ref}$) Map for Montana ($T_r$ = 1,033)**

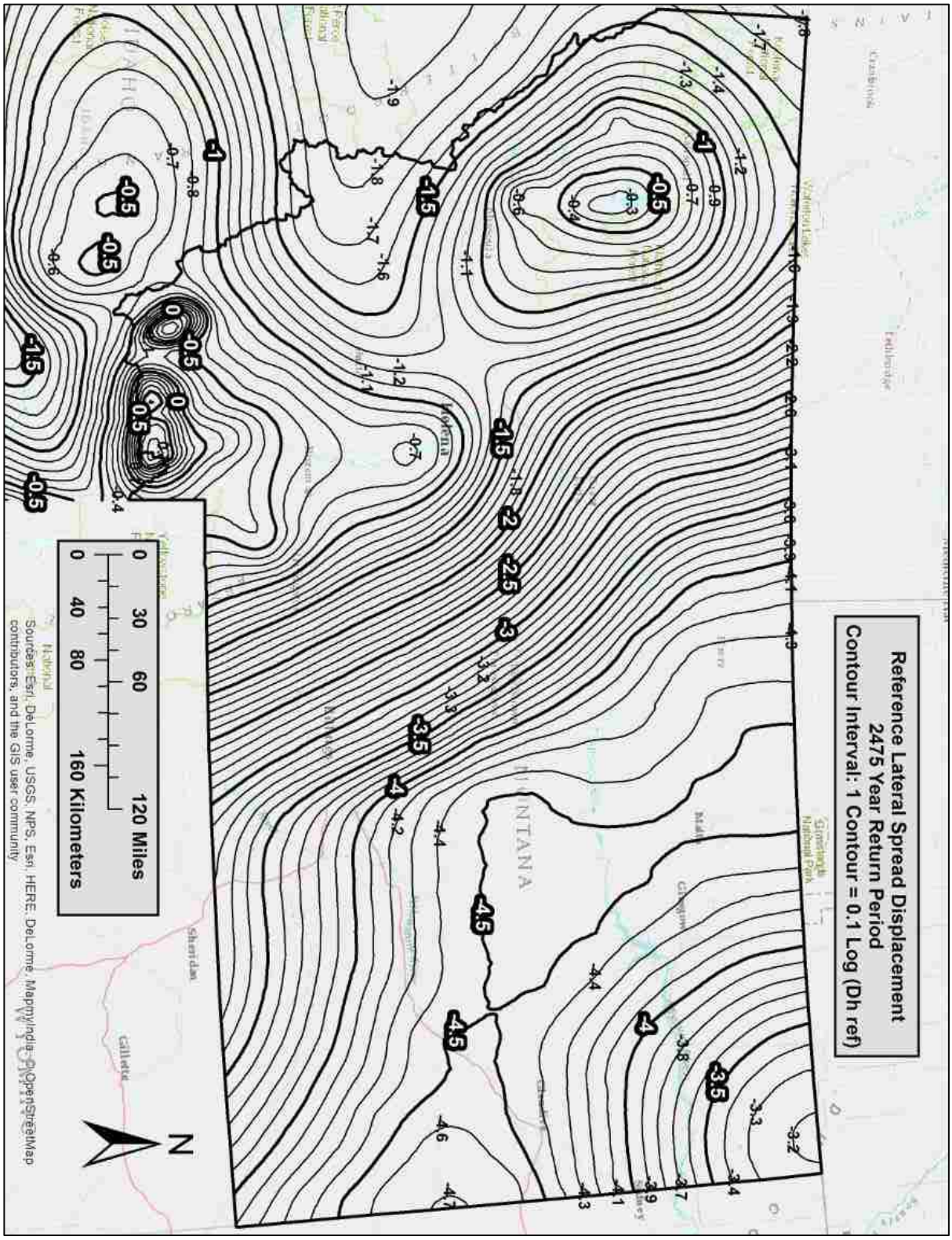


**Figure A-12: Lateral Spread Parameter ($D_H^{ref}$) Map for Montana ($T_r$ = 2,475)**

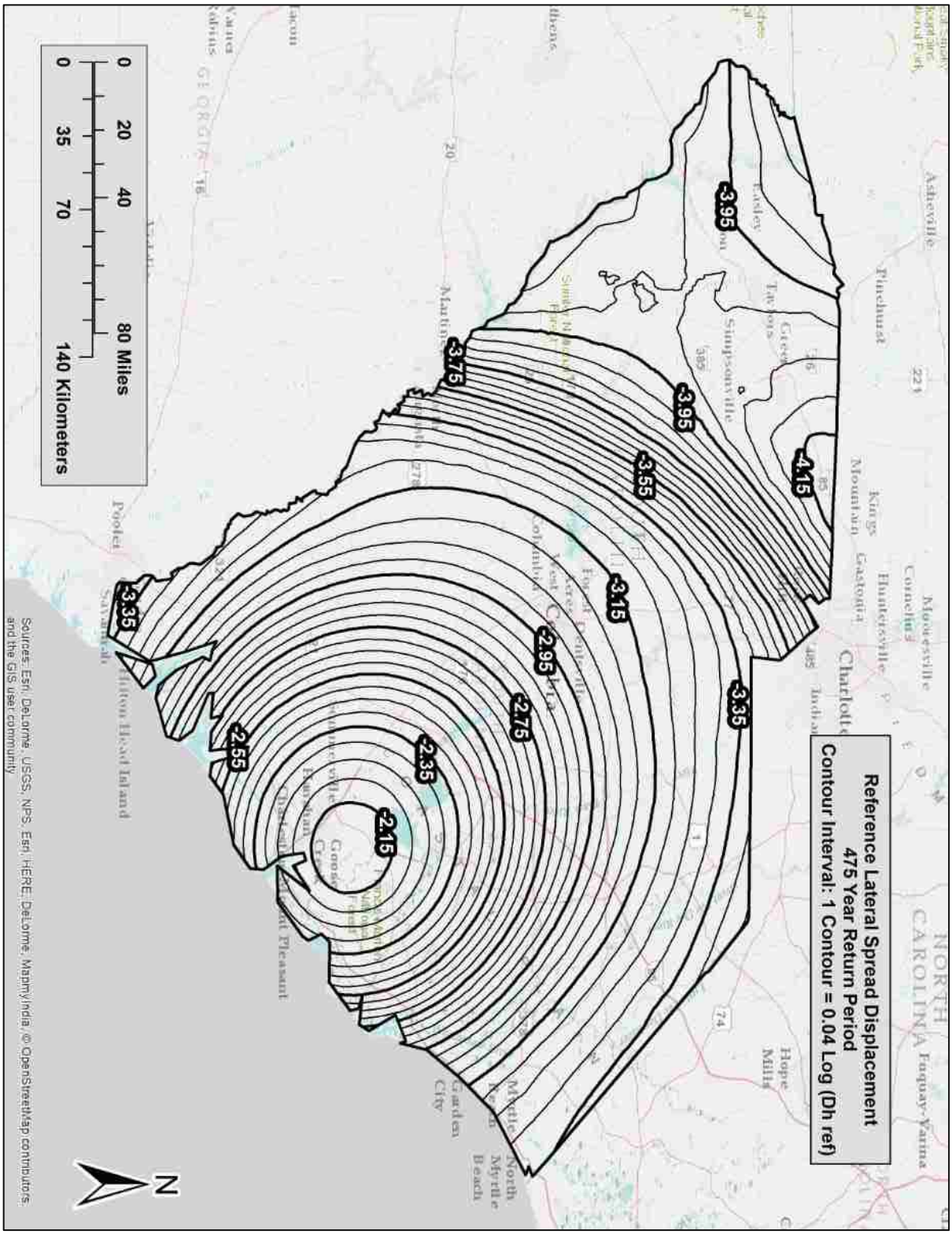


**Figure A-13: Lateral Spread Parameter ($D_H^{ref}$) Map for South Carolina ($T_r$ = 475)**

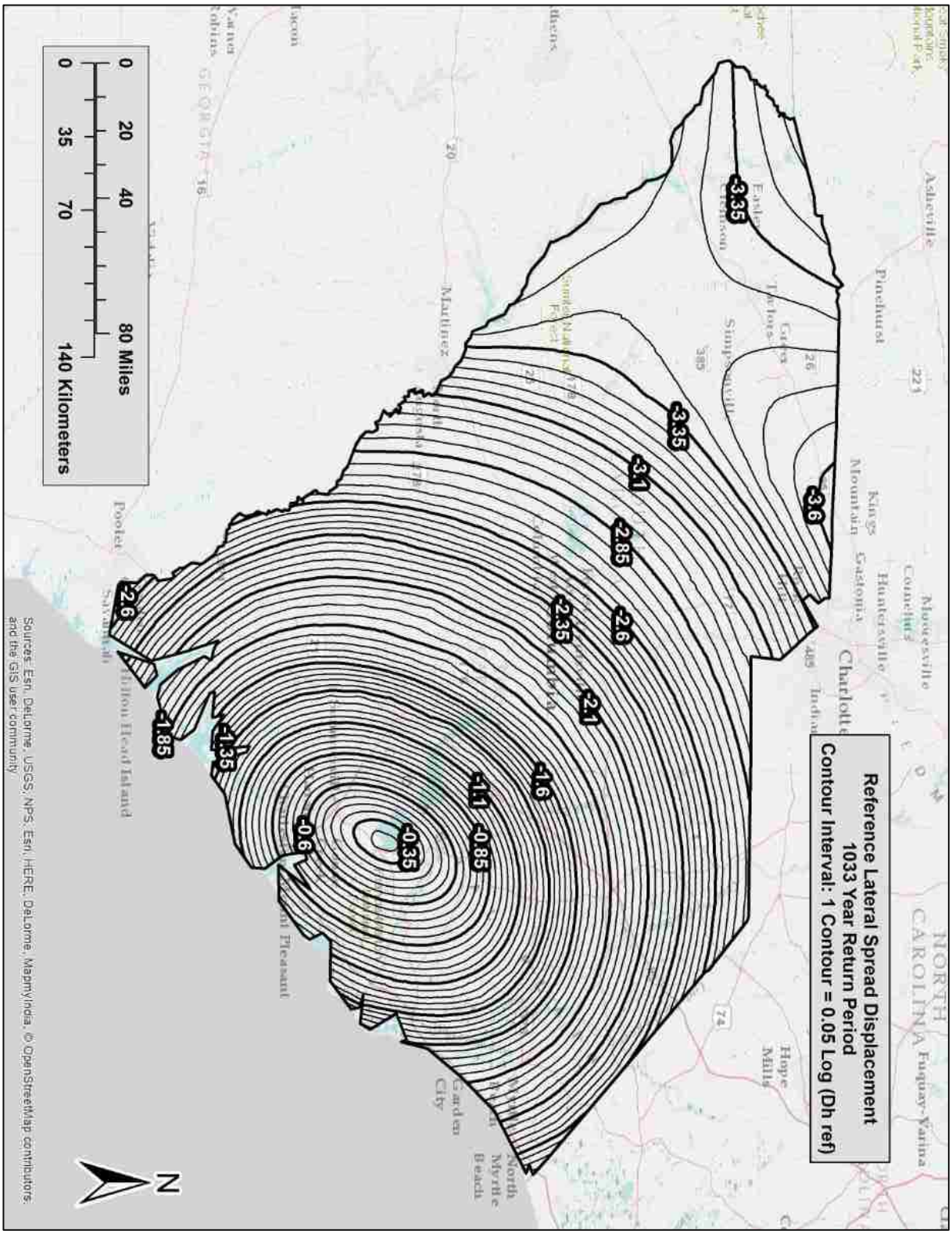


**Figure A-14: Lateral Spread Parameter ($D_H^{ref}$) Map for South Carolina ($T_r$ = 1,033)**

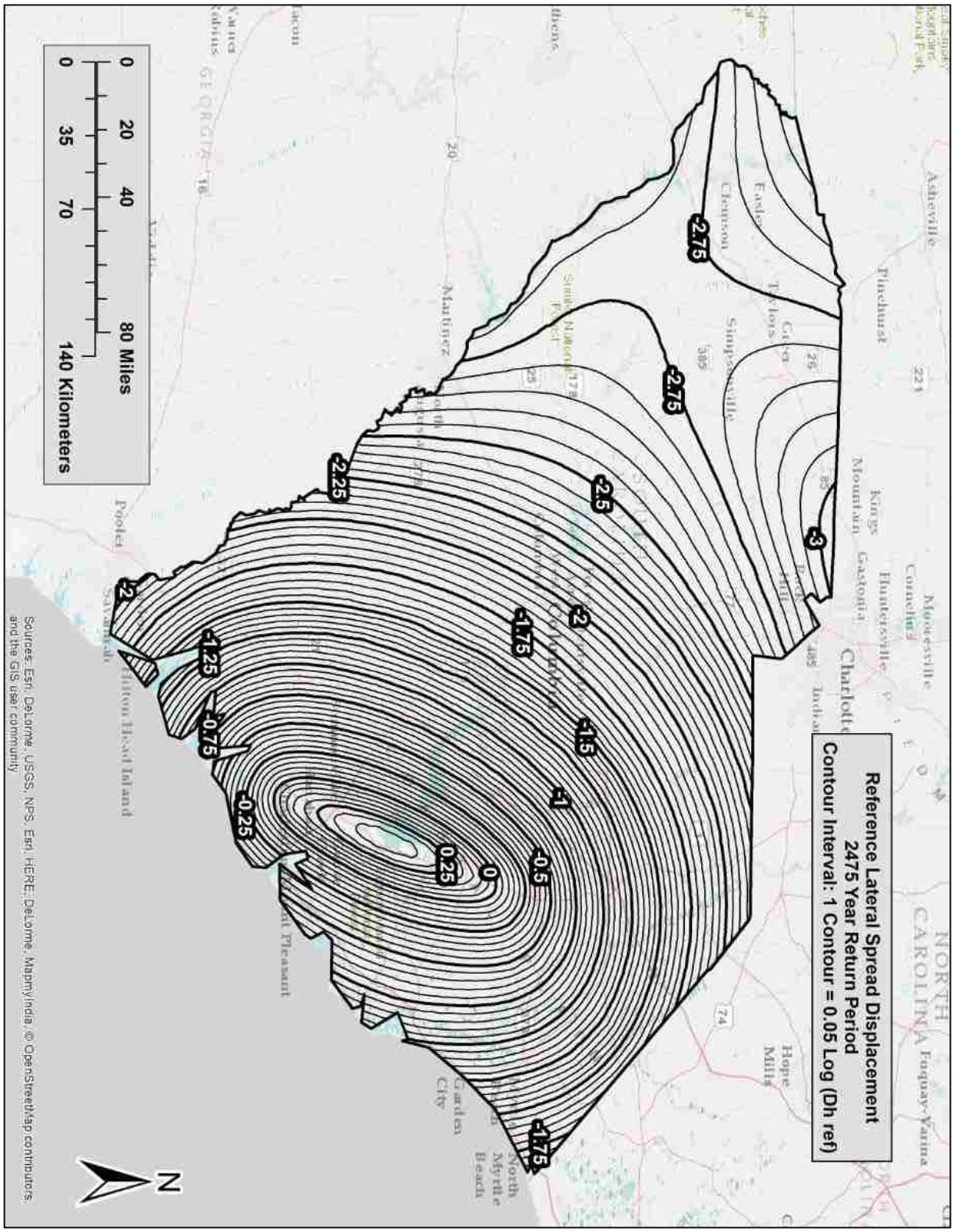


**Figure A-15: Lateral Spread Parameter ($D_H^{ref}$) Map for South Carolina ($T_r$ = 2,475)**

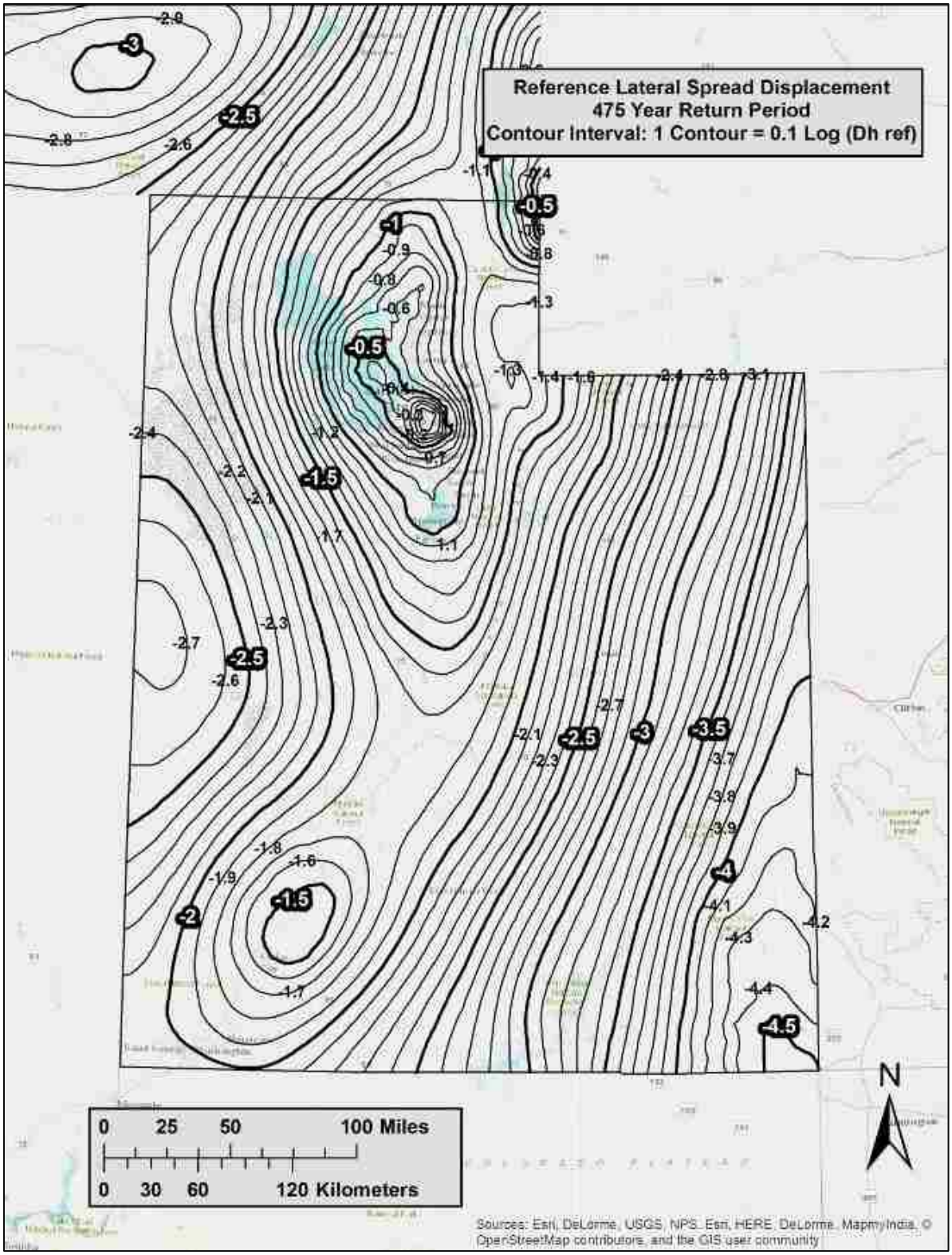


**Figure A-16: Lateral Spread Parameter ($D_H^{ref}$) Map for Utah ($T_r$ = 475)**

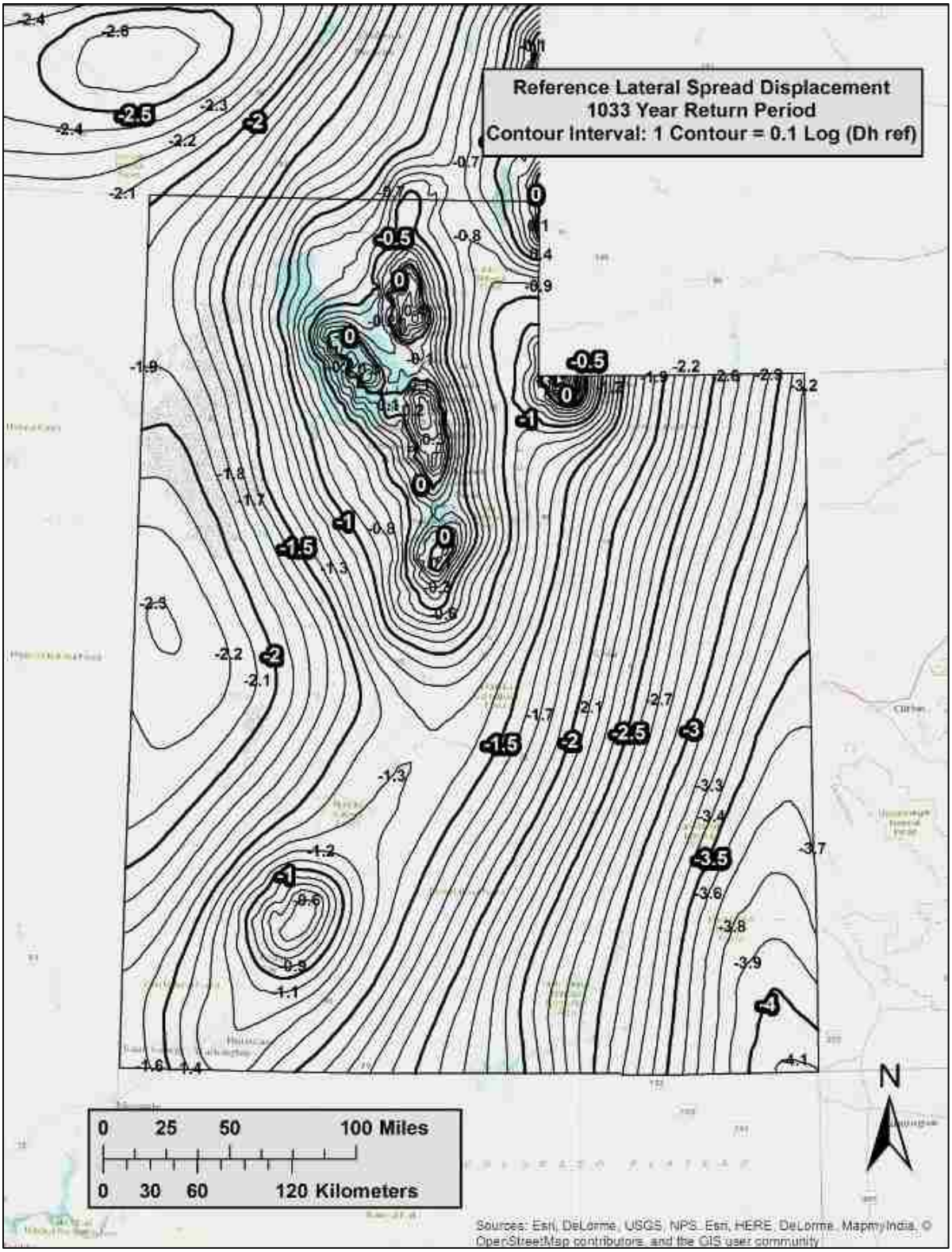


**Figure A-17: Lateral Spread Parameter ($D_H^{ref}$) Map for Utah ($T_r$ = 1,033)**

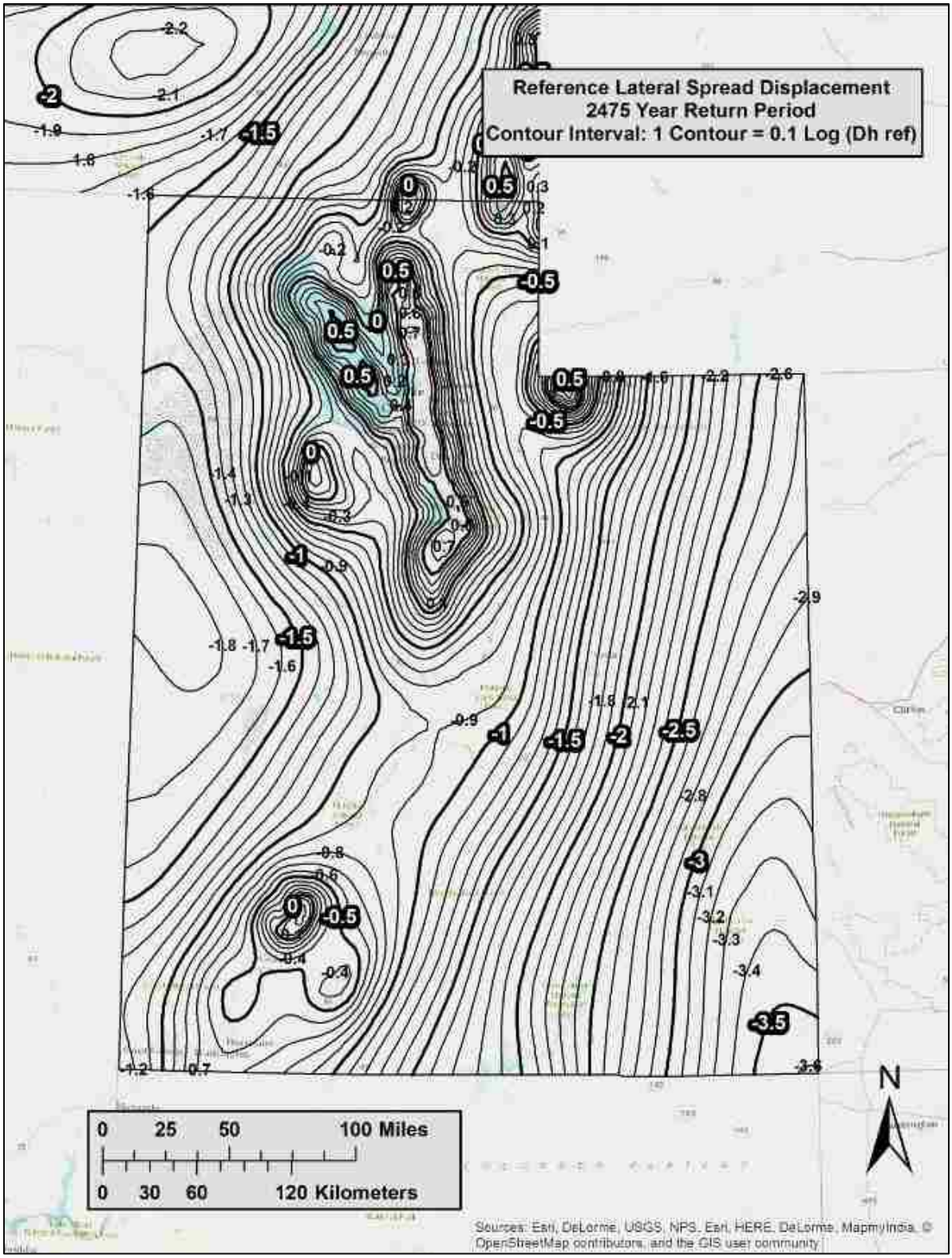


**Figure A-18: Lateral Spread Parameter ($D_H^{ref}$) Map for Utah ($T_r$ = 2,475)**

# APPENDIX B. SUPPLEMENTARY DETERMINISITIC DATA

## Faults Considered in Deterministic Analysis

| | | | | | Median Acceleration $T_R$ = 1033 | | | (Median + 1 St. Dev) Acceleration $T_R$ = 1033 | | |
|---|---|---|---|---|---|---|---|---|---|---|
| *San Francisco* | | **Seismic Source** | **Dist (km)** | **Mag** | ***PGA*** | $F_{pga}$ | $a_{max}$ | ***PGA*** | $F_{pga}$ | $a_{max}$ |
| | 1 | Northern San Andreas | 10.77 | 8.05 | 0.3175 | 1.183 | 0.3754 | 0.5426 | 1.0 | 0.5426 |
| | 2 | San Gregorio Connected | 16.64 | 7.5 | 0.2139 | 1.372 | 0.2935 | 0.3660 | 1.134 | 0.4150 |
| | 3 | Hayward-Rodgers Creek | 18.23 | 7.33 | 0.1918 | 1.416 | 0.2717 | 0.3282 | 1.172 | 0.3846 |
| | 4 | Mount Diablo Thrust | 36.08 | 6.7 | 0.1050 | 1.590 | 0.1670 | 0.1811 | 1.438 | 0.2604 |
| | 5 | Calaveras | 34.28 | 7.03 | 0.0981 | 1.6 | 0.1570 | 0.1682 | 1.464 | 0.2462 |
| *Salt Lake City* | | | | | | | | | | |
| | 1 | Wasatch Fault, SLC Section | 1.02 | 7 | 0.5911 | 1.0 | 0.5911 | 1.0050 | 1.0 | 1.0050 |
| | 2 | West Valley Fault Zone | 2.19 | 6.48 | 0.5694 | 1.0 | 0.5694 | 0.9842 | 1.0 | 0.9842 |
| | 3 | Morgan Fault | 25.04 | 6.52 | 0.0989 | 1.6 | 0.1583 | 0.1713 | 1.457 | 0.2497 |
| | 4 | Great Salt Lake Fault zone, Antelope Section | 25.08 | 6.93 | 0.1016 | 1.597 | 0.1622 | 0.1742 | 1.452 | 0.2529 |
| | 5 | Oquirrh-Southern, Oquirrh Mountain Fault | 30.36 | 7.17 | 0.0958 | 1.6 | 0.1532 | 0.1641 | 1.472 | 0.2415 |
| *Butte* | | | | | | | | | | |
| | 1 | Rocker Fault | 4.92 | 6.97 | 0.5390 | 1.0 | 0.5390 | 0.9202 | 1.0 | 0.9202 |
| | 2 | Georgia Gulch Fault | 45.91 | 6.42 | 0.0435 | 1.6 | 0.0696 | 0.0754 | 1.6 | 0.1206 |
| | 3 | Helena Valley Fault | 75.56 | 6.6 | 0.0294 | 1.6 | 0.0470 | 0.0507 | 1.6 | 0.0812 |
| | 4 | Canyon Ferry Fault | 81.32 | 6.92 | 0.0327 | 1.6 | 0.0523 | 0.0561 | 1.6 | 0.0898 |
| | 5 | Blacktail Fault | 84.27 | 6.94 | 0.0317 | 1.6 | 0.0508 | 0.0545 | 1.6 | 0.0872 |
| | 6 | Madison Fault | 86.51 | 7.45 | 0.0420 | 1.6 | 0.0671 | 0.0719 | 1.6 | 0.1150 |

**Characteristics of Rocker Fault (near Butte) and Calculations to Determine *PGA* and $M_w$.**

*M_w calculated based on
Wells and Coppersmith (1994): Length = 43 km
(Use "all" slip type, because it's a normal fault and the # of normal events is small)

*PGA calculated based on NGA equations (Linda Al Atik, PEER 2009)
BA08, CB08, and CY08 used with equal weighting

| | | | |
|---|---|---|---|
| M_w = | 6.97 | | |
| Dip = | 70 | degrees | (Another fault near Butte, has a dip of 70-75 degrees) |
| Depth to bottom of rupture = | 16 | km | (Assumed) |
| R_x = | 4.92 | km | (measured using Google Earth) |
| Z_TOR = | 0 | km | (Assumed) |
| Width = | 17.03 | km | |
| R_jb = | 0 | km | (Assuming the site is on the hanging wall side) |
| R_rup = | 1.68 | km | |
| V_s30 = | 760 | m/s | |
| U= | 0 | | |
| F_RV= | 0 | | |
| F_NM = | 1 | | |
| F_HW = | 1 | | |
| F_measured = | 0 | | |
| Z_1 = | DEFAULT | | |
| Z_2.5= | DEFAULT | | |
| F_AS= | 0 | | |
| HW Taper = | 1 | | |
| --> PGA (50%) = | 0.5390 | g | (From NGA spreadsheet) |
| --> PGA (84%) = | 0.9202 | g | (From NGA spreadsheet) |